USGS
science for a changing world

Prepared in Cooperation with the Oregon Water Resources Department

Groundwater Model of the Harney Basin, Southeastern Oregon

Scientific Investigations Report 2024–5017

U.S. Department of the Interior
U.S. Geological Survey

Covers. All photographs by Joseph Kennedy, U.S. Geological Survey, unless otherwise noted.

Front cover. Top and bottom: Irrigated fields near Dog Mountain in the Harney Basin lowlands as seen looking south from Wrights Point, Oregon. **Center-left:** Center pivot irrigation system using groundwater in the Harney Basin lowlands as seen looking north. Photograph by Amanda Garcia, U.S. Geological Survey. **Center-right:** Hibbard Spring on the southern edge of Warm Springs Valley as seen looking east.

Back Cover. Background: Irrigated fields near Dog Mountain in the Harney Basin lowlands as seen looking south from Wrights Point, Oregon. **Foreground:** Satellite image showing the irrigated fields in the Weaver Spring area and Harney Lake to the south. Image from Google Earth, copyright 2024.

Groundwater Model of the Harney Basin, Southeastern Oregon

By Stephen B. Gingerich, Darrick E. Boschmann, Gerald H. Grondin, and Halley J. Schibel

Prepared in cooperation with the Oregon Water Resources Department

Scientific Investigations Report 2024–5017

U.S. Department of the Interior
U.S. Geological Survey

U.S. Geological Survey, Reston, Virginia: 2024

Suggested citation:
Gingerich, S.B., Boschmann, D.E., Grondin, G.H., and Schibel, H.J., 2024, Groundwater model of the Harney Basin, southeastern Oregon: U.S. Geological Survey Scientific Investigations Report 2024–5017, 104 p., https://doi.org/10.3133/sir20245017.

Associated data for this publication:
Gingerich, S.B., 2024, MODFLOW 6 model used to simulate groundwater flow in the Harney Basin, southeastern Oregon: U.S. Geological Survey data release, https://doi.org/10.5066/P9OEKEIO.

ISSN 2328-0328 (online)

Acknowledgments

The authors gratefully acknowledge the Harney Groundwater Study Advisory Committee for their local knowledge, comments, questions, suggestions, and assistance. We also thank the residents of the Harney Basin, particularly those individuals who allowed access to property, wells, and springs for groundwater-level measurements and groundwater samples. Nicholas Corson-Dosch and Joseph Kennedy of the U.S Geological Survey helped with model pre- and post-processing routines.

Contents

Figures

Tables

Wells and springs have three identification systems. Example well: HARN0051319; 433425118561801; 23.00S/32.00E-18CCA01

Oregon State designation: HARN0051319; county name (HARN for Harney) and unique number within the county.

U.S. Geological Survey identifier: 433425118561801; first six digits are the latitude in degree-minute-seconds, the next seven digits are the longitude, and the last two digits indicate a unique number at that location.

Public Land Survey System designation: 23.00S/32.00E-18CCA01, shown on the following page.

Site Identification—Public Land Survey System in Oregon

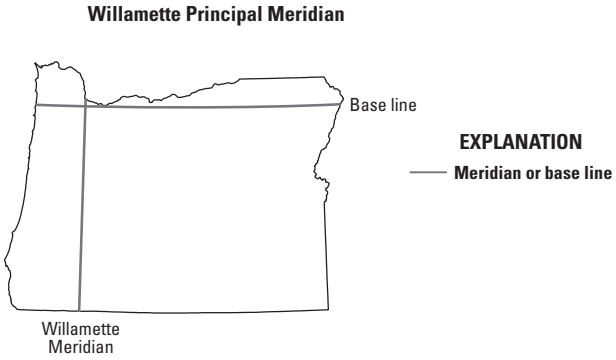

23.00S/32.00E-18CCA01

23.00S	32.00E	18	CCA	01
Township	Range	Section	Quarter-quarter-quarter section	Location sequence

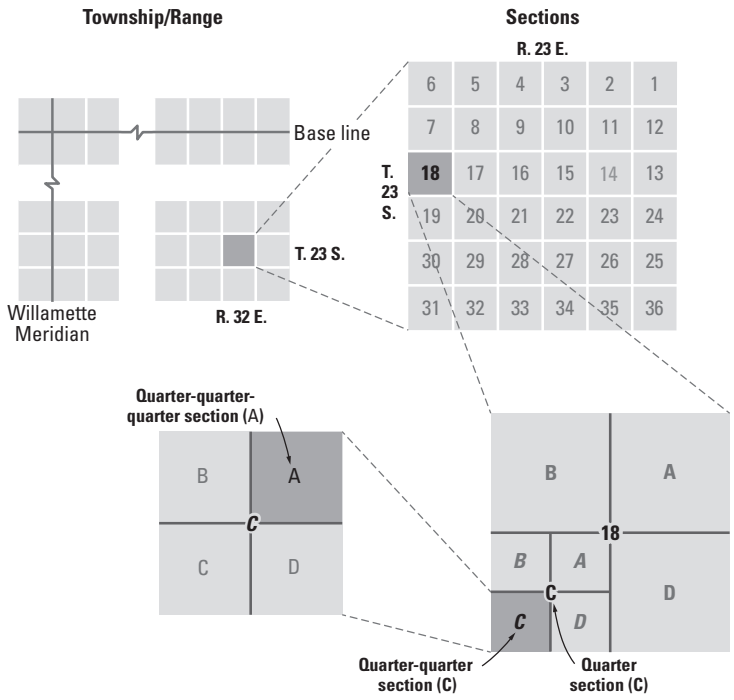

The PLSS system is based on the site's location in the Public Land Survey System. Four quadrants are formed by the intersection of the Willamette base line and principal meridian. The letters N or S locate the township north or south of the base line. The letters E or W locate the range east or west of the principal meridian. The first numeral indicates the township, the second the range, and the third the section in which the well is located. Letters following the section number locate the well within the section. The letters (A-D) are assigned within the section in a counter-clockwise direction beginning with "A" in the northeast quarter of the section. The first letter denotes the quarter section, the second the quarter-quarter section, and the third the quarter-quarter-quarter section. Letters are assigned within each divided subsection in the same manner. Where two or more wells are located within the smallest subdivision, a number indicating the order in which the wells are inventoried follows the letters. For example, well 23.00S/32.00E-18CCA01 is located in the NW 1/4, SW 1/4, SW 1/4, Section 18, T23S, R32E. It is the first inventoried well in that parcel.

Conversion Factors

U.S. customary units to International System of Units

Multiply	By	To obtain
	Length	
inch (in.)	2.54	centimeter (cm)
inch (in.)	25.4	millimeter (mm)
foot (ft)	0.3048	meter (m)
mile (mi)	1.609	kilometer (km)
	Area	
acre	4,047	square meter (m^2)
acre	0.4047	hectare (ha)
acre	0.4047	square hectometer (hm^2)
acre	0.004047	square kilometer (km^2)
square foot (ft^2)	929.0	square centimeter (cm^2)
square foot (ft^2)	0.09290	square meter (m^2)
square mile (mi^2)	259.0	hectare (ha)
square mile (mi^2)	2.590	square kilometer (km^2)
	Volume	
gallon (gal)	3.785	cubic decimeter (dm^3)
million gallons (Mgal)	3,785	cubic meter (m^3)
cubic foot (ft^3)	28.32	cubic decimeter (dm^3)
cubic foot (ft^3)	0.02832	cubic meter (m^3)
acre-foot (acre-ft)	1,233	cubic meter (m^3)
acre-foot (acre-ft)	0.001233	cubic hectometer (hm^3)
	Flow rate	
acre-foot per day (acre-ft/d)	0.01427	cubic meter per second (m^3/s)
acre-foot per year (acre-ft/yr)	1,233	cubic meter per year (m^3/yr)
acre-foot per year (acre-ft/yr)	0.001233	cubic hectometer per year (hm^3/yr)
foot per day (ft/d)	0.3048	meter per day (m/d)
foot per year (ft/yr)	0.3048	meter per year (m/yr)
cubic foot per second (ft^3/s)	0.02832	cubic meter per second (m^3/s)
million gallons per day (Mgal/d)	0.04381	cubic meter per second (m^3/s)
million gallons per day per square mile ([Mgal/d]/mi^2)	1,461	cubic meter per day per square kilometer ([m^3/d]/km^2)
	Hydraulic conductivity	
foot per day (ft/d)	0.3048	meter per day (m/d)
	Hydraulic gradient	
foot per mile (ft/mi)	0.1894	meter per kilometer (m/km)
	Transmissivity	
foot squared per day (ft^2/d)	0.09290	meter squared per day (m^2/d)

Datums

Vertical coordinate information is referenced to the North American Vertical Datum of 1988 (NAVD 88).

Horizontal coordinate information is referenced to the North American Datum of 1983 (NAD 83).

Elevation, as used in this report, refers to distance above the vertical datum.

Abbreviations

ET	evapotranspiration
HBGM	Harney Basin Groundwater Model
HU	hydrostratigraphic unit
MODFLOW 6	U.S. Geological Survey modular finite-difference groundwater-flow model
NAD 83	North American Datum of 1983
NAVD 88	North American Vertical Datum of 1988
NGVD 29	National Geodetic Vertical Datum of 1929
OWRD	Oregon Water Resources Department
PRISM	Parameter-Elevation Relationships on Independent Slopes Model
USGS	U.S. Geological Survey

Groundwater Model of the Harney Basin, Southeastern Oregon

By Stephen B. Gingerich[1], Darrick E. Boschmann[2], Gerald H. Grondin[2], and Halley J. Schibel[2]

Abstract

Groundwater development, mainly for large-scale irrigation, has increased substantially in the Harney Basin of southeastern Oregon since 2010. Concurrently, some areas of the basin experienced groundwater-level declines of more than 100 feet, and some shallow wells have gone dry. The Oregon Water Resources Department has limited new groundwater development in the basin until an improved understanding of the groundwater-flow system is available. The groundwater resources report by Gingerich and others (2022, U.S. Geological Survey Scientific Investigations Report 2021–5103, https://doi.org/10.3133/sir20215103) provides that understanding. This report describes the development of a numerical groundwater-flow model that can be used as a tool to help improve that understanding. The Harney Basin Groundwater Model was developed using the finite-difference groundwater-modeling software U.S. Geological Survey modular finite-difference groundwater-flow model (MODFLOW 6) and associated Python pre- and post-processing routines. The groundwater model encompasses the entire 5,240-square-mile Harney Basin and adjacent areas and is calibrated to the hydrologic conditions from 1930 to 2018. The model has a uniform grid consisting of 78,064 nearly square cells, each covering 2,005 by 2,007 feet (about 92 acres) and has 10 layers (780,640 total cells) representing the vertical distribution of hydrogeologic units. The results from the calibrated model simulations indicate that groundwater pumpage exceeded recharge since about the mid-1980s, resulting in an estimated net cumulative depletion of groundwater storage (discharge minus recharge) of about 840,000 acre-feet and also indicated declines in groundwater evapotranspiration and spring and stream discharge. Model simulations show as much as 100 feet of groundwater-level decline in some areas and more than 40 feet of decline in widespread areas in recent decades. Model simulations are consistent with field observations of groundwater levels through time.

Introduction

A numerical groundwater-flow model of the Harney Basin (Harney Basin Groundwater Model; HBGM) was developed to better understand the hydrologic conditions within the basin and to enable resource managers to test the conceptualization of the groundwater-flow system and accurately simulate its response to historical pumpage, current conditions, and future groundwater-withdrawal scenarios. The model was developed to meet one of the objectives in a cooperative agreement between the Oregon Water Resources Department (OWRD) and the U.S. Geological Survey (USGS) to conduct a groundwater-availability study of the Harney Basin.

The HBGM is a three-dimensional finite-difference numerical model based on the USGS three-dimensional modular finite-difference groundwater-flow model (MODFLOW 6; Langevin and others, 2017, 2022). Model development involved defining the model discretization, model boundaries, hydrologic properties of the geologic units, recharge, discharge, and anthropogenic stresses. The development and simulations of the model were facilitated using the FloPy Python package (Bakker and others, 2022). Model versions and packages used are shown in table 1 and are available in Gingerich (2024). The model was calibrated using a mixed iterative approach. Steady-state conditions, also called "initial conditions," were based on groundwater recharge estimates for conditions prior to 1930 and groundwater-level data from the 1930s (Piper and others, 1939), and the period 1930–2018 was used for the transient-state model.

The HBGM can be used to assess groundwater availability based on predicted future scenarios that describe different groundwater-management strategies and changes in natural recharge patterns. Resource managers and stakeholders can use results from future scenarios to gain insights for managing future groundwater resources and challenges. Numerical models are approximations of complex natural systems, and although they provide valuable insights and provide capability for exploring a range of resource-management alternatives, their limitations must be kept in mind moving forward.

[1]U.S. Geological Survey

[2]Oregon Water Resources Department

Table 1. Summary of U.S. Geological Survey modular finite-difference groundwater-flow model (MODFLOW 6) packages and processes used in the Harney Basin Groundwater Model, southeastern Oregon (Gingerich, 2024).

[Package and process descriptions in Langevin and others (2017)]

Computer program (packages processes)	Function
Drain (DRN) Package	Simulates a head-dependent flux boundary condition used to represent streams within the model to allow groundwater to flow out of the model under a regional gradient.
Evapotranspiration (EVT) Package	Specifies evapotranspirative flux leaving the model at the top surface.
Groundwater Flow (GWF) Model	Contains setup simulating a basic groundwater-flow model.
Initial Conditions (IC) Package	Contains the starting hydraulic head distribution. For the transient simulation, this is from the result of the pre-1390 steady-state simulation.
Iterative Model Solution (IMS)	Specifies nonlinear and linear settings for the solver equations.
List File (LIST)	Contains the output file for allocation information, values used by the GWF process, and calculated results, such as hydraulic head and the water budget.
Model Budget Files	Binary file of cell-by-cell flow throughout the simulation. Used for determining the water budget for the various processes simulated.
Node Property Flow (NPF) Package	Specifies the horizontal and vertical hydraulic conductivity distribution.
Observation (OBS) Utility	Provides options for extracting numeric values of groundwater level and drain flows of interest generated in the course of a model run.
Output Control (OC) Option	Specifies how and when heads and water budgets are printed to the listing file and/or written to a separate binary output file.
Recharge (RCH) Package	Specifies recharge flux entering the model at the top surface from precipitation and surface-water infiltration.
Simulation Name File	Contains names of files controlling all aspects of the simulation.
Storage (STO) Package	Specifies the storage property distribution for transient simulations.
Structured Discretization (DIS) Input File	Contains discretization information (such as cell size and location) for structured grids.
Temporal Discretization (TDIS) Package	Contains information controlling the length of stress periods and time steps used in the simulation.
Well (WEL) Package	Simulates pumpage from wells and contains well locations, depths, and withdrawal rates.

Purpose and Scope

The purpose of this report is to document the calibrated groundwater-flow model of the Harney Basin. Geologic mapping and interpretation performed since the 1930s helped define the geologic framework and controls on groundwater flow. Groundwater levels measured in wells during 1930–2018 were used to determine the groundwater-level elevations for history matching. Data available from wells during 1930–2021 and information recorded in drillers' logs were used to help define sources of groundwater and identify individual hydrostratigraphic units (HUs). Estimates of stream base flow during 1982–2016 were compared with model results of simulated discharge in upland streams.

The information contained herein builds upon nearly a century's worth of geologic mapping and hydrologic data collection. Much of the information is available in recent reports and published data sources describing the Harney Basin groundwater-flow system. The hydrologic framework is presented in Gingerich and others (2022), the hydrologic budget in Garcia and others (2022), the geology of the Harney Basin in Boschmann (2021), and the hydraulic characteristics of subsurface materials in Grondin and others (2021). Irrigation pumpage is described in Beamer and Hoskinson (2021), non-irrigation pumpage is summarized in Grondin (2021), and estimates from both sources are incorporated in Schibel and Grondin (2023).

This report describes the development and use of the model and includes two example simulations of hypothetical future (through 2100) groundwater withdrawal scenarios: (1) continued withdrawal at 2018 rates and (2) complete cessation of irrigation withdrawal after 2018. This report also contains discussion of model limitations.

Model Boundaries and Discretization

The HBGM includes the entire Malheur Lake watershed and surrounding areas that have water-bearing strata and alluvial deposits. The model is bounded on the northwest, west, and southwest by the basin topographic divides, on the south by Home Creek and topographic divides, on the northeast by the forks of the Malheur River, and on the southeast by topographic divides and discharge areas of the Alvord Desert (fig. 1). The boundary in the vicinity of the Alvord Desert is outside the Harney Basin and assumed far enough away from the topographic divide along the top of Steens Mountain so as to be unaffected by groundwater flow in the basin. The flank of Steens Mountain east of the topographic divide is included to allow for the model to determine the position of the groundwater divide beneath the crest of the mountain rather than assuming it coincides with the topographic divide. This approach was used because the asymmetry of Steens Mountain (gently sloping on the west flank and steeply sloping on the east flank) could shift the groundwater divide westward relative to the surface-water divide. Where other topographic divides defined the boundaries of the model, they were simulated as no-flow boundaries; where rivers and streams formed boundaries, they were simulated as head-dependent flow boundaries.

The area simulated was discretized using a rectangular finite-difference model grid consisting of rows and columns of square cells. Each cell of the model grid represents a small part of the landscape. The averaged value for each parameter of the groundwater-flow system was assigned as the model input for each active cell. Every active cell in the model area is assigned a value for all necessary model input parameters, thereby describing the areal and vertical distribution of the aquifer properties.

Spatial Discretization

The finite-difference grid, designed to represent topography, surficial deposits, and subsurface strata, consists of 328 roughly east-west rows and 238 roughly north-south columns of nearly square cells 2,007 (east to west) by 2,005 ft (north to south). The total model grid covers an area of 11,269 square miles. In the vertical dimension, the model grid has 10 layers. About 62 percent of the 780,640 cells (48,016 cells in each of layers 1–10) are within the active area of the hydrologic model; groundwater flow is only simulated in active model cells (fig. 1). The top of the model (layer 1) represents the land-surface elevation and ranges from 3,259-foot (ft) elevation along the South Fork Malheur River to 9,573-ft elevation at the summit of Steens Mountain. The elevation for the top of layer 1 was determined by overlaying the model grid on a 10-meter digital elevation model of the area and calculating the average elevation within each model cell. Layers 1–5 are each 100-ft thick, and layers 6–10 are of varying thickness to encompass the depth from the bottom of layer 5 (500 ft below ground surface) to the bottom of the model grid, which is at 2,085-ft elevation everywhere. Thicknesses of cells in layers 6–10 range from 135 to 1,397 ft. The bottom of the model is a no-flow boundary.

Temporal Discretization

The total simulation period used for calibration of the HBGM spans 89 years, from January 1930 through December 2018. The first stress period (representing pre-1930 conditions) is steady-state, defining the initial condition for the transient-state simulation (1930–2018). Time segments during which user-specified model inflows (such as recharge from precipitation and streamflow infiltration) and outflows (such as groundwater pumpage and evapotranspiration [ET]) are considered constant are referred to as “stress periods.” Time-varying stresses are simulated by changing these model inputs from one stress period to the next. The transient-state simulation (1930–2018) has 12 monthly stress periods each year, for a total of 1,068 stress periods (stress periods 2–1,069).

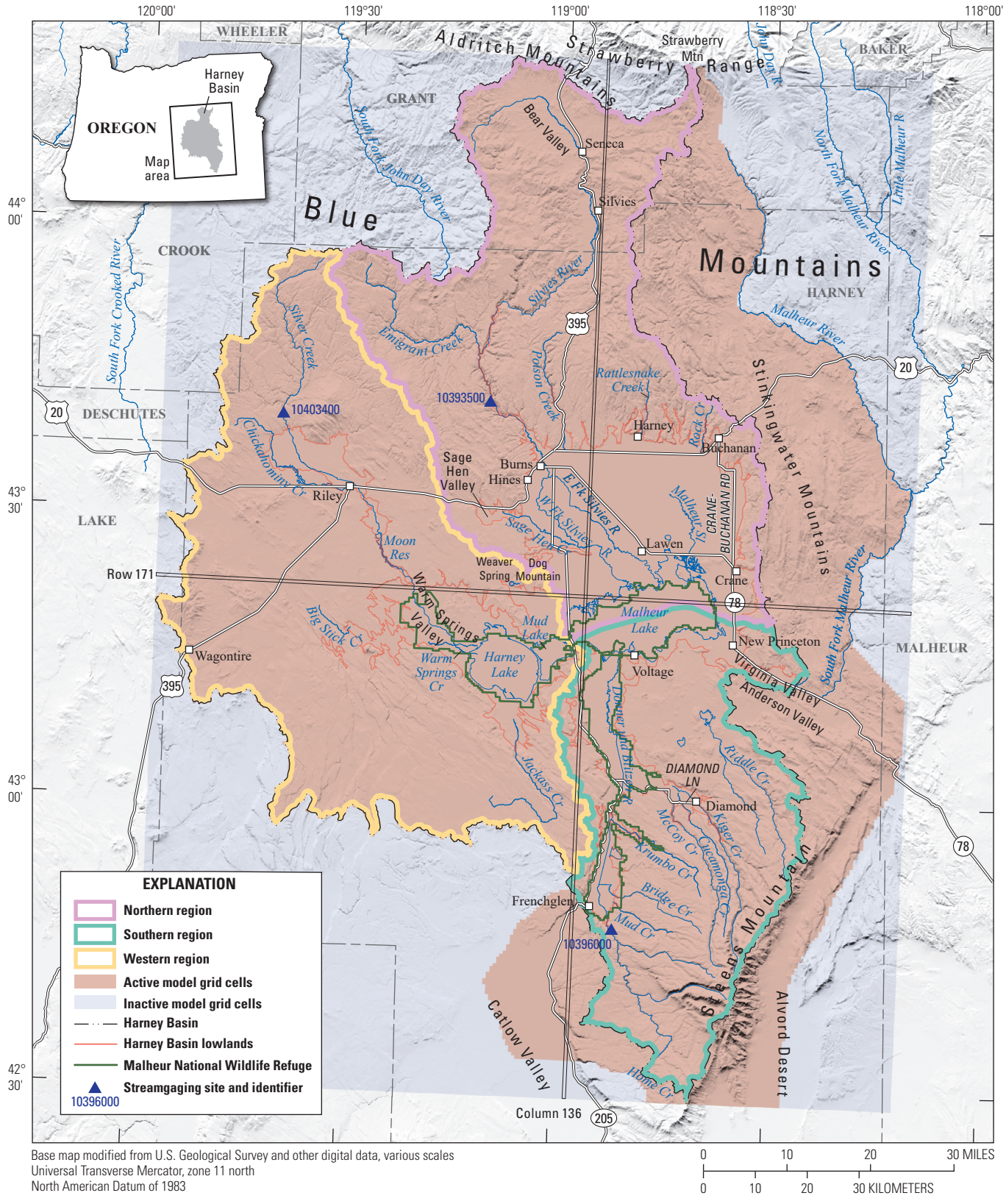

Figure 1. Location simulated in the Harney Basin Groundwater Model, Harney Basin, southeastern Oregon. Regional definitions were taken from Garcia and others (2022).

Hydraulic Properties

Individual model cells were assigned hydraulic properties based on the predominant hydrostratigraphic unit (HU) (figs. 2–3) represented by that cell (see app. 1 for the distribution of HUs in layers 1–10). The thickness of each HU was estimated on the basis of published descriptions (Boschmann, 2021; Gingerich and others, 2022), drillers' logs (Oregon Water Resources Department, 2019), and the following assumptions:

- The top of the Marine sedimentary rocks HU was assumed to dip southeastward beneath all other units (fig. 3*B*).
- The top of the Upland volcanic rocks HU was assumed to form a bowl-shaped depression beneath the central part of the basin.
- The Silicic lava flows and domes HU was generally assumed to be at least 500-ft thick around the periphery of each unit and thicker in the center.
- The Dry Mountain lavas HU was assumed to be 400–600-ft thick and dome shaped with a diameter of roughly 7.5 miles in layer 4.
- The High Lava Plains basalt HU was assumed to be about 200-ft thick.
- The Proximal vent deposits HU was assumed to be about 200-ft thick, except in the Weaver Spring area where an abundance of drillers' logs showed the deposits as thick as 400 ft.
- The Voltage basalt HU was assumed to be about 200-ft thick except in the drainage leaving Virginia Valley toward the Malheur River Basin where this HU is up to 400-ft thick to represent its canyon-filling geometry.

The hydraulic properties assigned to each corresponding model layer represent the ability of the various hydrostratigraphic units to transmit water and store or release water. Hydraulic properties in the basin rocks and sediments differ according to depositional characteristics, grain size, cementation, and the degree of sorting of the sediments, which are dependent on lithology and depositional environment. Thus, considerable spatial variation exists in the hydraulic properties of the groundwater-flow system. The water-transmitting properties of hydrostratigraphic units are represented by their horizontal and vertical hydraulic conductivities. The storage properties of hydrostratigraphic units are represented by specific yield in the unconfined model layers and by specific storage in the confined model layers. The relation among hydrostratigraphic units in the Harney Basin and hydraulic properties has been described in previous reports (Grondin and others, 2021; Gingerich and others, 2022). Areas with similar geologic features and hydrologic properties were grouped together into hydrostratigraphic units and generally assigned the same hydraulic properties. The final calibrated values of the hydraulic properties for each similar area were determined through an iterative calibration approach.

Representation of the subsurface is increasingly generalized with depth in the deeper model layers due to a paucity of subsurface data, especially in the upland areas. Along the eastern side of the Harney Basin boundary, the HUs were extended beyond the hydrostratigraphic unit map of Gingerich and others (2022) to fill in the rest of the simulated area based on the geologic units of Walker and Repenning (1965) and Greene and others (1972) and the correlations of Boschmann (2021) and Grondin and others (2021).

Hydraulic Conductivity

Hydraulic conductivity is the volume of water that will flow through a unit cross section of a porous medium (the rock or deposit), measured at right angles to the direction of flow, under a unit head gradient (Lohman, 1972). Hydraulic conductivity is dependent on the physical properties of any given rock or deposit (framework, porosity, pore size, and pore connectivity) and the physical properties of the fluid flowing through the rock or deposit. Horizontal and vertical hydraulic conductivity values for hydrostratigraphic units represented by the HBGM are required as model input. Initial estimates of hydraulic conductivity were calculated from specific-capacity tests reported on drillers' logs and a few long-term aquifer tests (Grondin and others, 2021; Gingerich and others, 2022) and were adjusted during the calibration process. As much as possible, entire hydrostratigraphic units beneath the uplands were kept homogeneous to provide a calibration that honored the sparse measured data without overparameterizing the model. Calibrated horizontal hydraulic conductivity values range from 0.002 to 4,790 feet per day (ft/d), and calibrated vertical hydraulic conductivity values range from 0.00004 to 28 ft/d (table 2). These horizontal and vertical hydraulic conductivity values are assigned to model cells according to the distributions shown on figures 4 and 5. Plots of vertical hydraulic conductivity in layers 2–4 and 6–9 are similar and are not included for brevity in this report.

The hydraulic conductivity values were modified separately beneath some lowland areas to provide better calibration where groundwater-level observations are more abundant or where regional hydraulic conductivity estimates were problematic. These areas, referred to as the Lowland deposits, the Virginia/Anderson Valley permeable zone, and the Western permeable zone, are described below.

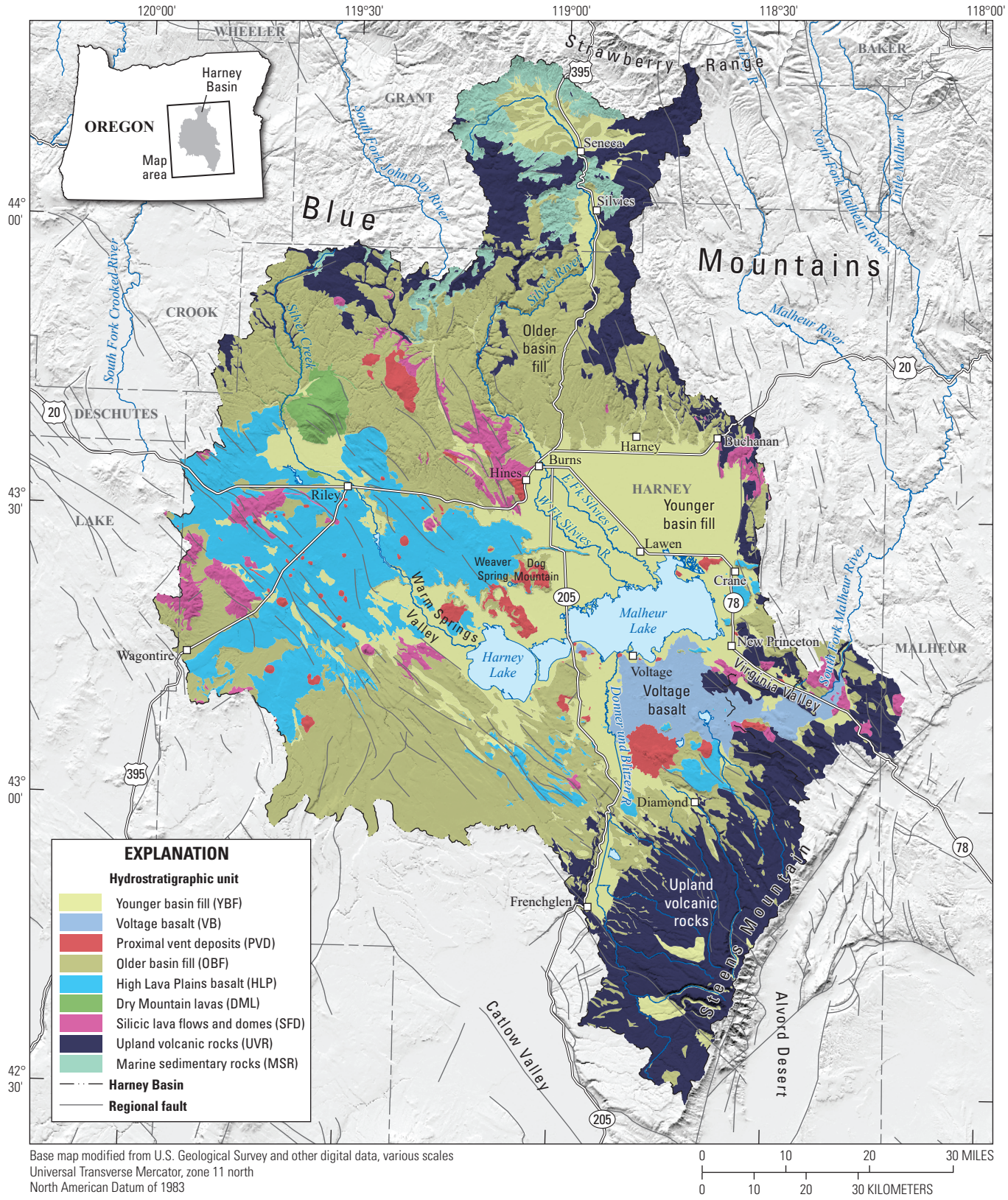

Figure 2. Surficial distribution of the hydrostratigraphic units, Harney Basin, southeastern Oregon (from Gingerich and others [2022]). Regional faults modified from Walker (1963), Brown and Thayer (1966), Walker and others (1967), Swanson (1969), Greene and others (1972), and Walker and Repenning (1965).

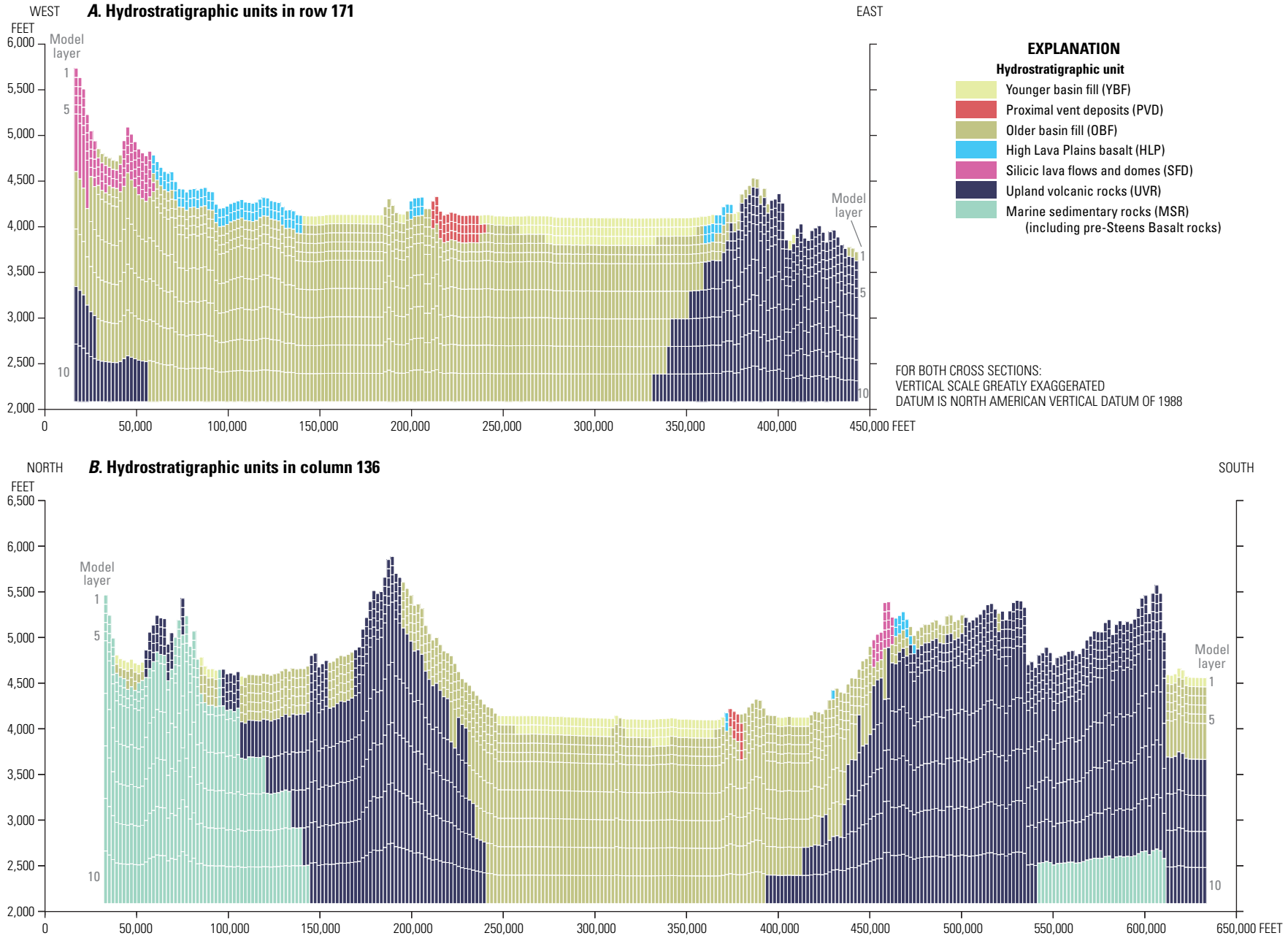

Figure 3. Hydrostratigraphic unit distributions (*A*) in east-west row 171 and (*B*) in north-south column 136 in the Harney Basin Groundwater Model (Gingerich, 2024), Harney Basin, southeastern Oregon. Row and column locations shown on figure 1.

Table 2. Summary of calibrated hydraulic properties used in the Harney Basin Groundwater Model (Gingerich, 2024), Harney Basin, southeastern Oregon.

[Specialized zones are areas of the model where the commonly used parameters were modified to provide better calibration. **Abbreviation**: ft/d, foot per day]

Hydrostratigraphic unit	Horizontal hydraulic conductivity (ft/d)	Vertical hydraulic conductivity (ft/d)	Specific yield (unitless)	Specific-storage (foot–1)
Younger basin fill (YBF)	5	0.05	0.05	7.5×10^{-5}
Voltage Basalt (VB)	2,800	28	0.005	1.0×10^{-7}
Proximal vent deposits (PVD)	40–100	2–10	0.05	1.0×10^{-7}
High Lava Plains basalt (HLP)	150–300	1.5–3.0	0.05	1.0×10^{-7}
Older basin fill (OBF)	0.043	0.0043	0.05	5.0×10^{-7}
Dry Mountain lavas (DML)	0.49	0.049	0.05	1.0×10^{-7}
Silicic lava flows and domes (SFD)	0.1	0.01	0.05	1.0×10^{-7}
Upland volcanic rocks (UVR)	0.04–0.06	0.004–0.006	0.005	1.0×10^{-7}
Pre-Steens Basalt rocks	0.005	0.0005	0.005	1.0×10^{-7}
Marine sedimentary rocks (MSR)	0.002	0.0002	0.01	1.0×10^{-7}
Specialized zones				
Lowland deposits[1]				
Layer 1	1.1–4,790	0.001–4.79	0.1–0.2	7.5×10^{-5}
Layer 2	0.8–984	0.0008–0.984	0.1	7.5×10^{-5}
Layer 3	0.2–371	0.0002–0.371	0.1	7.5×10^{-5}
Layer 4	0.1–245	0.0001–0.245	0.1	7.5×10^{-5}
Layer 5	0.04–148	0.00004–0.148	0.1	7.5×10^{-5}
Layer 6	0.04–74	0.00004–0.074	0.1	7.5×10^{-5}
Layer 7	0.04–15	0.00004–0.015	0.1	7.5×10^{-5}
Layer 8	0.04–3.0	0.00004–0.003	0.1	7.5×10^{-5}
Layer 9	0.04–0.6	0.00004–0.0006	0.1	7.5×10^{-5}
Virginia/Anderson Valley[2]	400	4	0.005–0.05	1.0×10^{-7}
Western permeable zone[3]	250	2.5	0.05	1.0×10^{-7}

[1]Lowland deposits: Area beneath lowlands combining Younger basin fill and Older basin fill in model layers 1–9 with hydraulic conductivity estimated by kriging of hydraulic conductivity estimates from Grondin (2021).

[2]Virginia/Anderson Valley: Area where the hydraulic conductivity of SFD and UVR was increased in layers 1–5 to improve model calibration.

[3]Western permeable zone: Area where hydraulic conductivity of various hydrostratigraphic units where increased in layers 3–6 to improve model calibration.

Lowland Deposits

Much of the lowlands is underlain by the Younger basin fill and Older basin fill HUs (fig. 2). The Younger basin fill HU is estimated to be 100–300 ft thick and in many places beneath the lowlands, indistinguishable from the underlying Older basin fill HU (Gingerich and others, 2022). Estimates of transmissivity for the Younger basin fill HU (n=43) have a median of 710 feet squared per day (ft^2/d) and an interquartile range of 210–3,500 ft^2/d and estimates of transmissivity for the Older basin fill HU (n=944) have a median of 980 ft^2/d and an interquartile range of 340–3,000 ft^2/d; however, the entire range of estimates spans six orders of magnitude (10^0–10^5 ft^2/d) (Gingerich and others, 2022). The Younger basin fill HU is generally finer grained toward the center of the valley where low energy fluvial and lacustrine processes dominate and coarser grained toward the margins where higher energy streams enter the valley floor from the upper elevation parts of their catchments.

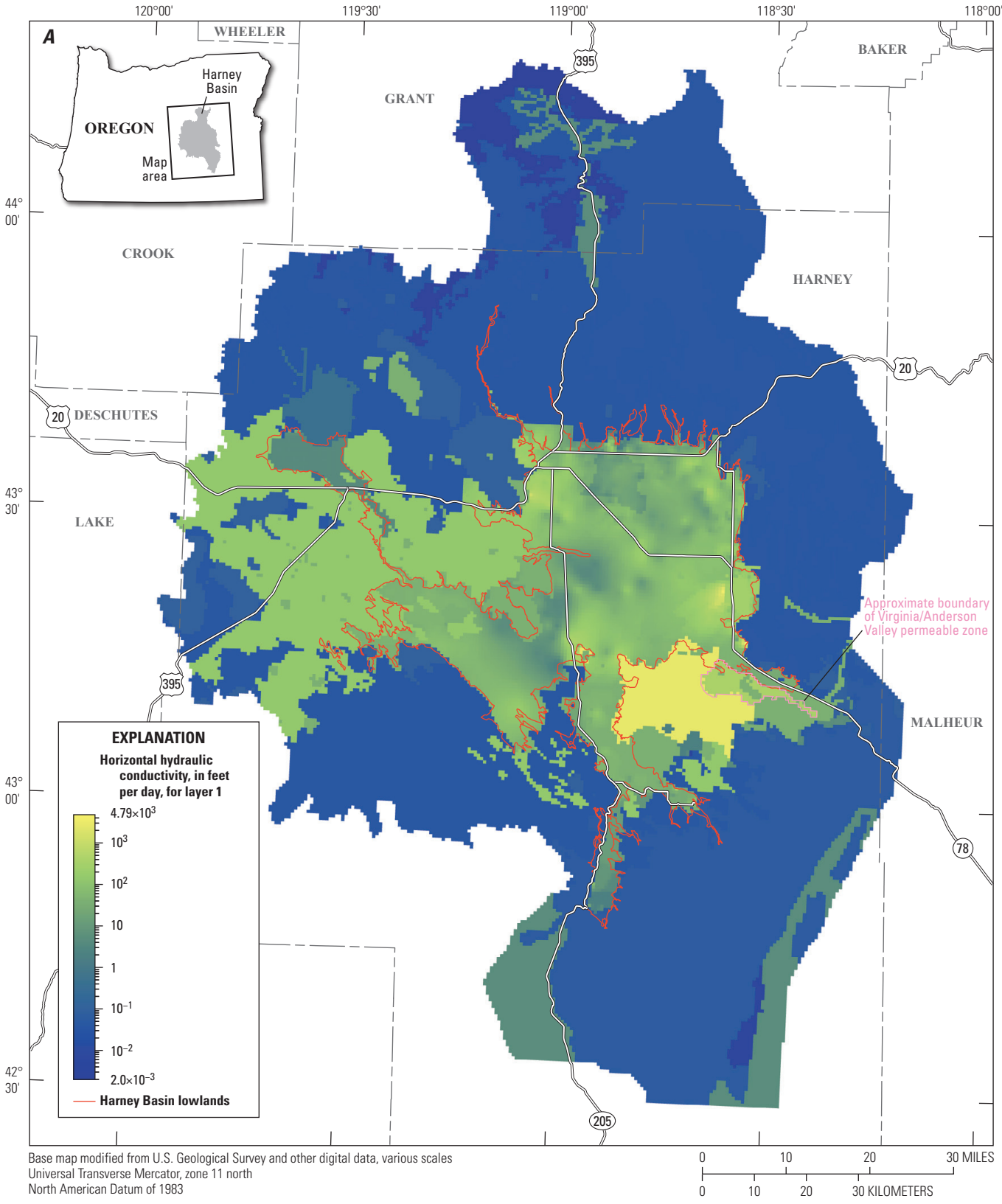

Figure 4. Distribution of horizontal hydraulic conductivity simulated in layers 1–10 of the Harney Basin Groundwater Model (Gingerich, 2024), Harney Basin, southeastern Oregon.

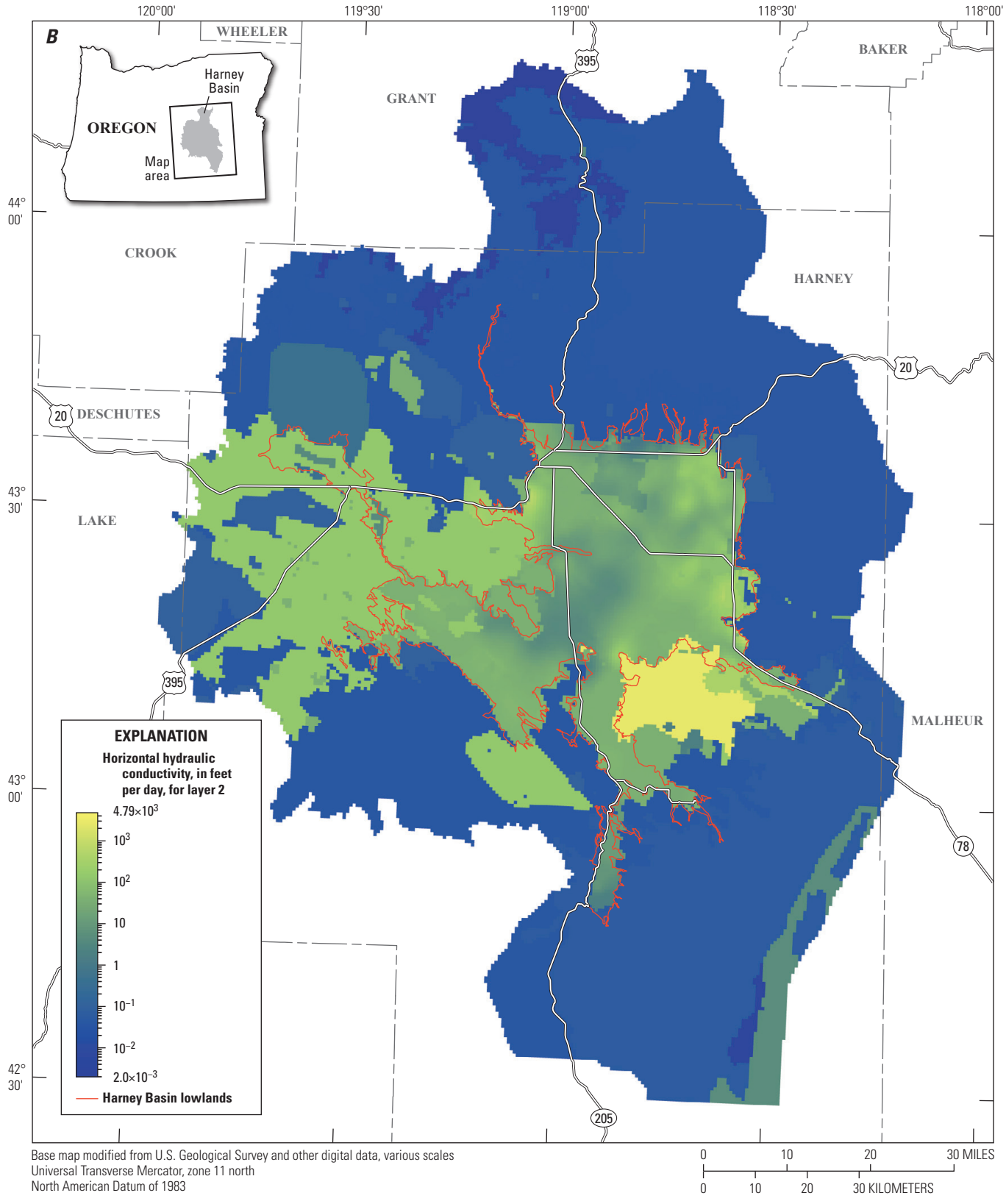

Figure 4.—Continued

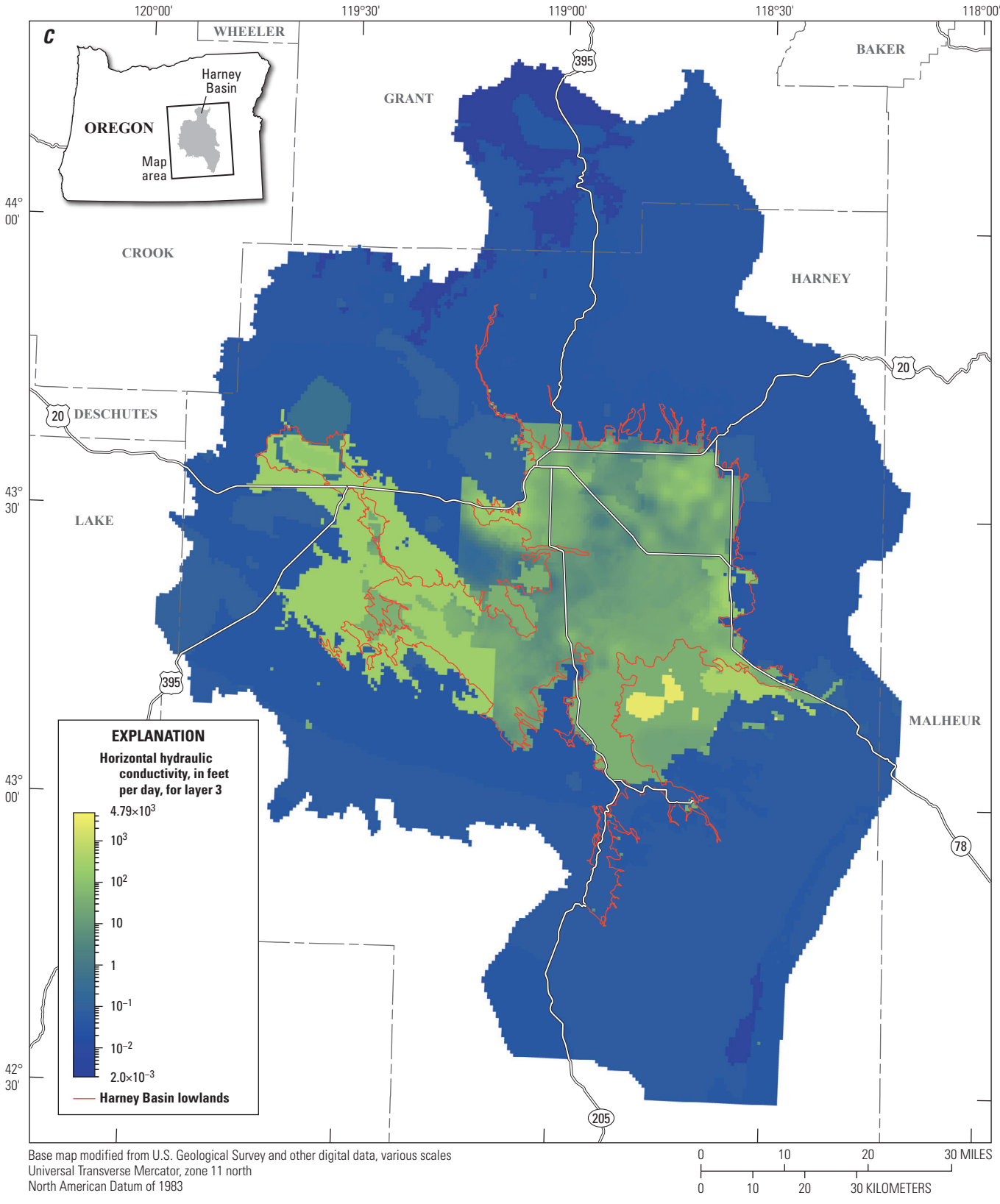

Figure 4.—Continued

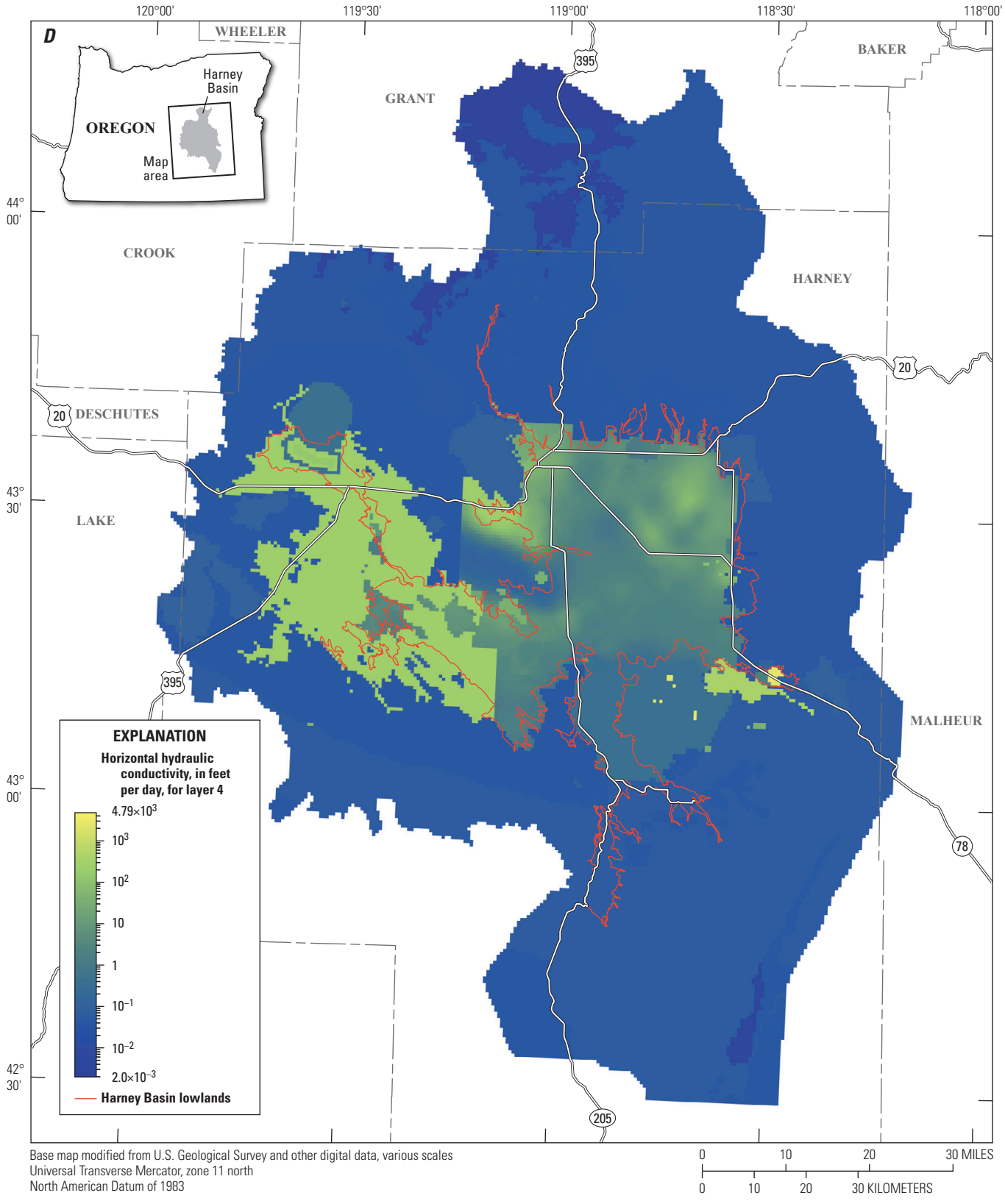

Figure 4.—Continued

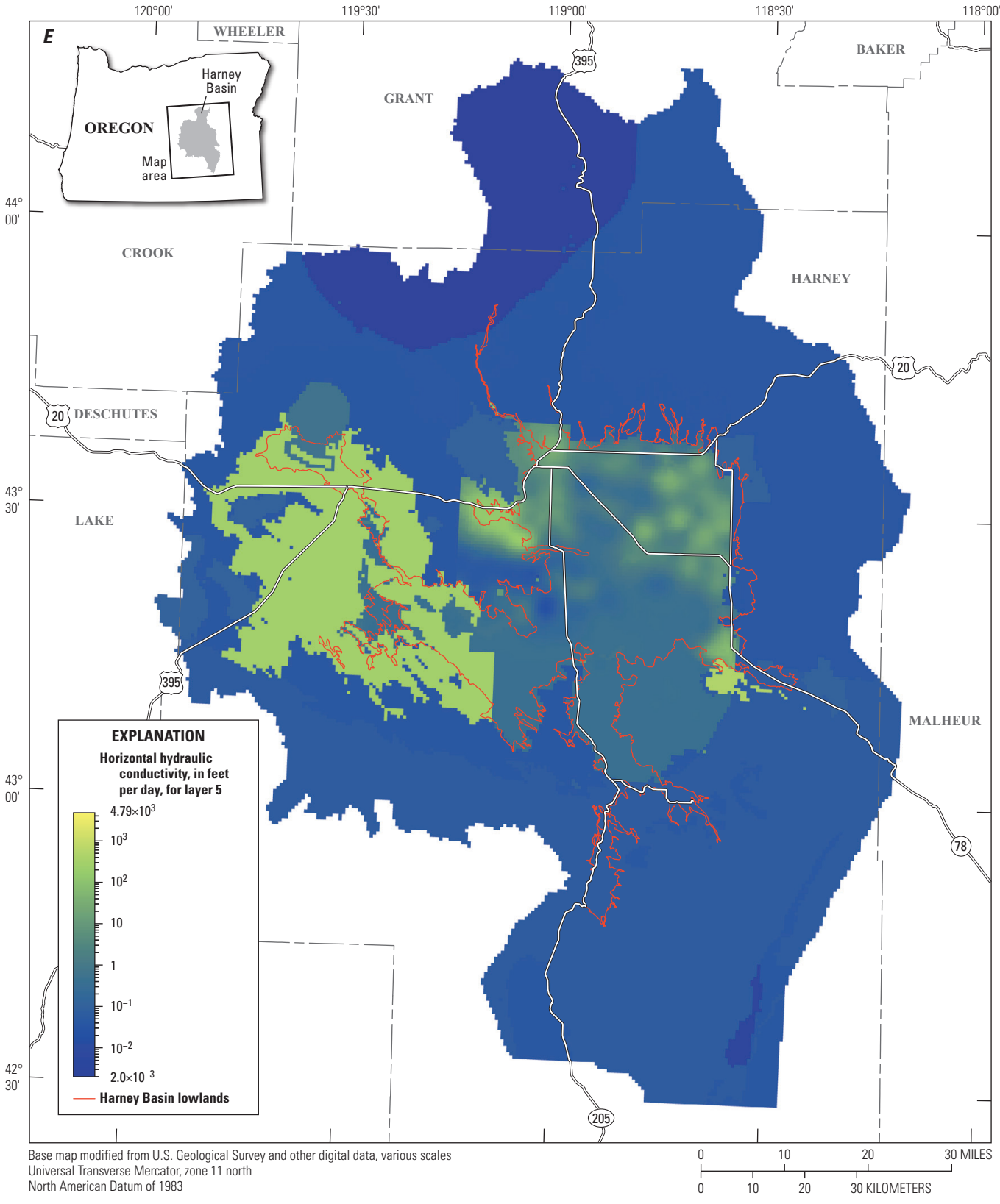

Figure 4.—Continued

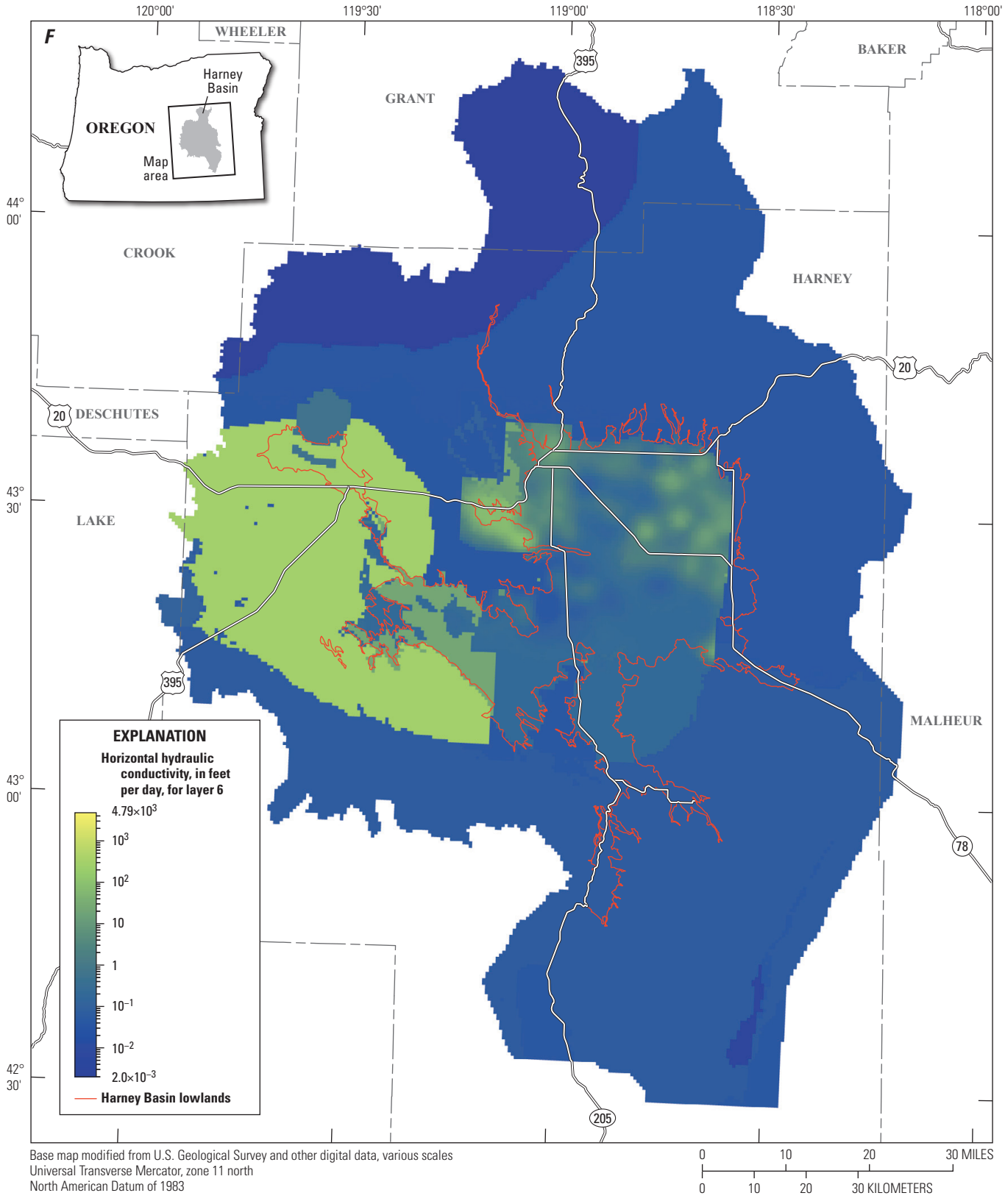

Figure 4.—Continued

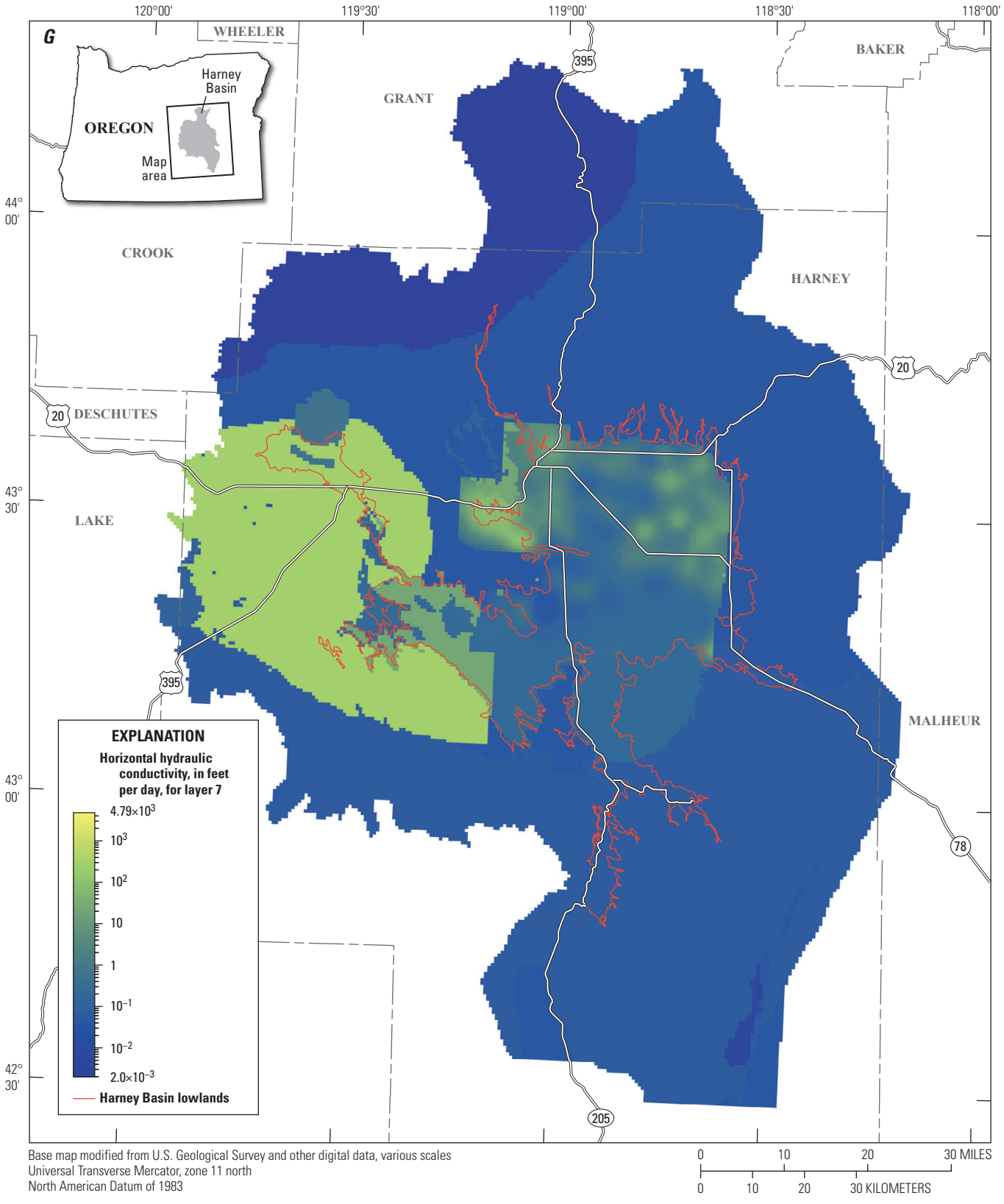

Figure 4.—Continued

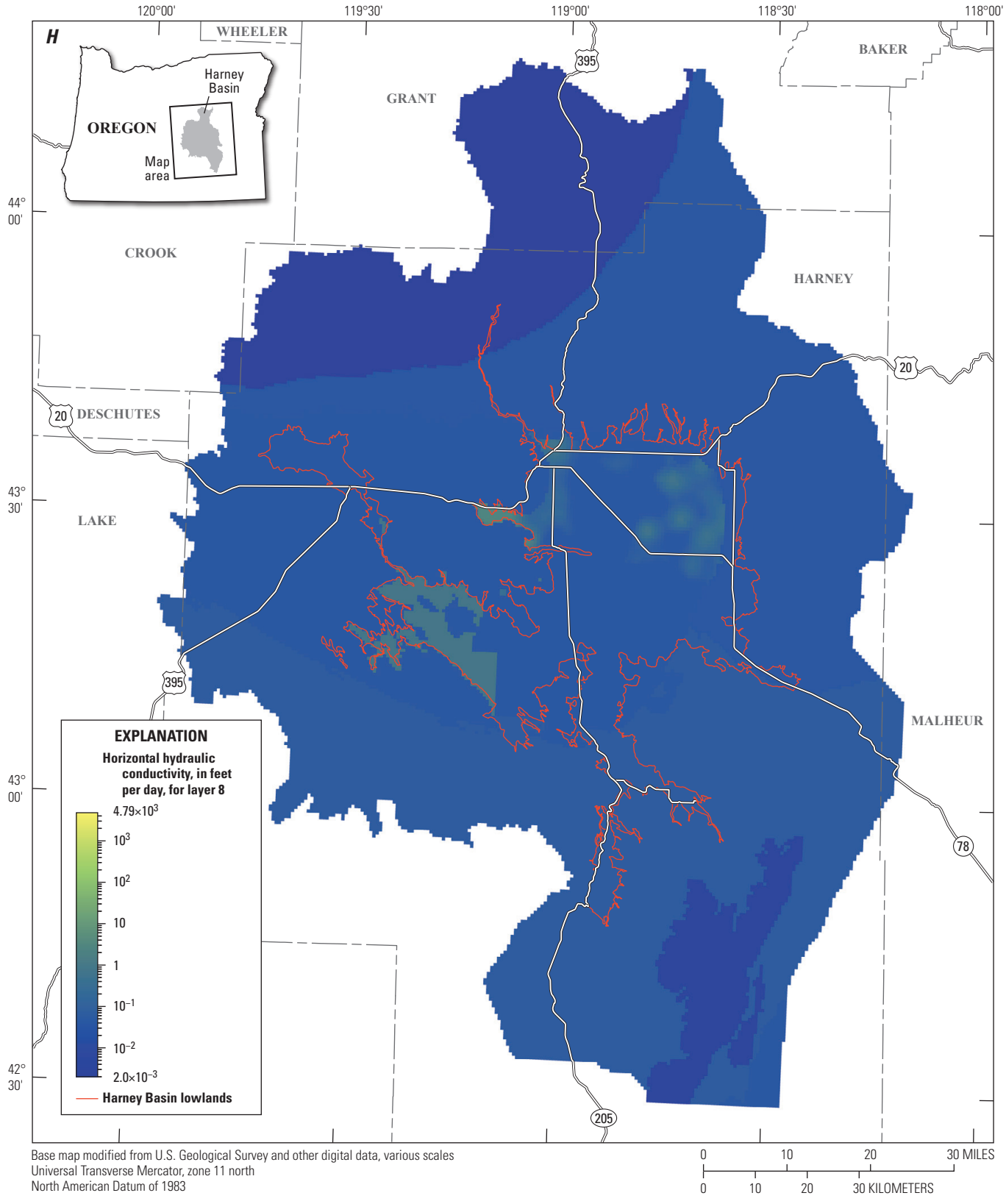

Figure 4.—Continued

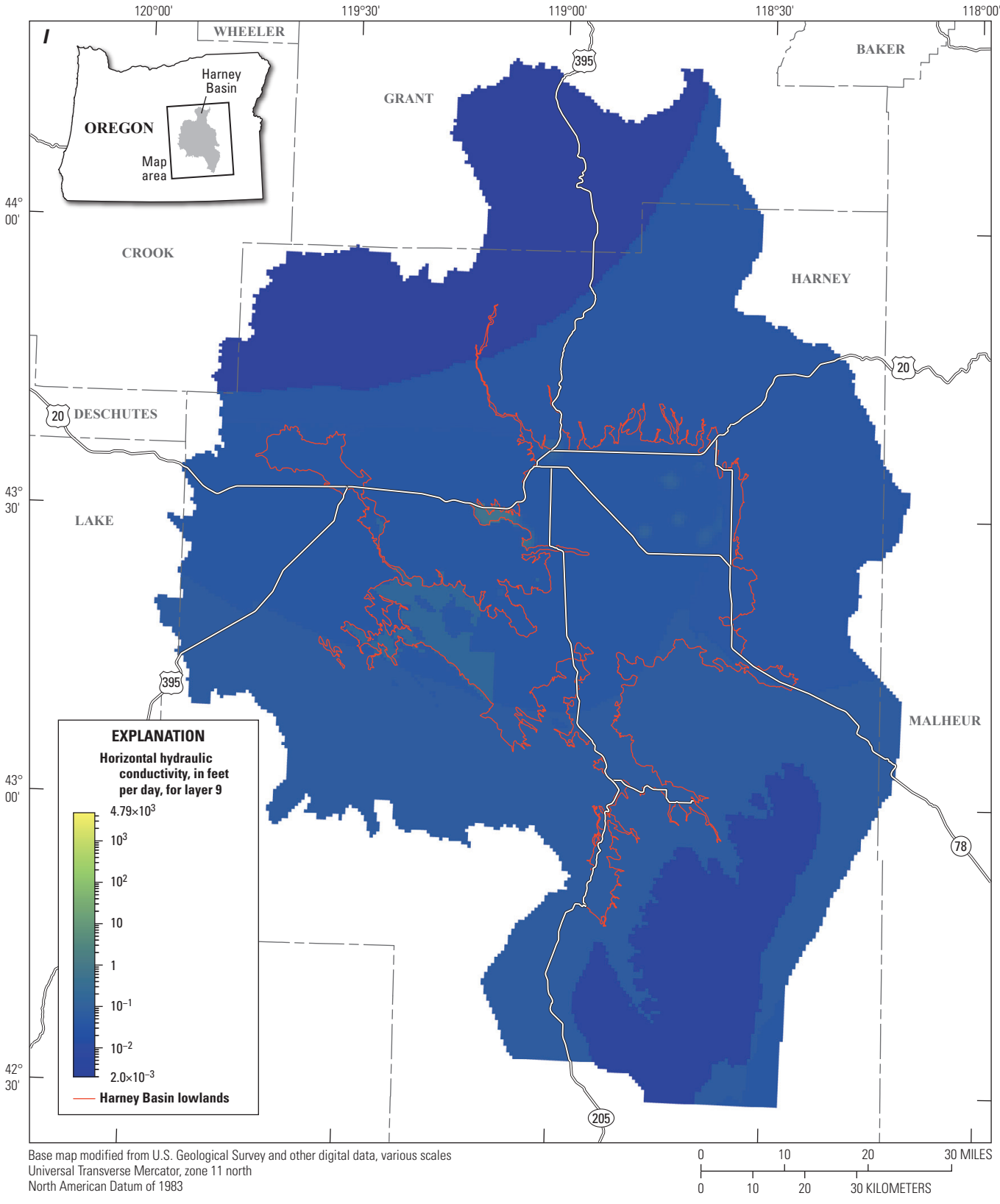

Figure 4.—Continued

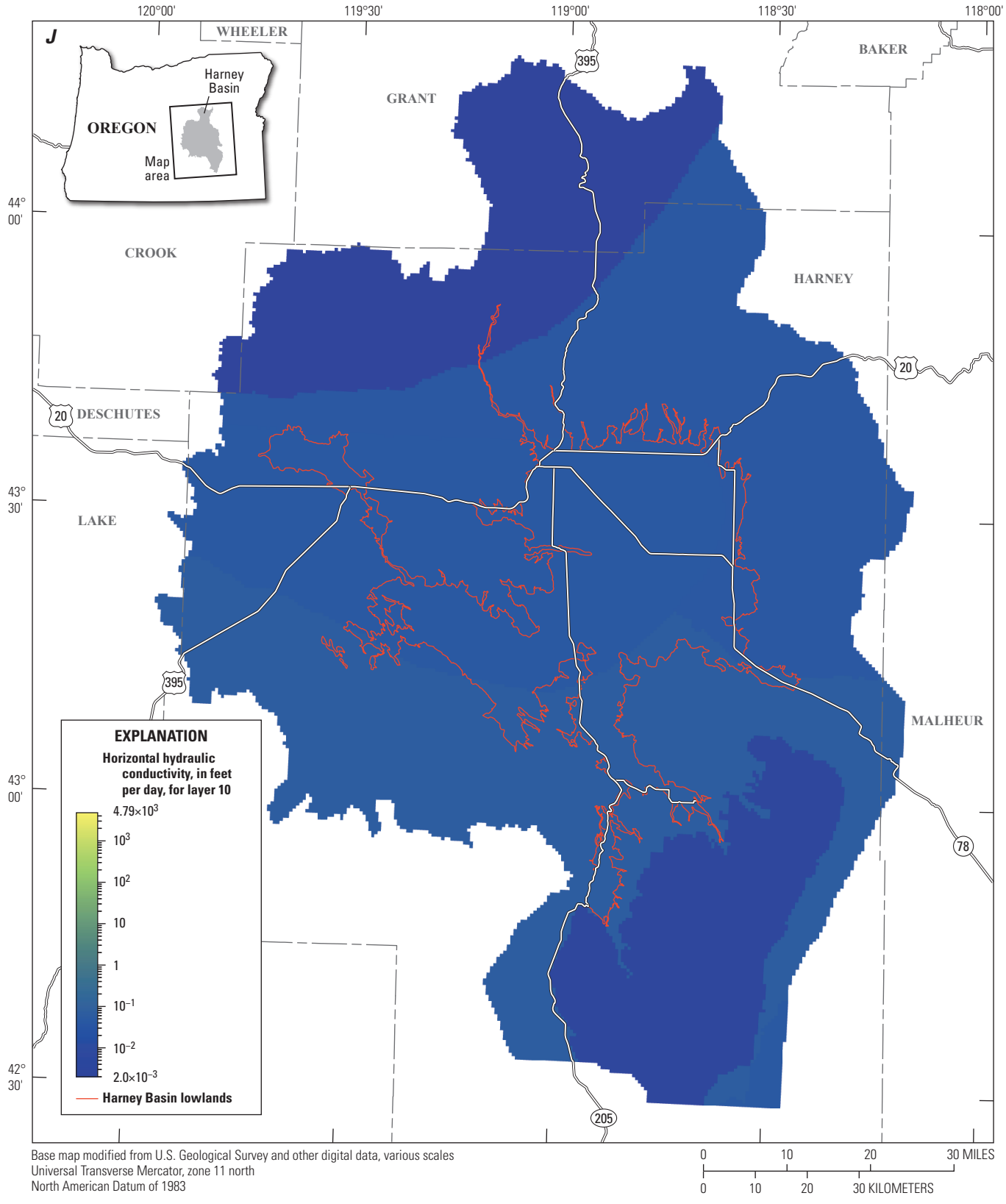

Figure 4.—Continued

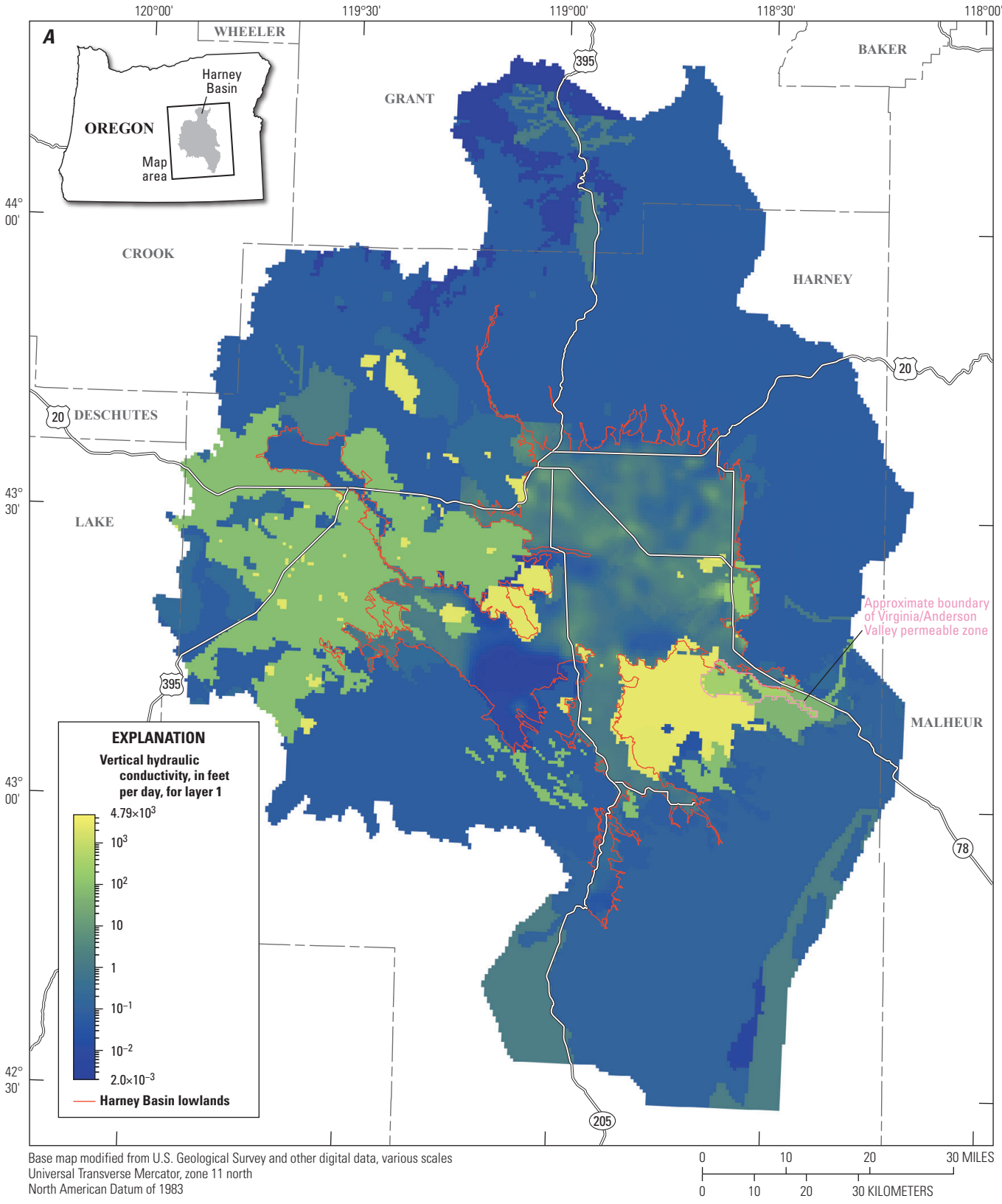

Figure 5. Distribution of vertical hydraulic conductivity simulated in layers (*A*) 1, (*B*) 5, and (*C*) 10 of the Harney Basin Groundwater Model (Gingerich, 2024), Harney Basin, southeastern Oregon.

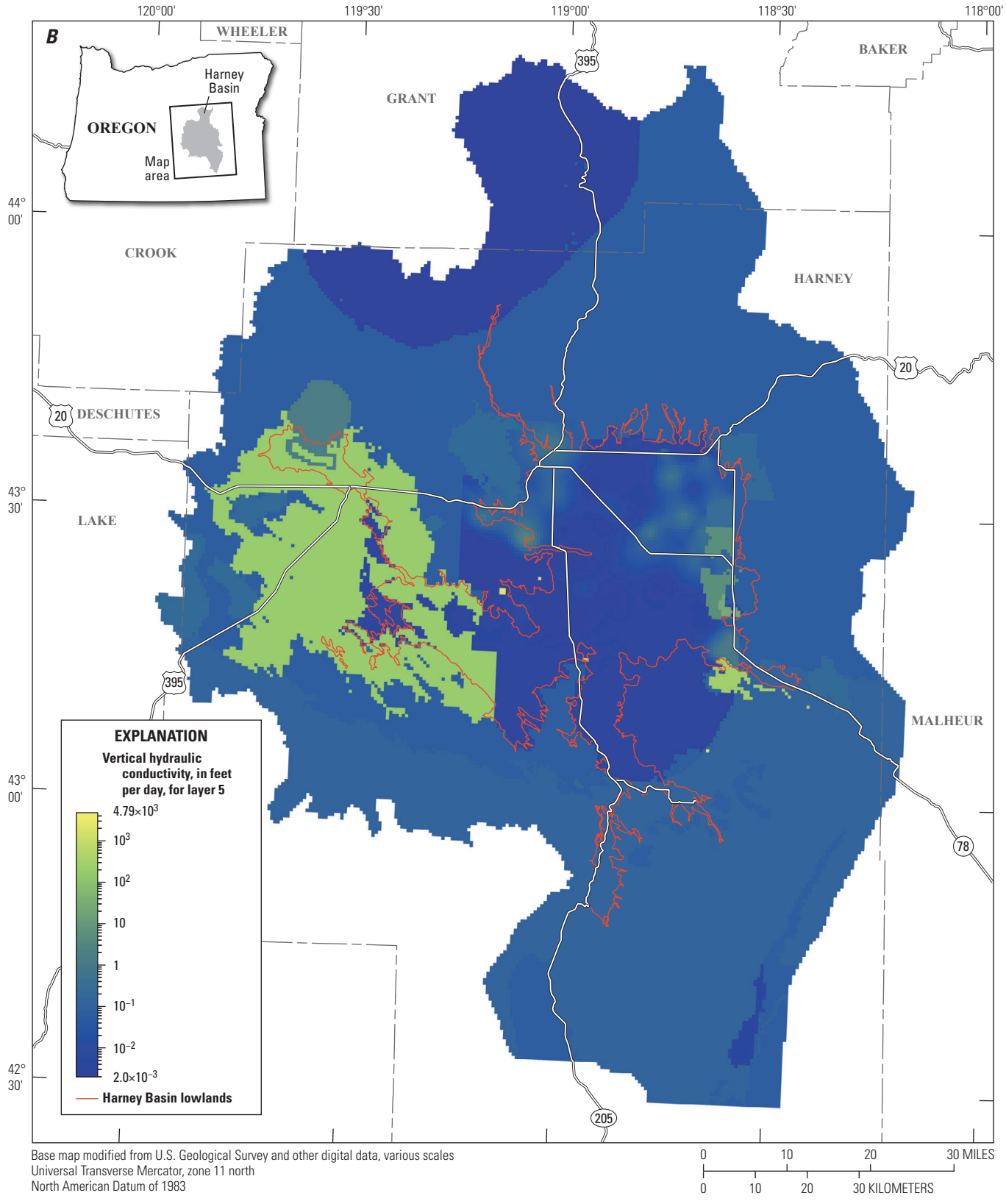

Figure 5.—Continued

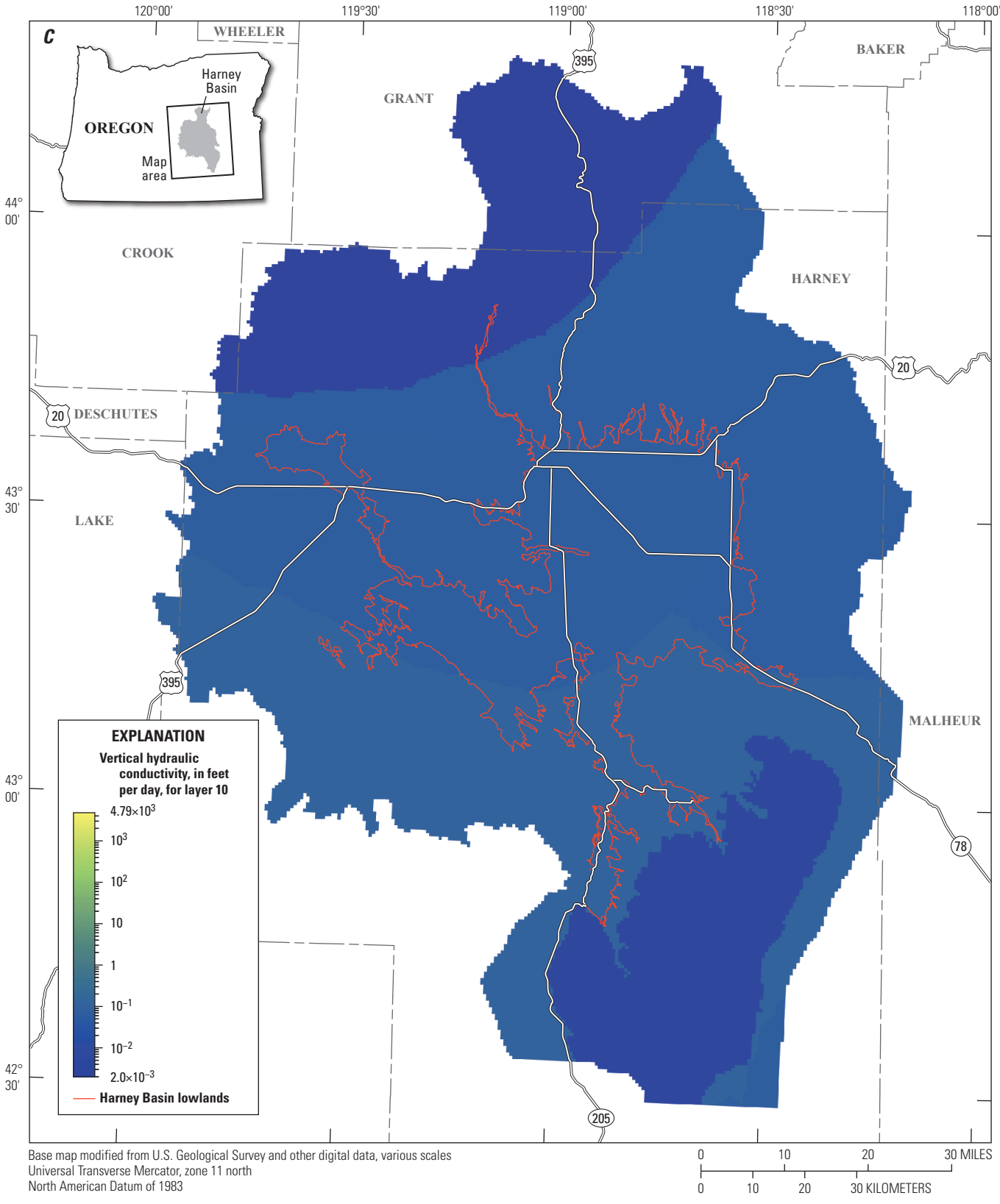

Figure 5.—Continued

In order to represent the complex pattern of hydraulic conductivity in the lowland deposits, a kriged surface was created for each of layers 1–5 using the estimates of transmissivity that Grondin and others (2021) made from well-yield tests and the location and open interval of the wells for which each transmissivity estimate was made. Each value of the kriged surface was normalized to the median transmissivity of all of the estimates to provide a distribution of scaling factors and multiplied by the median value to create a lowland hydraulic conductivity distribution for layers 1–5. Layers 6–9 were populated by subsequently using the maximum value of either half of the hydraulic conductivity in the overlying cell or 0.04 ft/d. The resulting lowland hydraulic conductivity distribution generally has higher values around the margins of the lowlands and in the shallower layers and generally lower values toward the center of the basin and in deeper layers (fig. 4). Irrigation well locations generally are associated with areas of higher hydraulic conductivity.

Virginia/Anderson Valley Permeable Zone

An area underlain by the Silicic flow and domes HU and Upland volcanic rocks HU nominally separating Virginia and Anderson Valleys is represented with values of hydraulic conductivity higher than expected (table 2) based on the reported values for these units (fig. 4). This modification allows easier flow of water between these areas and results in more accurate simulation of the lower groundwater levels measured in wells throughout this area. Using the relatively low values of hydraulic conductivity initially estimated for these two HUs (Grondin and others, 2021) resulted in simulated groundwater levels that were far too high when compared with measured groundwater levels in much of the surrounding area. Subsurface geologic information from mapping and boreholes in this area is sparse, and the only indication of the hydraulic properties of the rocks in the area is the estimate of higher hydraulic conductivity values needed to match groundwater levels in the model. Because this area is along or outside the eastern periphery of the basin boundary, the relative effect of modifying this area has little effect on other parts of the lowlands.

Western Permeable Zone

A high-permeability zone is located beneath the Silver Creek floodplain and a broad area surrounding it. Wells near the head of the floodplain penetrate a higher-permeability sequence about 200–300 ft below ground surface. Farther southeast, near Highway 20, this zone of higher-permeability rocks is penetrated as shallow as 50 ft below the surface (Gingerich and others, 2022). The high-permeability sequence is at least 300-ft thick in the deepest wells; however, no wells appear to penetrate entirely through the sequence, so the maximum thickness is unknown. This high-permeability zone is not correlated with any particular HU but seems to encompass parts of the Older basin fill, High Lava Plains basalt, and Dry Mountain lava HUs and may be the result of faulting in this part of the basin. To represent this zone in the model, an area of relatively higher horizontal hydraulic conductivity (250 ft/d) was created in layers 3–6, covering an area of about 950 square miles beneath the Silver Creek floodplain and surrounding areas to the west and south (fig. 4). The extent of this area was guided by the distribution of similar groundwater levels throughout this area (Gingerich and others, 2021), assumed to indicate the presence of the high-permeability zone.

Specific Yield and Specific Storage

Water is stored and released from an aquifer by two processes: (1) the filling and draining of pores due to gravity and (2) the expansion and compression of water and the aquifer framework (the rock or rock particles that support the open spaces in which water resides) (Freeze and Cherry, 1979). The term “specific yield” is associated with the filling and draining of pores in an unconfined aquifer. When water drains from an unconfined aquifer, the water is replaced by air as the pores become unsaturated. Specific yield is a much larger contribution to the total storativity of an aquifer than “specific storage,” which is the term used to represent the expansion and compression of water and the aquifer framework. Specific yield applies only to unconfined parts of groundwater-flow systems and represents the drainable porosity as the groundwater-table elevation changes within the water-bearing unit. For confined portions of groundwater-flow systems, water is released from storage when pumpage causes a decrease in pressure. The associated change in pressure is rapidly transmitted through the confined portions of the groundwater-flow system; water is released through a slight compression of the geologic framework and the expansion of water. When a confined layer releases water in this manner, the pores remain saturated.

The top layer of the model (layer 1) is simulated as unconfined, and the remaining layers (layers 2–10) are simulated under convertible conditions; therefore, specific yield and specific storage are specified in the MODFLOW 6 Storage (STO) Package (Langevin and others, 2022). In this way, the storage properties of confined layers can change if groundwater levels drop below their upper surface and they become unconfined. Initial estimates of specific yield and specific storage were based on other groundwater-flow models constructed for other volcanic groundwater basins in Oregon (Gannett and Lite, Jr., 2004; Gannett and others, 2012; Gannett and others, 2017) and adjusted during model calibration. Final estimates of specific yield range from 0.005 to 0.2, and final estimates of specific storage range from 1×10^{-7} to 7.5×10^{-5} ft^{-1} (table 2; fig. 6). Plots of storage properties in layers 3–4 and 6–9 are similar and are not included for brevity in this report.

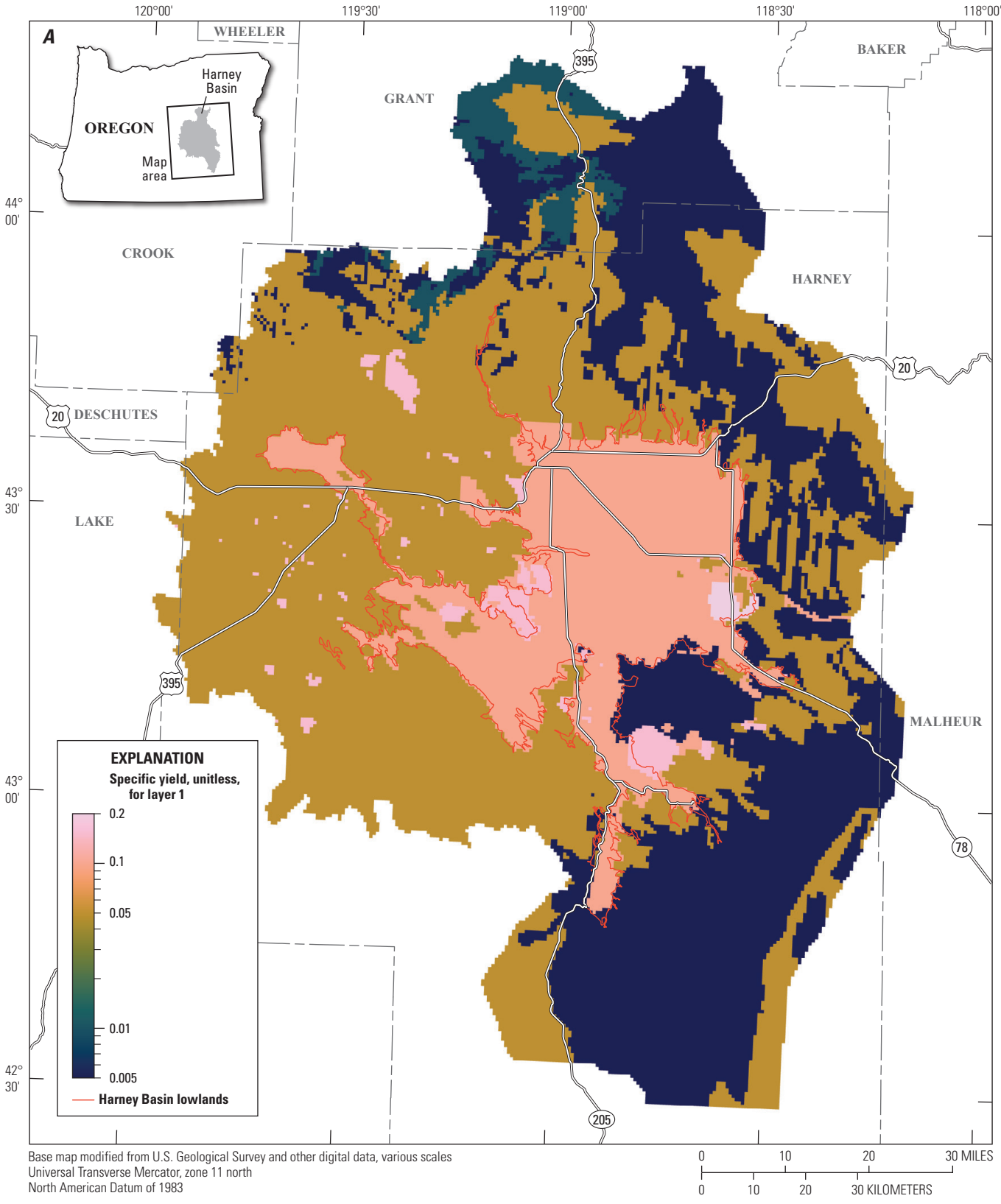

Figure 6. Distribution of storage properties simulated: (*A*) specific yield in layer 1, (*B*) specific storage in layer 2; (*C*) specific storage in layer 5, and (*D*) specific storage in layer 10 of the Harney Basin Groundwater Model (Gingerich, 2024), Harney Basin, southeastern Oregon.

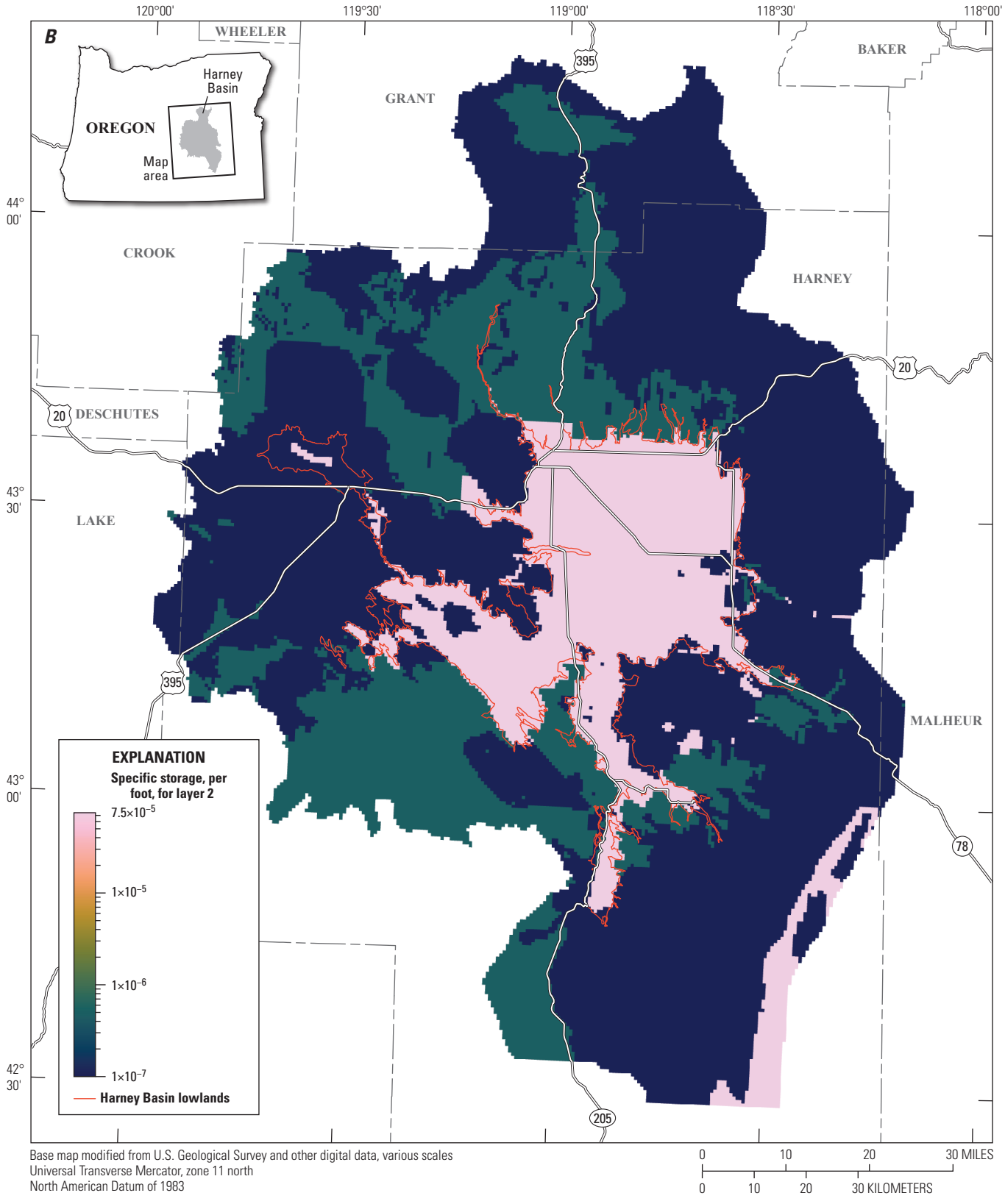

Figure 6.—Continued

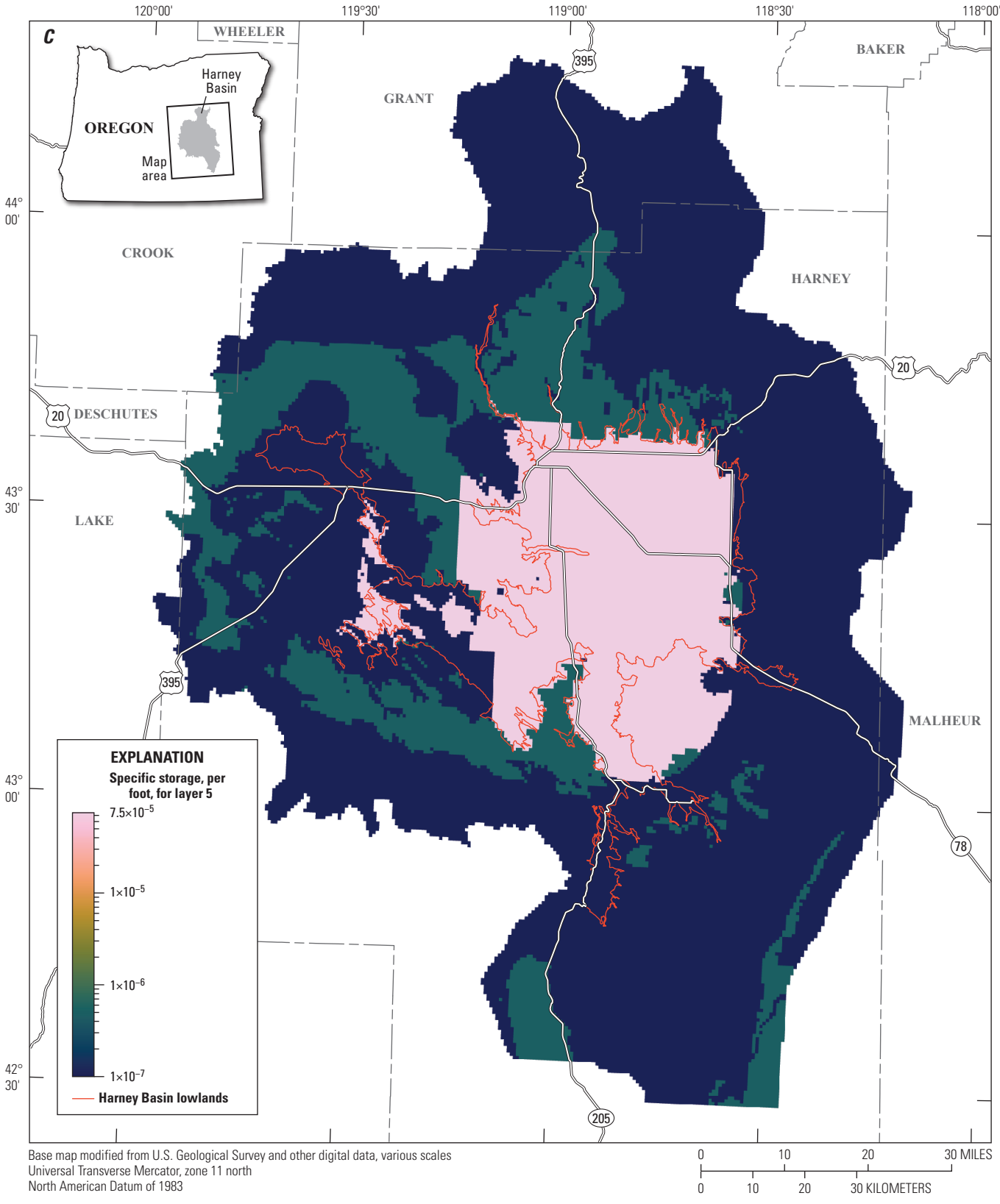

Figure 6.—Continued

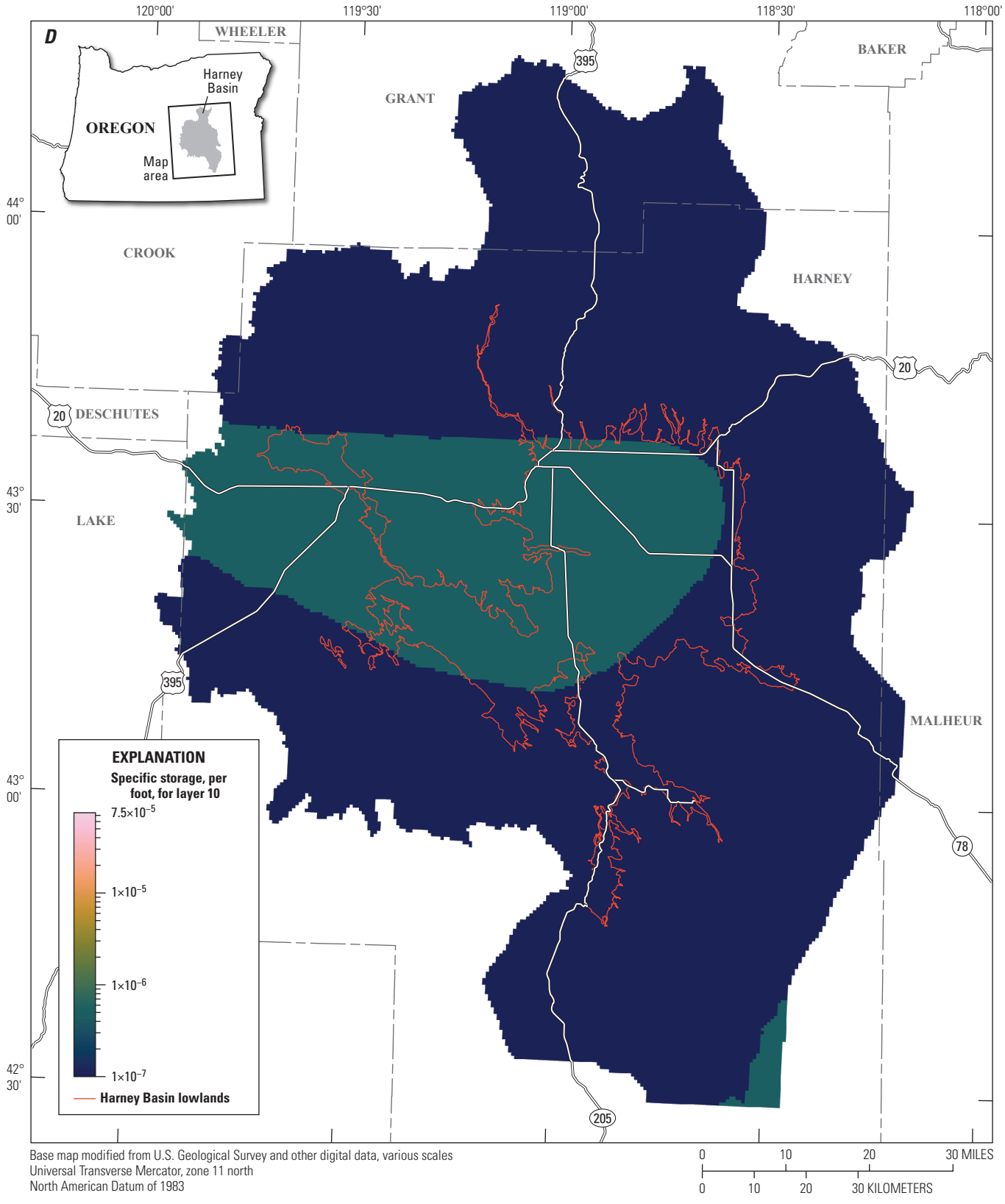

Figure 6.—Continued

Simulation of Recharge

Recharge to Harney Basin comes mainly from natural sources. As discussed in Garcia and others (2022) and Gingerich and others (2022), the primary source of natural recharge to the uplands is infiltration of precipitation and snowmelt. In the lowlands, the main source of recharge is infiltration of streamflow and seasonal floodwater along streams and rivers flowing from the uplands. Natural recharge from precipitation and surface-water infiltration was simulated using the Recharge (RCH) Package. This package allows a specified amount of groundwater to recharge the water table within the upper-most active layer (specified-flow boundary). The estimate of average annual natural recharge during 1982–2016 was the initial basis of recharge estimates.

A variety of methods were used to create the initial recharge estimates. The spatial distribution of upland recharge was determined from a Soil-Water-Balance (SWB) model of the Harney Basin (Corson-Dosch and Garcia, 2022; Garcia and others, 2022). The upland recharge was augmented with the estimate of recharge provided by surface-water infiltration where streams enter the lowlands and lose water to the subsurface (Garcia and others, 2022). The areas receiving surface-water infiltration were determined from mapped streams, streamflow and seepage measurements, and satellite imagery. The infiltrated volumes of surface water for each of the Northern, Southern, and Western areas delineated by Garcia and others (2022) were distributed to either stream channels or floodwater infiltration areas through an iterative process. Total mean annual upland recharge through precipitation and snowmelt in the study area during 1982–2016 is 288,000 acre-feet per year (acre-ft/yr) (Garcia and others, 2022), and this is augmented by 116,000 acre-ft/yr of surface-water infiltration in the lowlands (fig. 7).

Because the recharge estimate for 1982–2016 represents one mean annual value for the entire period, a method was developed to temporally scale the estimate for each year of the 1930–2018 transient model simulation. A relation between Silvies River annual mean streamflow at streamgaging station 10393500 (fig. 1) and annual recharge estimated from the SWB model (Corson-Dosch and Garcia, 2022) during 1982–2016 was developed as follows:

$$R = 0.0045S + 0.453 \quad (1)$$

where

R is annual mean SWB upland recharge, in inches, and

S is annual mean Silvies River discharge at streamgaging station 10393500, in cubic feet per second.

The annual mean Silvies River discharge at streamgaging station 1039350 during each year of 1930–2018 was used in equation 1 to generate the mean upland recharge estimate for each year. Discharge at streamgaging station 10393500 is available from the USGS during 1903–2012 (U.S. Geological Survey, 2024a, https://waterdata.usgs.gov/monitoring-location/10393500/) and OWRD from 2013 to 2018 (Oregon Water Resources Department, 2024, https://apps.wrd.state.or.us/apps/sw/hydro_report/gage_data_request.aspx?station_nbr=10393500). The recharge estimate for each year was then divided by the mean recharge during 1930–2018 to derive a scaling factor for each year (fig. 8). The scaling factor was used to adjust the spatially distributed upland recharge each year during the simulation.

Annual scaling factors were also derived for the streamflow infiltration estimate for the Northern and Western regions using annual mean Silvies River flow (streamgaging station 10393500) and the Southern region using annual mean Donner und Blitzen River flow (streamgaging station 10396000 discharge from 1911 to 2018 is available at U.S. Geological Survey, 2024b, https://waterdata.usgs.gov/monitoring-location/10396000/; fig. 1). The scaling factors for streamflow were multiplied by the spatial distribution of average streamflow and flooding and combined to get annual total recharge estimates for each year during 1930–2018.

The annual recharge to the study area during the entire transient simulation averaged 452,000 acre-feet (acre-ft), consisting of 294,000 acre-ft of precipitation and snowmelt recharge in the uplands and 158,000 acre-ft of streamflow infiltration in the lowlands. In the Harney Basin, much of the recharge from streamflow infiltration is generated from groundwater discharge to streams in the uplands (Garcia and others, 2022). For initial conditions (the steady-state [pre-1930] condition), the average recharge distribution was scaled by 0.782 based on the ratio of Silvies River flow during 1923–29 relative to the annual mean flow during 1930–2018.

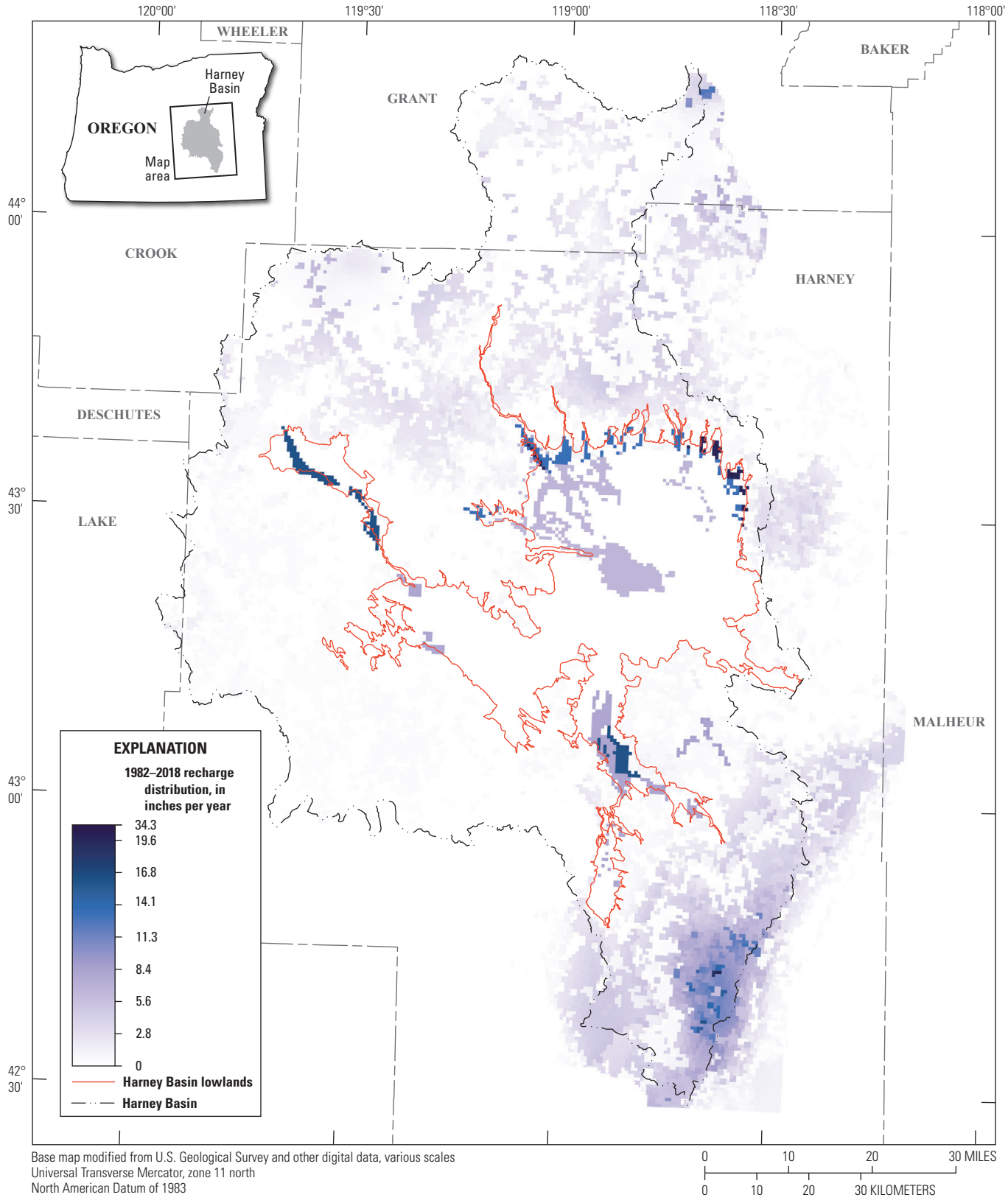

Figure 7. Distribution of average 1982–2016 recharge for the Harney Basin Groundwater Model (Gingerich, 2024), Harney Basin, southeastern Oregon.

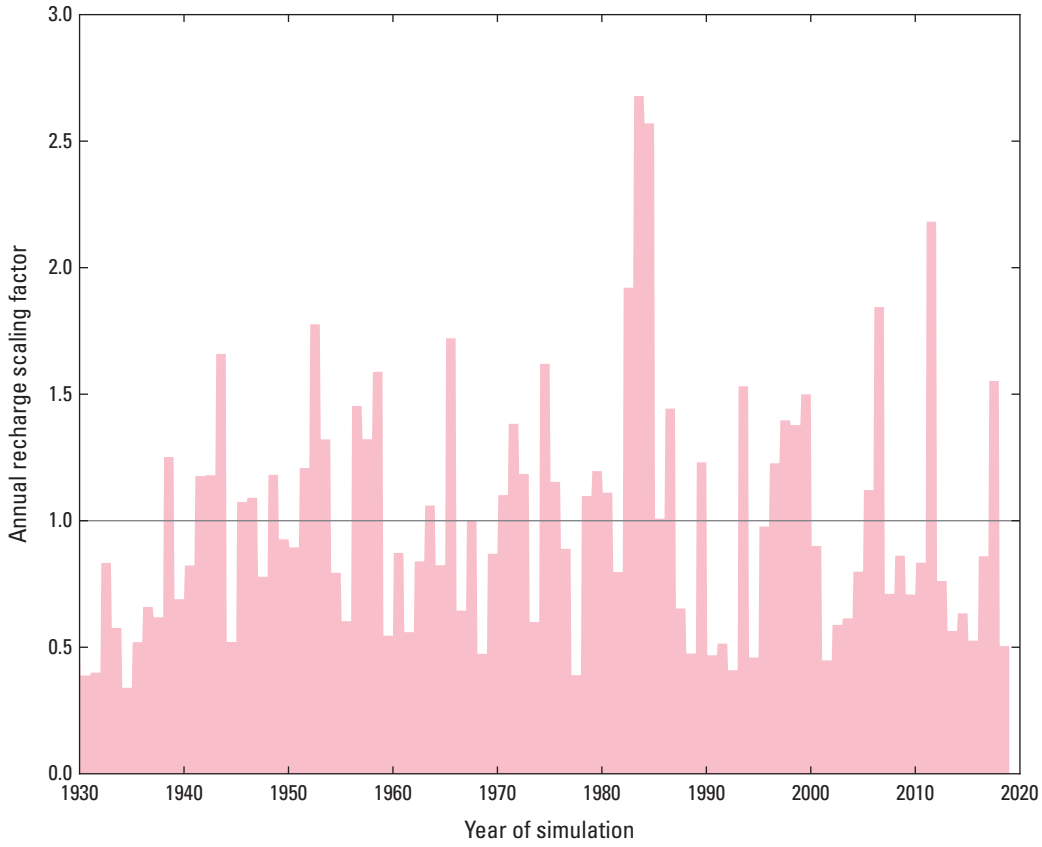

Figure 8. Recharge multiplier for each transient stress period (1930–2018) for the Harney Basin Groundwater Model (Gingerich, 2024), Harney Basin, southeastern Oregon.

Simulation of Discharge

Prior to the onset of artificial groundwater discharge through pumpage in the Harney Basin, groundwater discharge consisted of ET, discharge at streams and springs, and a small amount of flow through Virginia Valley into the Malheur River Basin (Garcia and others, 2022). As the groundwater resources of the basin were developed, groundwater pumpage became the dominant form of groundwater discharge. All of these mechanisms of groundwater discharge are simulated in the HBGM.

Natural Discharge

Total upland and lowland natural discharge during 1982–2016 occurred as groundwater flow to stream base flow (the groundwater component of streamflow) and spring discharge (247,900 acre-ft/yr), ET (119,000 acre-ft/yr) and a minor amount as underflow to the Malheur River Basin (3,100 acre-ft/yr) (Garcia and others, 2022). Natural discharge through springs and stream base flow in the HBGM is simulated using the MODFLOW 6 Drain (DRN) Package. Evapotranspiration is simulated using the Evapotranspiration (EVT) Package. The model boundaries include the Malheur River, so an estimate of underflow leaving through Virginia Valley toward the Malheur River Basin can be determined from the HBGM water-budget file using the USGS computer program Zonebudget for MODFLOW 6 (Langevin and others, 2022).

Streams

Streams are represented in the HBGM using the DRN package. The DRN package is used rather than a stream package in order to enable the specification of groundwater discharge from streams and to improve numerical stability and model run times. The head-dependent discharge to drains and streams are formulated the same in both packages. By using the DRN package, accounting of flow along stream reaches, normally done automatically by a stream or river package, is by necessity performed outside the model. In subsequent sections of this report, this distinction was set aside, only stream and spring discharge is referred to, regardless of the approach of using the DRN package for the simulations.

Streams are simulated by 9,437 drain cells positioned along the stream network in the HBGM (fig. 9). The elevation of each drain cell was initially determined from a 10-meter digital elevation model and later manually adjusted as

needed for improved accuracy based on visual inspection of topographic maps that depicted stream, spring, and wetland locations. The hydraulic conductance of the interface between the aquifer and the drain (streambed conductance) is set at an arbitrary high value (10,000 ft^2/d) to allow groundwater to freely discharge to each stream or spring represented by a drain cell. Groundwater discharge to a particular stream or segment of stream having a streamgaging station is determined during model post processing by summing all of the discharge for the drain cells representing that stream upstream of the streamgaging station location.

Evapotranspiration

Evapotranspiration from groundwater is simulated using the MODFLOW 6 ET (EVT) Package. Characteristics of ET from groundwater, estimated for Harney Basin by Garcia and others (2022), are distributed spatially across the model and represented using a head-dependent flow boundary (fig. 10). The elevation of the ET surface (land surface) was set equal to the elevation of the top of layer 1. Simulated maximum ET flow rates ranges from $2.0x10^{-6}$ to $6.63x10^{-3}$ ft/d (fig. 10). Simulated ET extinction depth (basically, the maximum rooting depth of phreatophytes) ranges from 0 to 30 ft depending on the plant community (fig. 11). The simulated ET rates only occur where groundwater is sufficiently shallow to represent wetlands and shallow groundwater discharge areas.

Groundwater Pumpage

Groundwater is pumped for irrigated agriculture, livestock watering, municipal and community supply, rural domestic supply, and commercial-industrial uses. By 2017–18, groundwater pumpage accounted for about 50 percent of groundwater discharge from the Harney Basin lowlands (Garcia and others, 2022). Estimated pumpage volumes, as well as the spatial distribution of wells in the HBGM, are specified using the Well (WEL) Package. Wells are represented in the model as specified flow boundaries. Estimates of 1930–2018 conditions are from pumpage values and well locations, open intervals, and installation dates provided in Schibel and Grondin (2023). Monthly pumpage was estimated at a decadal scale for the six decades during 1930–90 and yearly for selected years during 1991–2018 (table 3; figs. 12–13). For 1930–90, the monthly estimates for each decade provided were repeated for each year of the decade. For 1991–2018, pumpage estimates of 13 selected years were provided and values for the missing years were assigned on the basis of adjacent-year estimates (table 3). The 13 years of selected pumpage data were the years estimated by Beamer and Hoskinson (2021) on the basis of available satellite ET data. Irrigation pumpage has a seasonal schedule during May–September of each year with zero irrigation pumpage during the other months. Municipal and community supply, rural domestic supply, and commercial-industrial pumpage vary for each month throughout the year, and livestock pumpage is constant for each month of the year (Schibel and Grondin, 2023). The consistent monthly pumpage shown during 1970–90 was mainly industrial use by the Hines lumber Company (Grondin, 2021). The highest monthly irrigation pumpage estimates typically occur during July of each year. The maximum monthly estimate of total pumpage for the entire area in the transient simulation is in July 2017; pumpage totals about 46,000 acre-ft (fig. 12). The average annual pumpage for 2017 is the highest yearly rate in the simulation at 149,000 acre-ft. Layers 9 and 10 had no pumpage because no production wells pump from this deeply in the basin.

For wells that have open intervals that extend over two or more layers of the HBGM, pumpage is distributed over all of the layers penetrated. Pumpage for each layer is weighted by the layer thickness relative to the total thickness of all the penetrated layers. For wells open to just two or more layers of layers 1–5, this amounts to an even distribution of pumpage to each layer, because layers 1–5 were each 100-ft thick. Wells that had open intervals extending less than 10 ft into a model layer generally were represented by shorter open intervals to exclude these layers unless a drillers' log indicated a large yield from this part of the well. Wells penetrating deeper than layer 5 have a higher proportion of pumpage coming from layers 6, 7, or 8 because these layers have variable thicknesses greater than 100 ft depending on their location in the model. Each well is individually represented in the HBGM input files and the MODFLOW 6 program aggregates the withdrawal rates for all wells in the same layer, row, and column of the model.

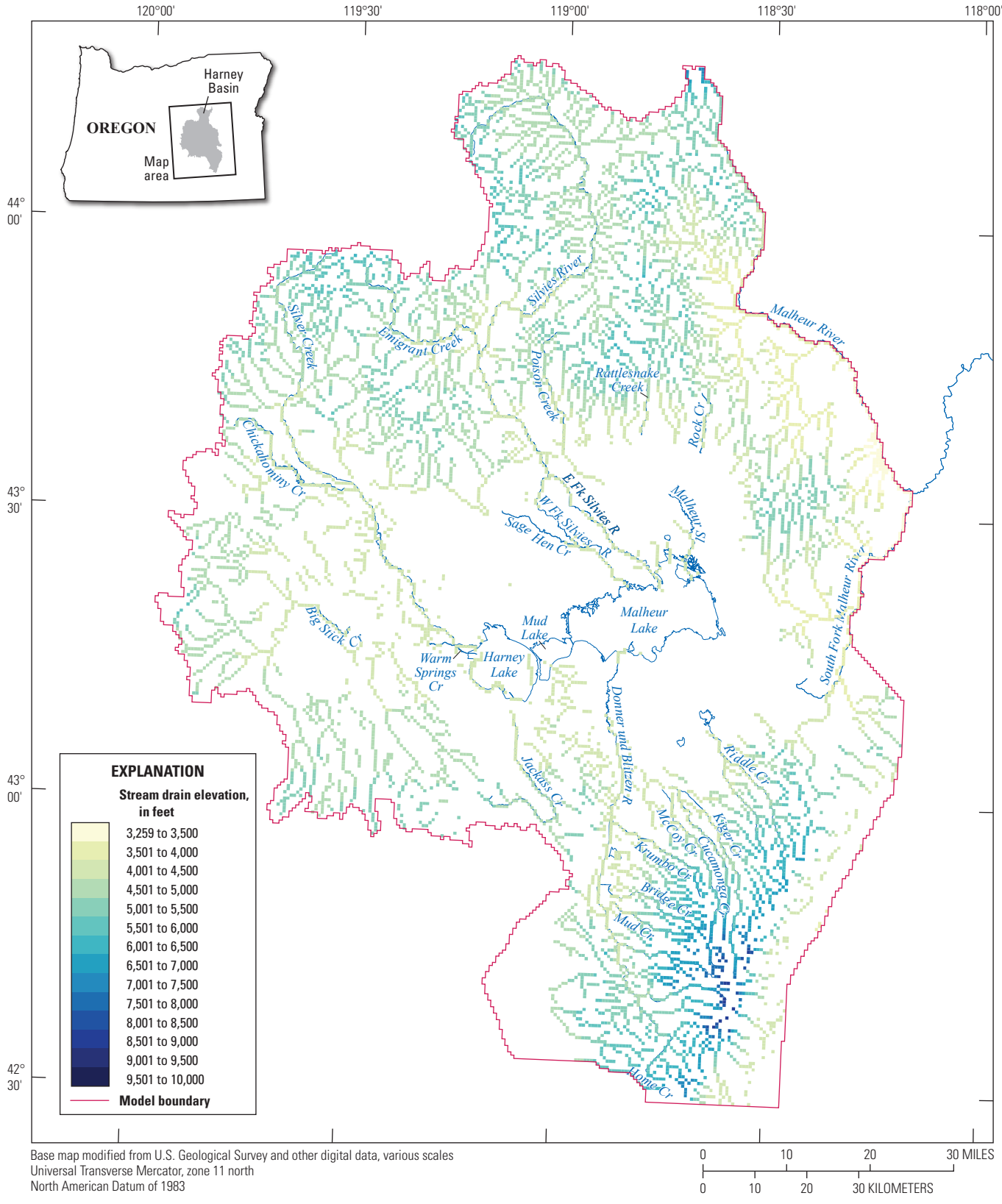

Figure 9. Locations and elevations of drain cells used to represent the stream network in the Harney Basin Groundwater Model (Gingerich, 2024), Harney Basin, southeastern Oregon.

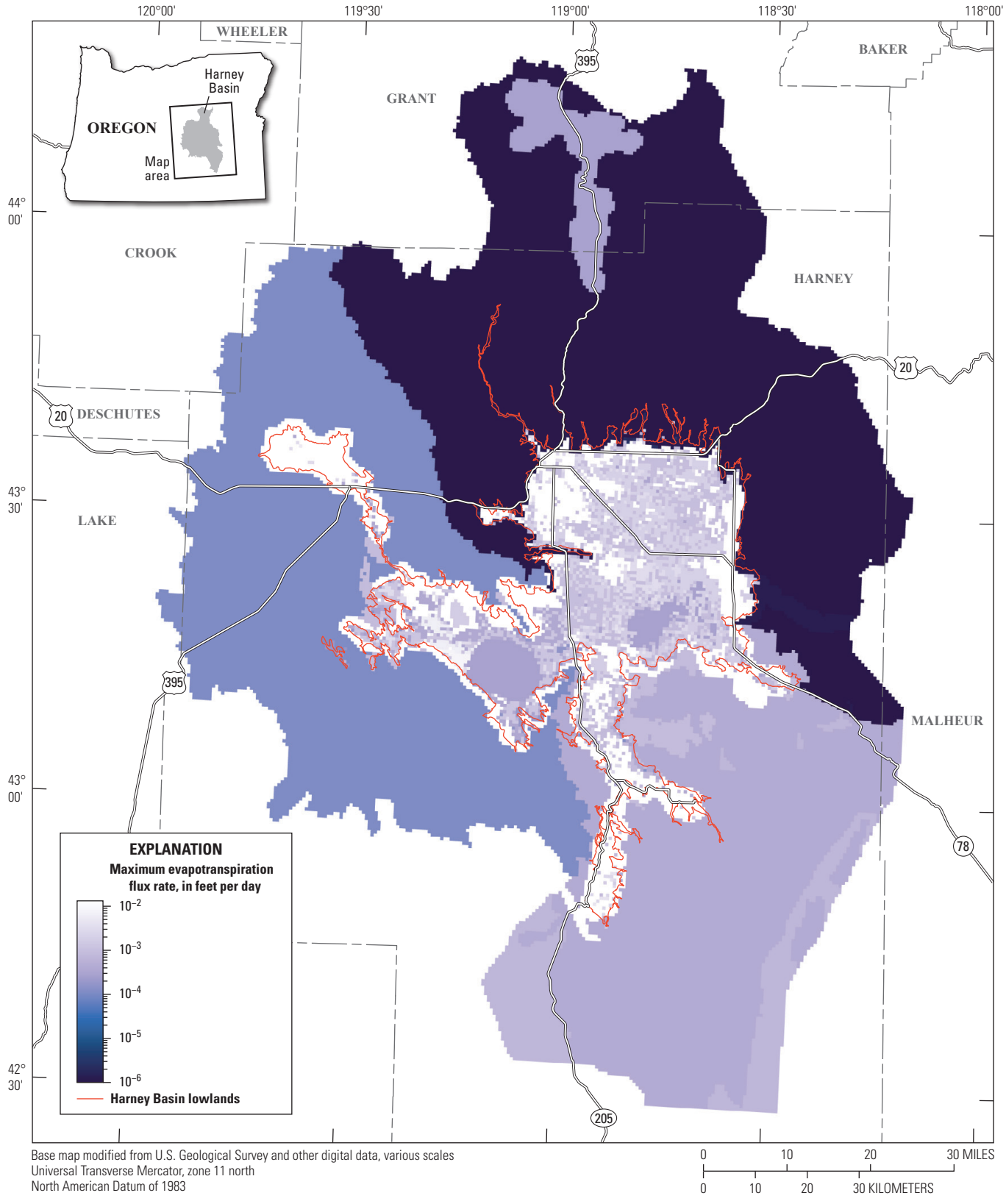

Figure 10. Distribution of simulated maximum evapotranspiration flow rate for the Harney Basin Groundwater Model (Gingerich, 2024), Harney Basin, southeastern Oregon.

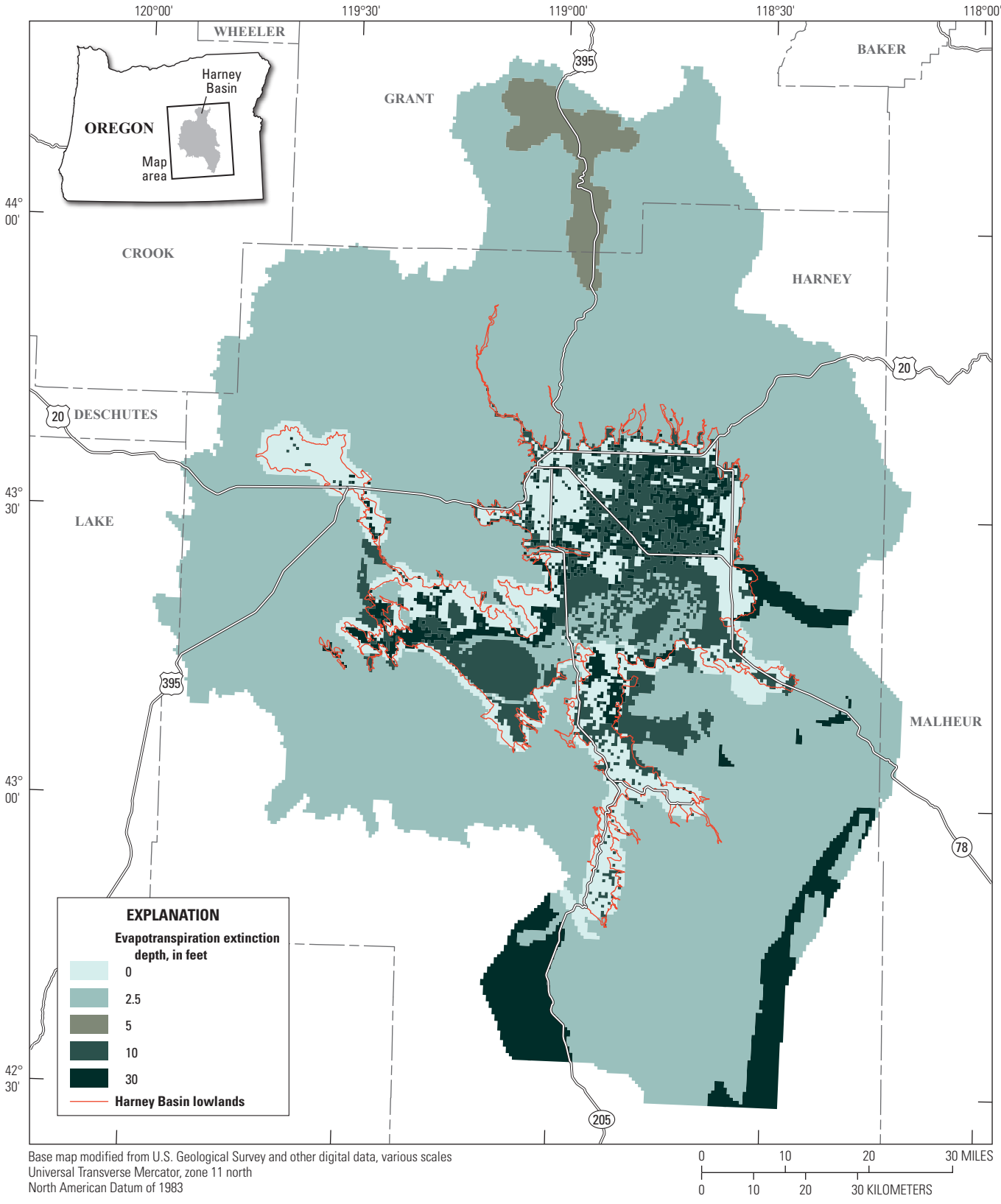

Figure 11. Distribution of simulated evapotranspiration extinction depth for the Harney Basin Groundwater Model (Gingerich, 2024), Harney Basin, southeastern Oregon.

Table 3. Summary of pumpage inputs to the groundwater model of Harney Basin, southeastern Oregon (Gingerich, 2024).

[All pumpage data from Schibel and Grondin (2023)]

Year with estimated monthly pumpage	Model input
1930s	Mean monthly values for the decade used each year
1940s	Mean monthly values for the decade used each year
1950s	Mean monthly values for the decade used each year
1960s	Mean monthly values for the decade used each year
1970s	Mean monthly values for the decade used each year
1980s	Mean monthly values for the decade used each year
1990	Monthly values for 1990
1991	Monthly values for 1991
1992	Monthly values for 1992
1994	Monthly values for 1993, 1994, 1995, 1996
2000	Monthly values for 1997, 1998, 1999, 2000
2001	Monthly values for 2001, 2002
2005	Monthly values for 2003, 2004, 2005, 2006
2009	Monthly values for 2007, 2008, 2009
2011	Monthly values for 2010, 2011, 2012
2014	Monthly values for 2013, 2014
2015	Monthly values for 2015 only
2016	Monthly values for 2016 only
2017	Monthly values for 2017 only
2018	Monthly values for 2018 only

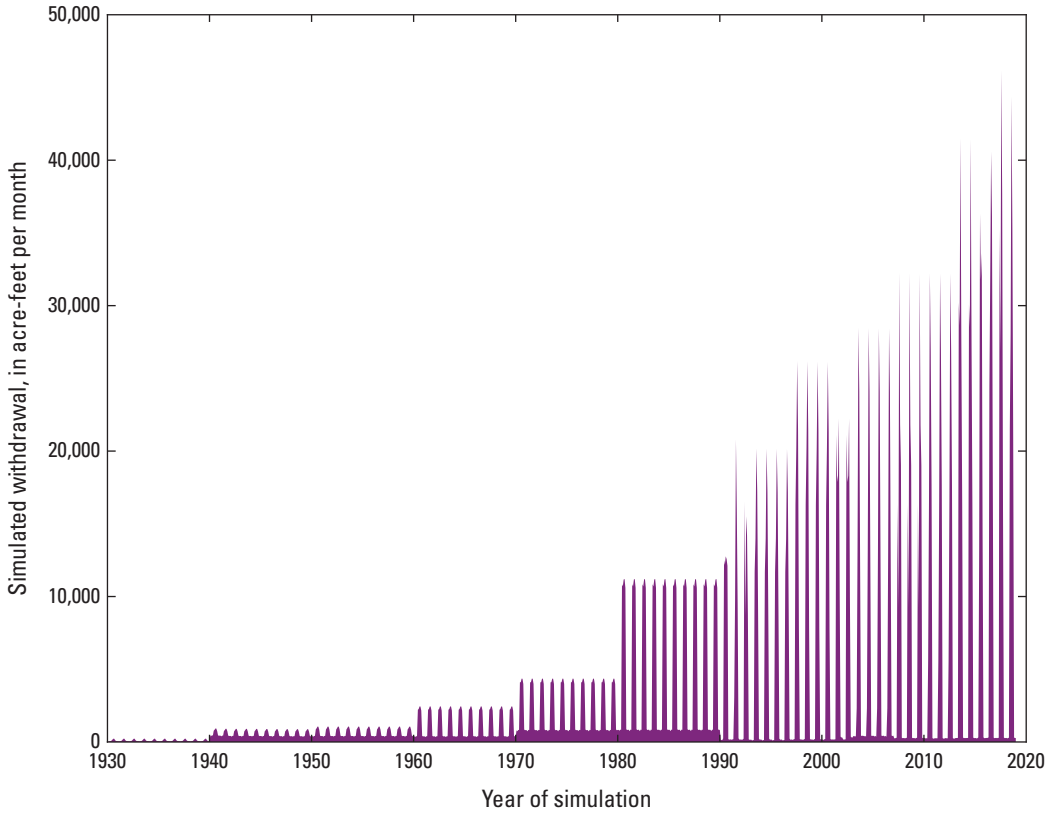

Figure 12. Simulated total well withdrawal volume for each transient stress period during 1930–2018 for the Harney Basin Groundwater Model (Gingerich, 2024), Harney Basin, southeastern Oregon.

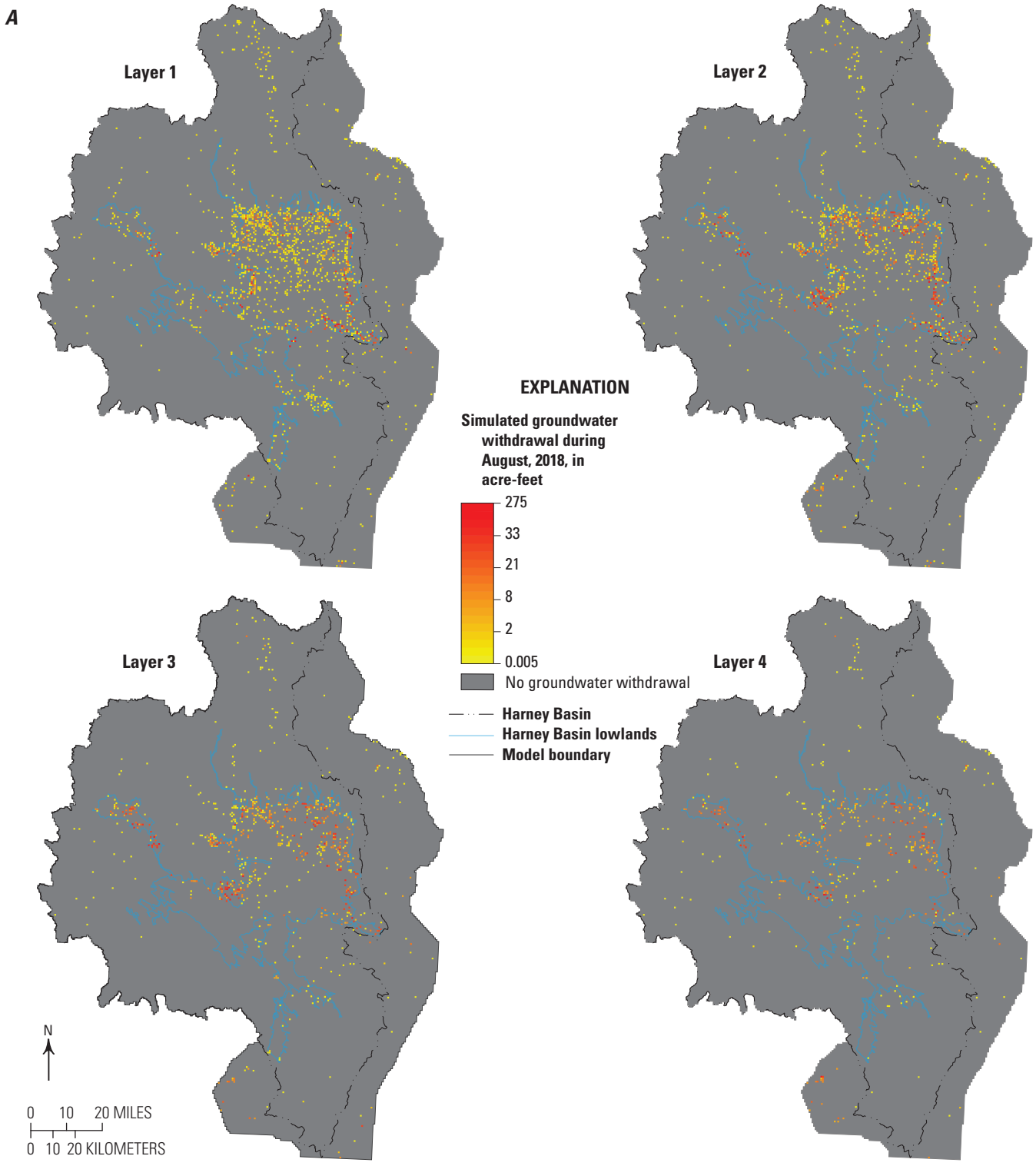

Figure 13. Distribution of simulated withdrawal wells for irrigation, municipal, domestic, and ranching uses during August 2018 in individual model cells for layers 1–8 of the Harney Basin Groundwater Model (Gingerich, 2024), Harney Basin, southeastern Oregon.

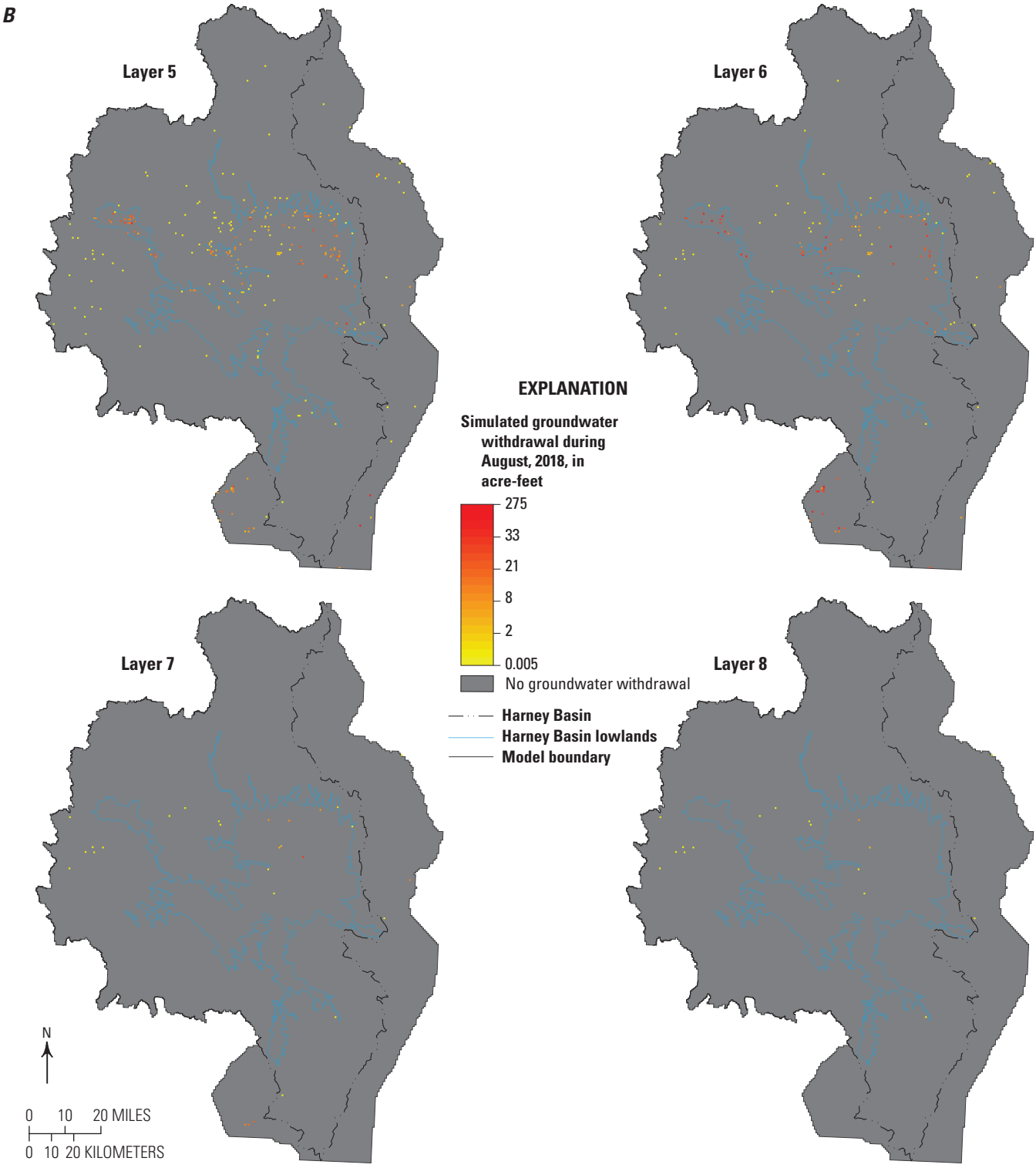

Figure 13.—Continued

Model Calibration and Results

Model calibration is the process by which model parameters and the hydrogeologic framework are adjusted to achieve the best match between measured and simulated variables such as hydraulic head (groundwater levels) and groundwater discharge to streams and springs (this is sometimes referred to as "model fit"). The model calibration process provides insight into model conceptualization, limitations of the current model, and a foundation for future model refinements. The HBGM was calibrated using an iterative method, during which certain model parameters were adjusted within reasonable ranges after many successive model runs to improve the model fit. Hydraulic properties, ET parameters, and lowland recharge locations were modified as part of this process.

Comparison Between the Simulated Results and Measured Data

The ability of the transient groundwater-flow model to accurately represent the measured data was evaluated throughout the calibration process. Measured data include the groundwater-levels from 186 wells across the basin (figs. 14–21) and base-flow estimates at 21 streams with streamflow estimates (fig. 22). The comparison of measured and simulated data provides an indication of model performance spatially and temporally.

Simulated groundwater levels are compared directly with measured groundwater-level elevations for observation wells open to a single model layer. For observation wells open to multiple consecutive model layers, the composite groundwater level is compared along with the range of simulated groundwater levels for all of the penetrated layers. No wells in the model are open to multiple nonconsecutive model layers. The composite groundwater level (or head) is calculated using the following weighting scheme:

$$Head_{composite} = \frac{\sum_1^n Head_n Thick_n}{\sum_1^n Thick_n} \quad (2)$$

where

n is the model layer penetrated by a well,

$Head_n$ is the model-calculated hydraulic head for layer n,

$Thick_n$ is the thickness of layer n, and

$Head_{composite}$ is the composite hydraulic head for well penetrating n model layers.

Because the top five layers of the model are all 100 ft thick, the $Head_{composite}$ for any wells penetrating less than 500 ft effectively simplify to just the mean of the simulated hydraulic heads for the penetrated layers. Measures of model fit to groundwater levels included the following:

- Measured groundwater-level elevations compared to simulated hydraulic heads on a 1:1 graph, and
- Hydrographs showing measured and simulated groundwater-level elevations for the transient-state simulation period (1930–2018).

Model-simulated groundwater discharge to streams was used to calibrate and constrain the model representation of the upland groundwater-flow system. Estimates of base flow during 1982–2016 at selected stream locations having streamgaging stations or base-flow measurements (Garcia and others, 2022) were compared to model-simulated groundwater discharge to streams. Simulated groundwater discharge values needed for comparison were determined by summing the discharge for all stream reaches upstream of the streamgaging station or measurement location and calculating the annual average during 1982–2016 from the transient simulation. Measures of model fit to upland base flow were based on estimated base flow compared to simulated stream discharge on a 1:1 graph.

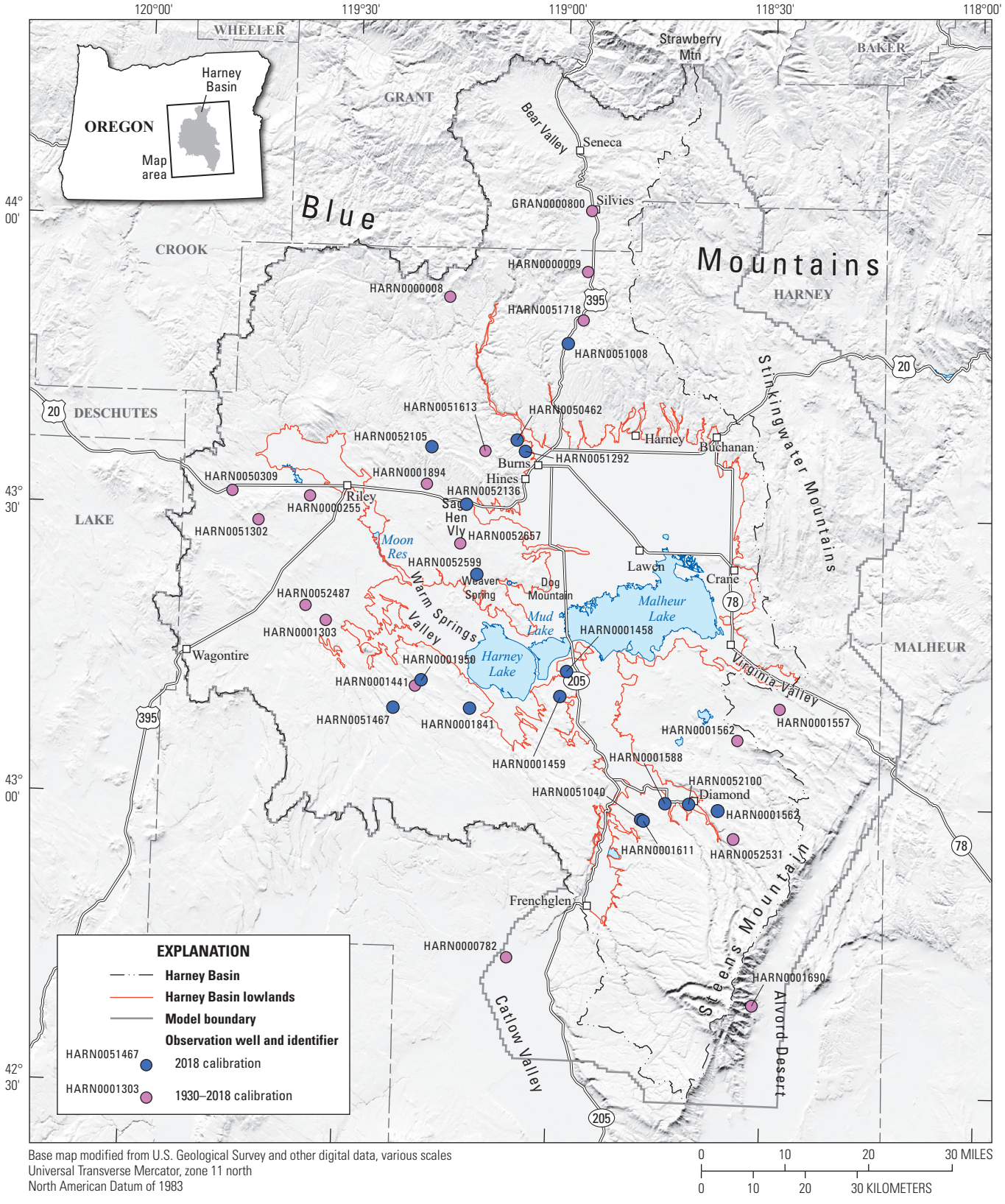

Figure 14. Locations of selected wells in the Uplands used for comparison of measured and simulated groundwater-level elevations from the Harney Basin Groundwater Model (Gingerich, 2024), Harney Basin, southeastern Oregon.

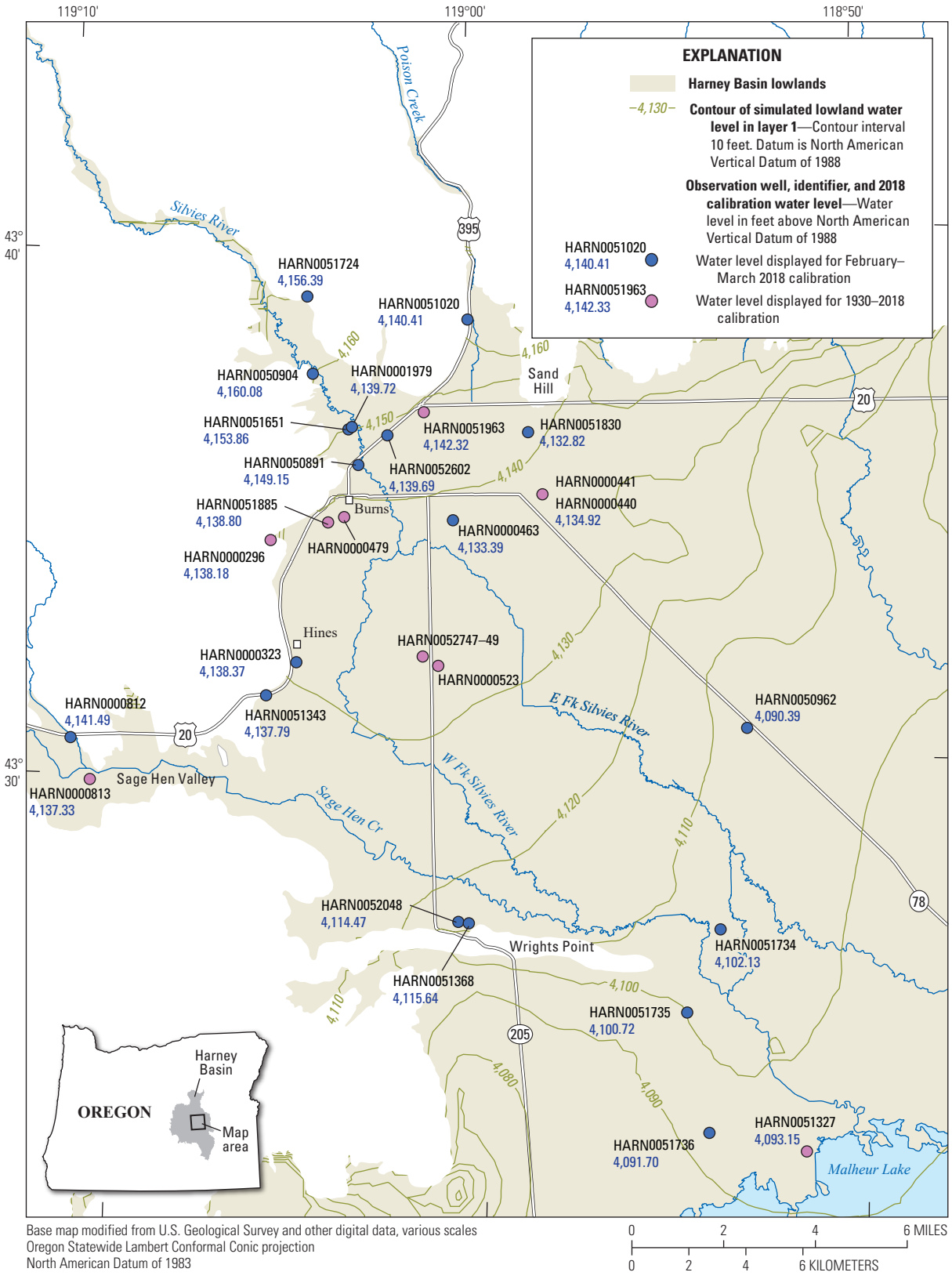

Figure 15. Locations of selected wells in the Silvies River floodplain area used for comparison of measured and simulated groundwater-level elevations from the Harney Basin Groundwater Model (Gingerich, 2024), Harney Basin, southeastern Oregon.

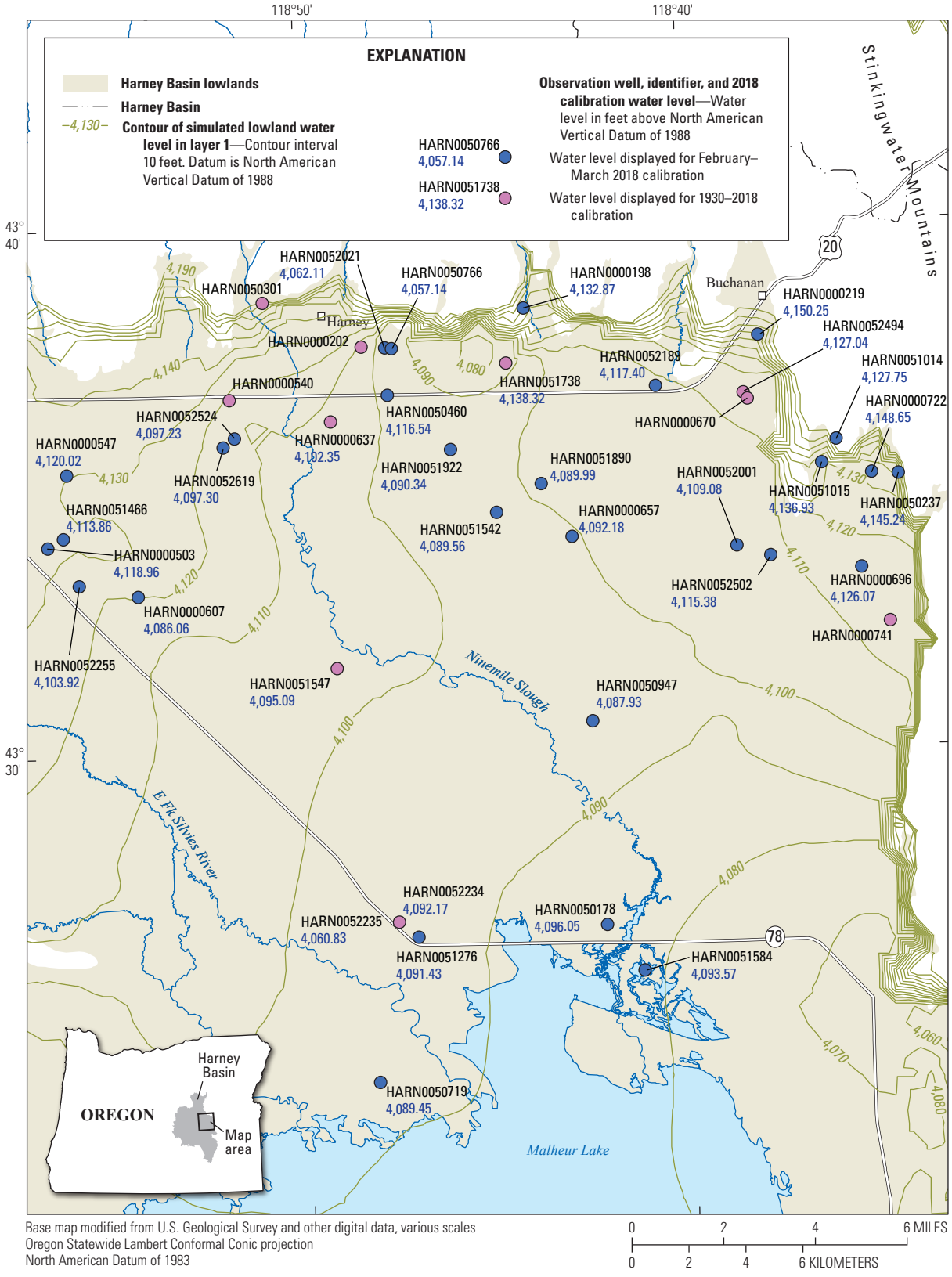

Figure 16. Locations of selected wells in the Northern lowlands area used for comparison of measured and simulated groundwater-level elevations from the Harney Basin Groundwater Model (Gingerich, 2024), Harney Basin, southeastern Oregon.

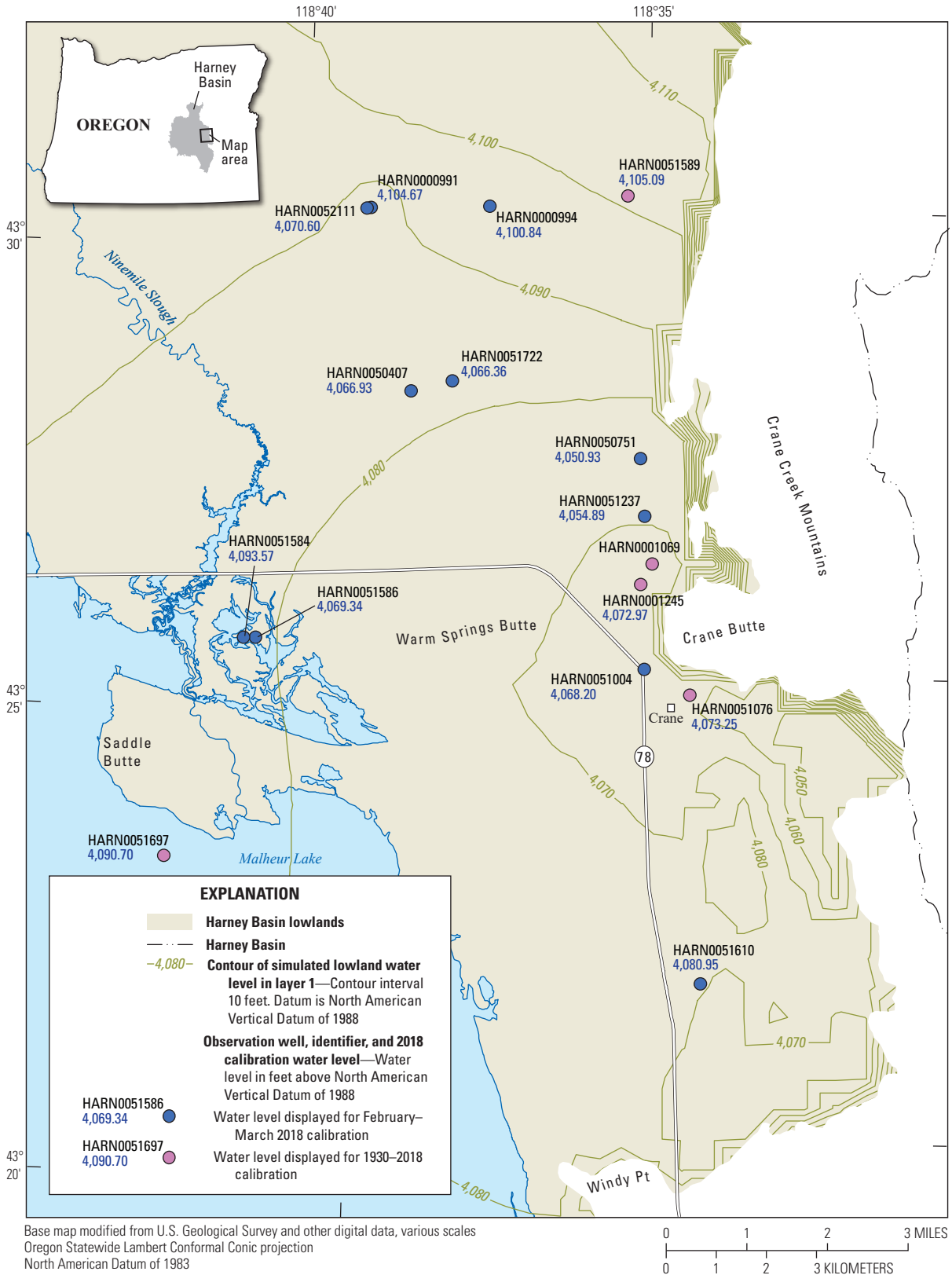

Figure 17. Locations of selected wells in the Crane area used for comparison of measured and simulated groundwater-level elevations from the Harney Basin Groundwater Model (Gingerich, 2024), Harney Basin, southeastern Oregon.

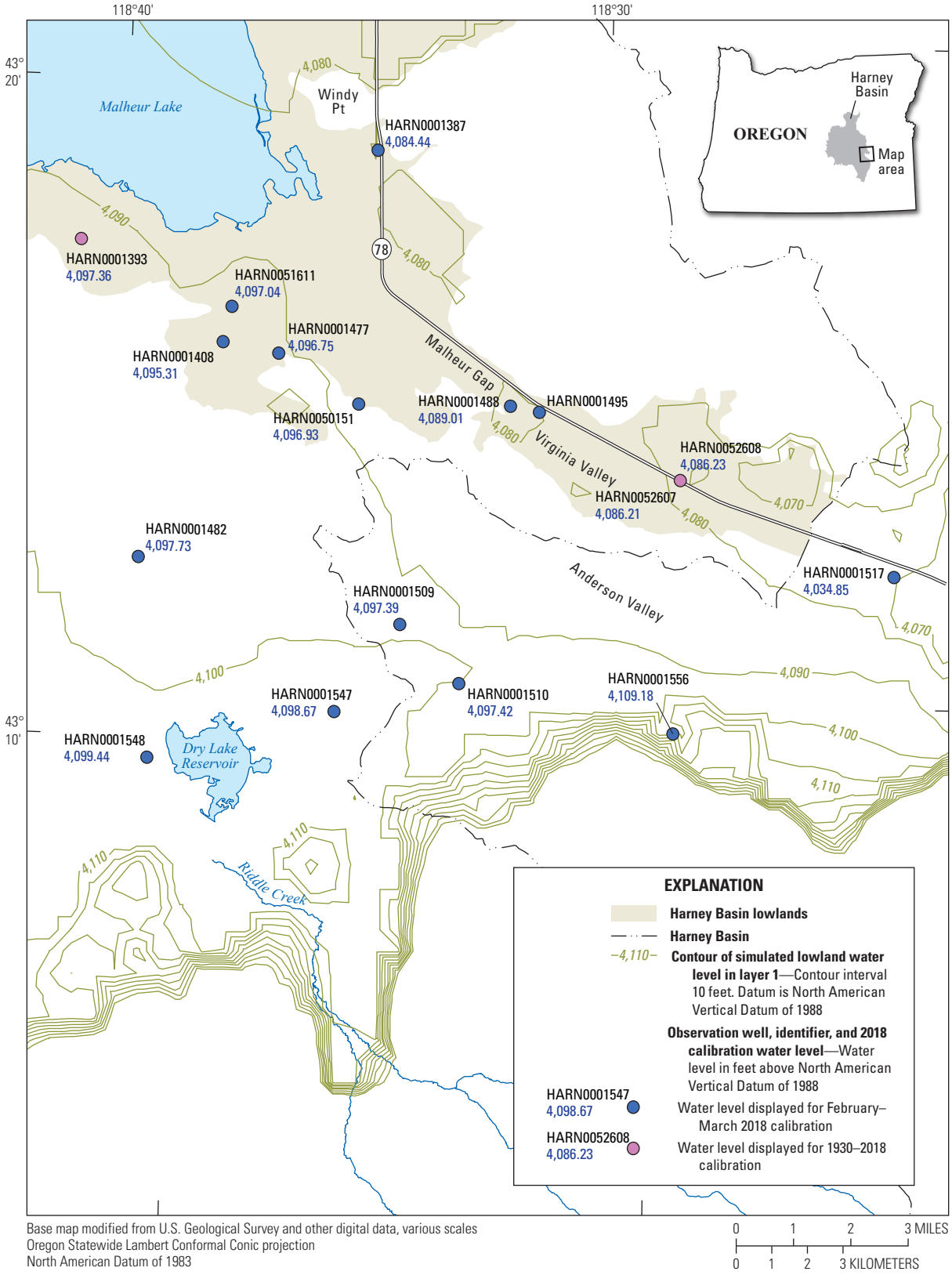

Figure 18. Locations of selected wells in the Virginia Valley area used for comparison of measured and simulated groundwater-level elevations from the Harney Basin Groundwater Model (Gingerich, 2024), Harney Basin, southeastern Oregon.

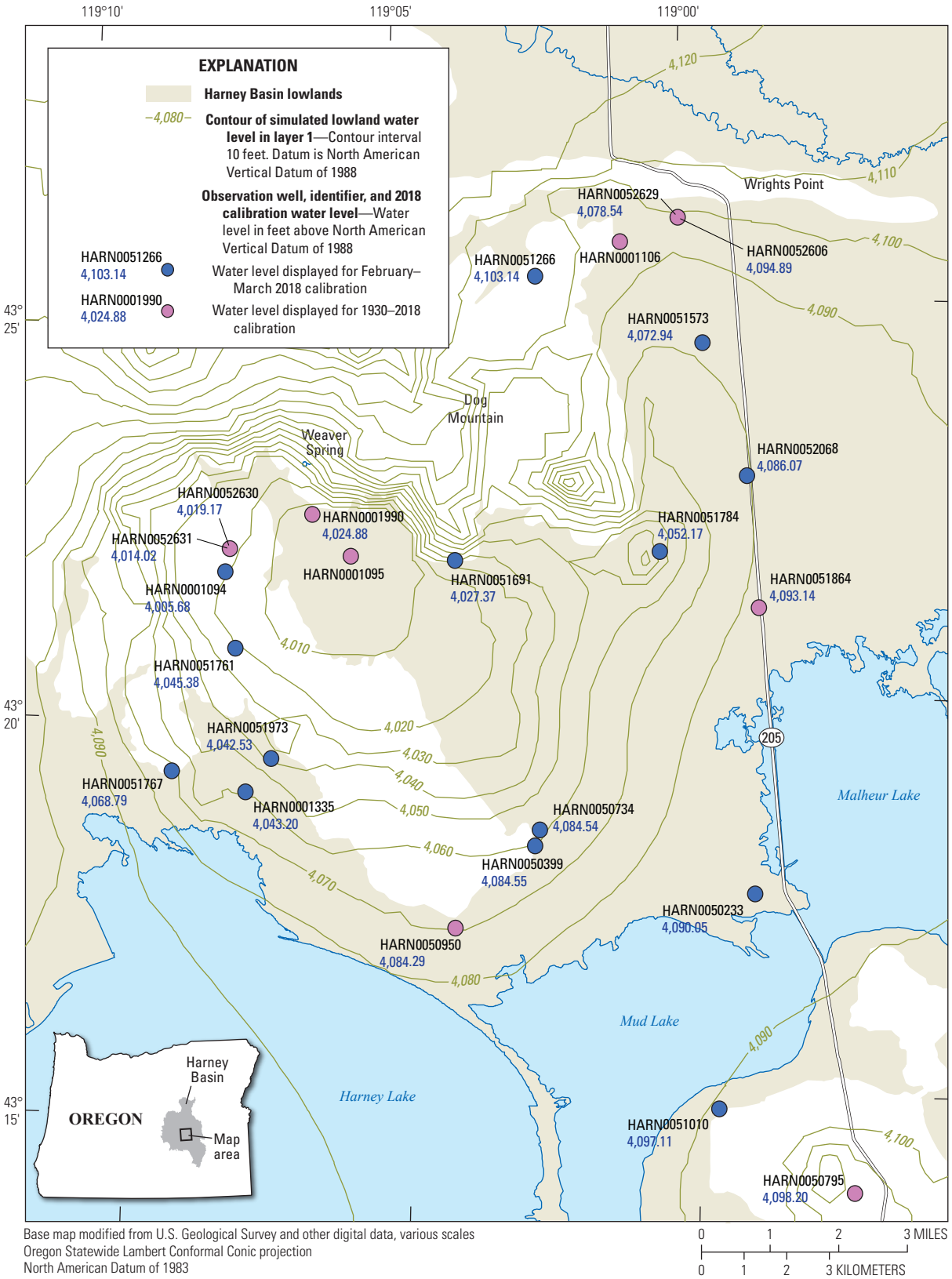

Figure 19. Locations of selected wells in the Weaver Spring area used for comparison of measured and simulated groundwater-level elevations from the Harney Basin Groundwater Model (Gingerich, 2024), Harney Basin, southeastern Oregon.

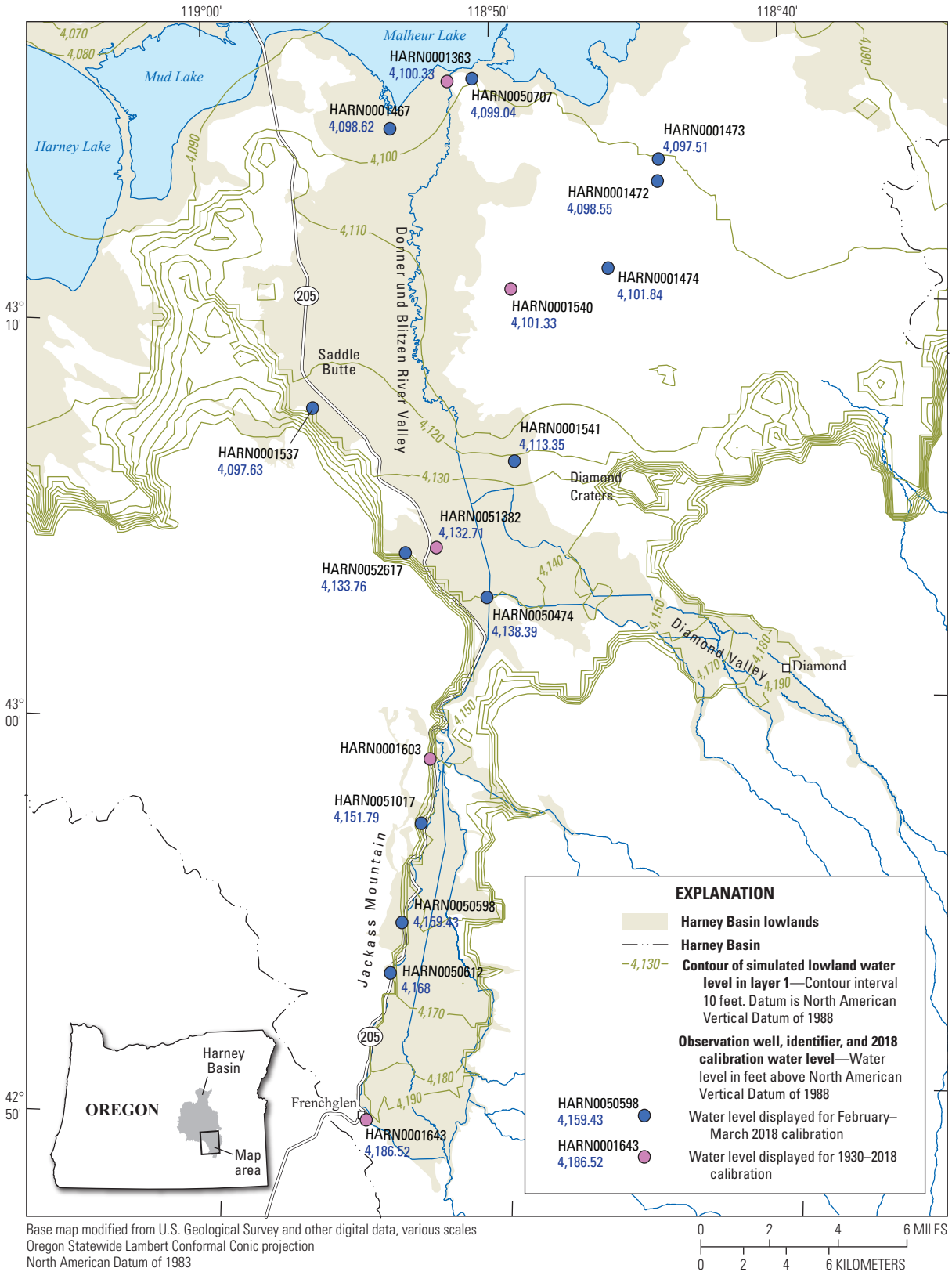

Figure 20. Locations of selected wells in the Donner und Blitzen River floodplain area used for comparison of measured and simulated groundwater-level elevations from the Harney Basin Groundwater Model (Gingerich, 2024), Harney Basin, southeastern Oregon.

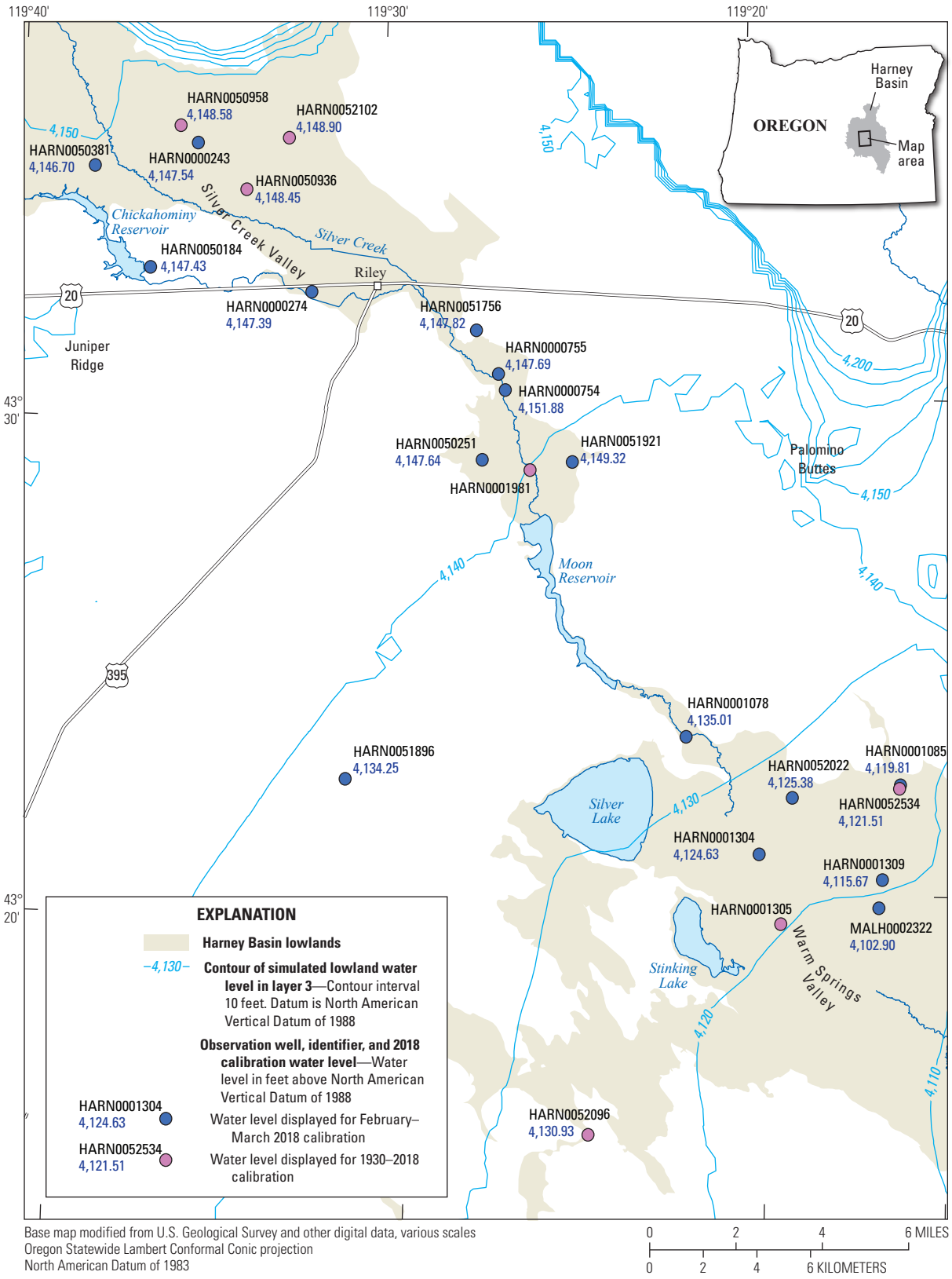

Figure 21. Locations of selected wells in the Silver Creek floodplain area used for comparison of measured and simulated groundwater-level elevations from the Harney Basin Groundwater Model (Gingerich, 2024), Harney Basin, southeastern Oregon.

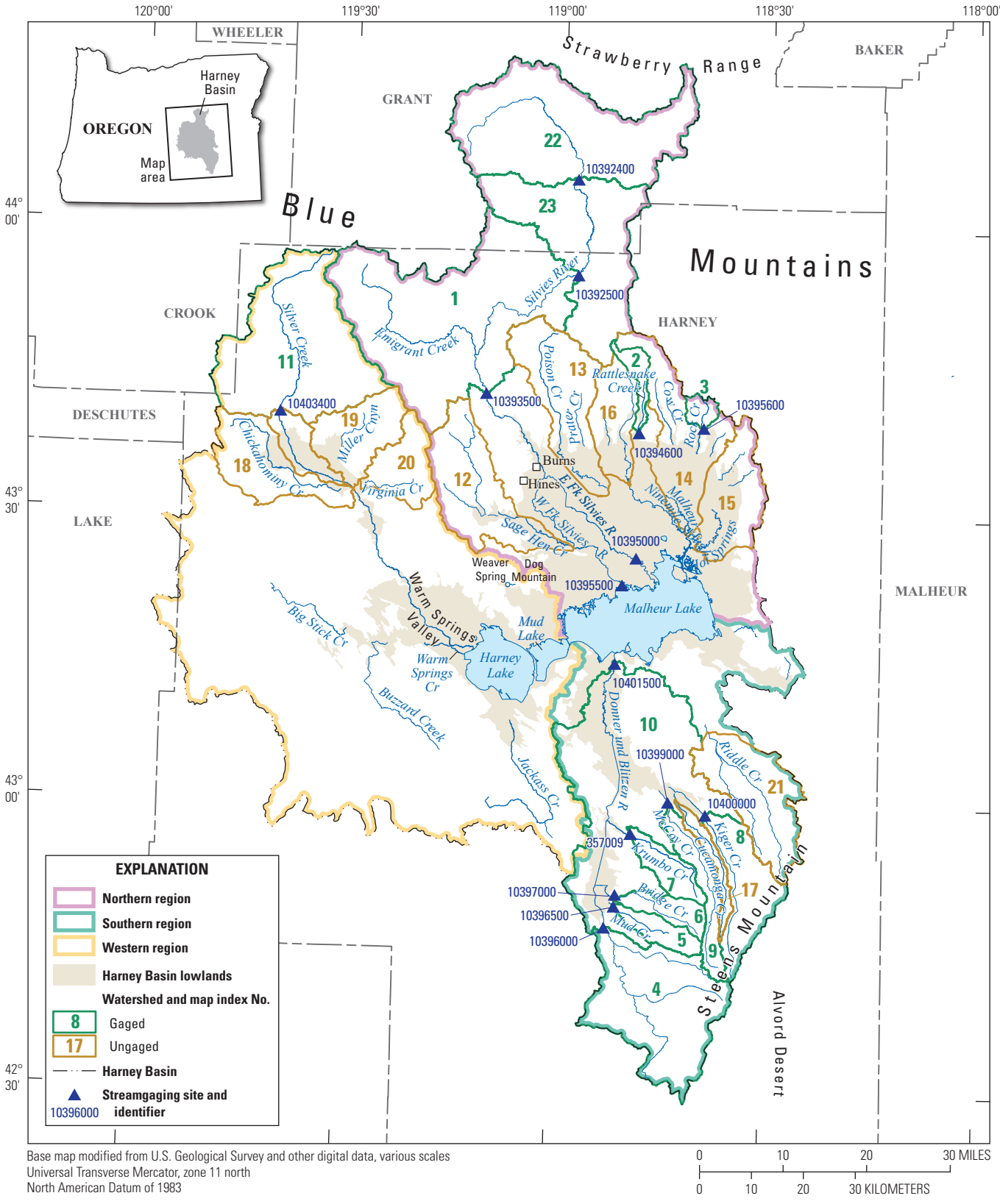

Figure 22. Locations of streamgaging stations and watersheds used for comparison of estimated base flow and simulated drain discharge in the Harney Basin Groundwater Model (Gingerich, 2024), Harney Basin, southeastern Oregon. Streamgaging station numbers and watershed map index numbers listed in table 4.

Comparison of Measured and Simulated Groundwater Levels

To determine how well the HBGM results reflect the measured data, one measure of model fit compares groundwater levels measured during February–March 2018 to the simulated groundwater levels representing the same time on a graph; an exact match would cause all observations to lie on the one-to-one (1:1) correlation line. The February–March 2018 period is a time when groundwater levels are least affected by the yearly May–October irrigation withdrawals. The simulated groundwater levels for the HBGM are plotted relative to the measured groundwater levels for various regions throughout the basin (figs. 23–30). Simulated groundwater levels that are above the 1:1 correlation line indicate that the model overestimates the measured groundwater levels; conversely, simulated groundwater levels that are below the line indicate the model underestimates the measured groundwater levels (the difference between measured and simulated values is the "residual"). Additionally, a vertical line stretching from the minimum to the maximum simulated groundwater level for each layer penetrated by the well is plotted to show the range used to calculate the weighted mean groundwater level. Due to uncertainty in

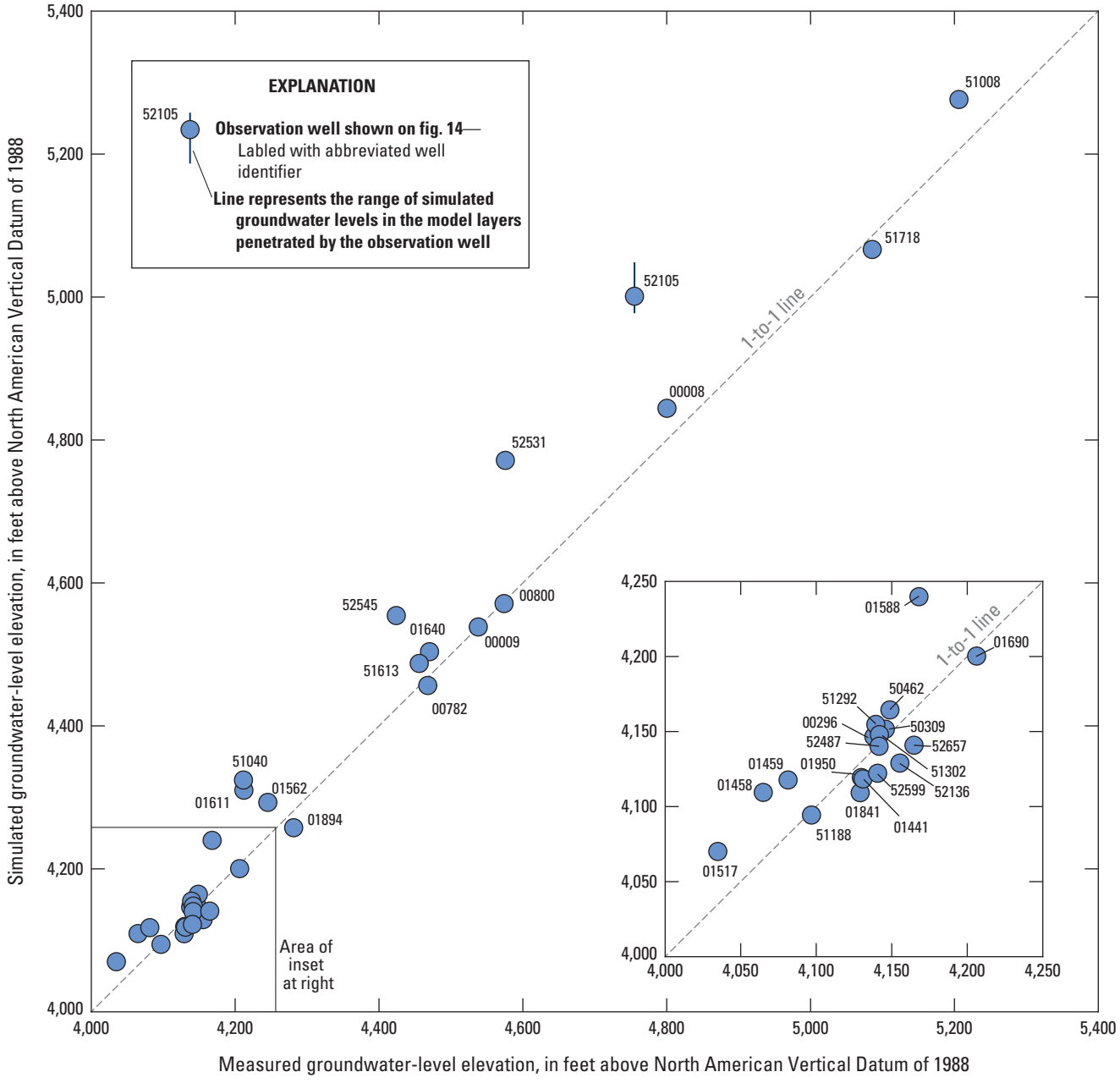

Figure 23. Measured and simulated groundwater-level elevations during February–March 2018 for wells in the Uplands in the Harney Basin Groundwater Model (Gingerich, 2024), Harney Basin, southeastern Oregon. Well locations shown on figure 14.

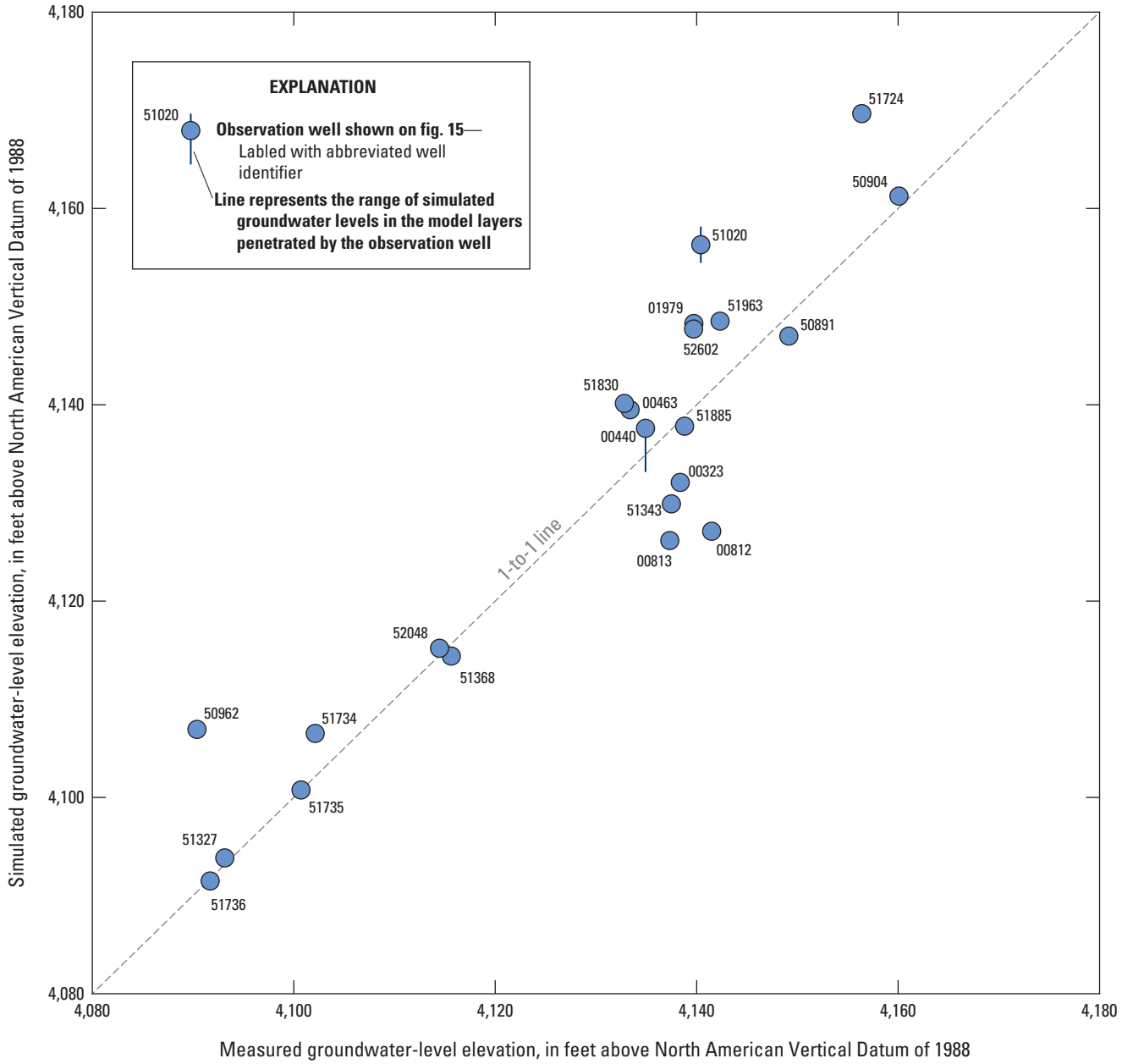

Figure 24. Measured and simulated groundwater-level elevations during February–March 2018 for wells in the Silvies River floodplain area in the Harney Basin Groundwater Model (Gingerich, 2024), Harney Basin, southeastern Oregon. Well locations shown on figure 15.

the construction of many of the wells in which groundwater levels were measured, any simulated groundwater level falling within this range can be considered an acceptable match. Overall, the measured and simulated groundwater levels in the various areas generally follow a 1:1 correlation line. Violin plots of the fit in the uplands and lowlands (including subareas of the lowlands) show the distribution of residuals across the Harney Basin (fig. 31). The median of the residuals for 33 wells in the uplands (fig. 23) is 8.4 ft with an interquartile range of −10.5–44.5 ft, indicating that the model simulates upland groundwater levels that are slightly higher than measured. Given the large area represented, the range in land-surface elevation (3,260–9,570 ft), the areas of steep terrain, and the variety of geologic units represented, the model fit is considered reasonable for representing the upland groundwater-flow processes.

The overall model fit of groundwater levels in the lowlands is slightly high but varies by area. The median of the residuals for 153 wells in the lowlands is 0.7 ft with an interquartile range of −4.7 to 7.6 ft. The areas that have simulated groundwater levels higher than measured groundwater levels include the Northern lowlands area (median=6.8 ft, n=38), the Donner und Blitzen River (median=1.8 ft, n=13), and the Silvies River floodplain

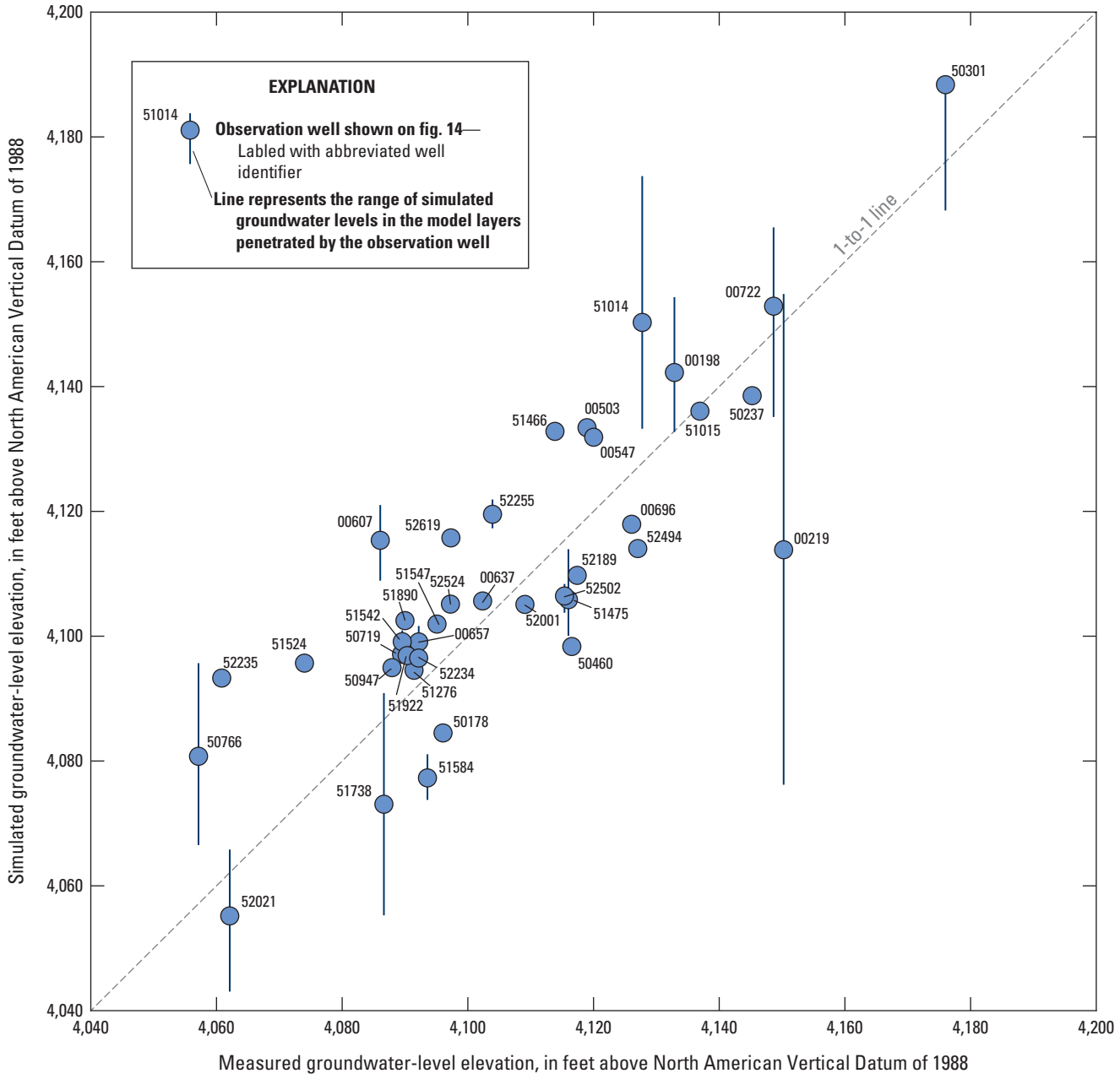

Figure 25. Measured and simulated groundwater-level elevations during February–March 2018 for wells in the Northern lowlands area in the Harney Basin Groundwater Model (Gingerich, 2024), Harney Basin, southeastern Oregon. Well locations shown on figure 16.

(median=1.0 ft, n=22). The areas that have simulated groundwater levels lower than measured groundwater levels include the Crane area (median=−3.8 ft, n=13), the Virginia Valley area (median=−1.7 ft, n=18), the Weaver Spring area (median=−1.7 ft, n=22), and the Silver Creek floodplain area (median=−0.1 ft, n=23). The areas with the most pumping wells (Weaver Spring, the Northern lowlands, and Crane areas) generally have the largest spread in the interquartile range highlighting the difficulty in simulating the complexly layered Younger Basin fill and Older Basin fill HUs and the numerous wells pumping from multiple depths in these areas.

To evaluate the ability of the HBGM to simulate changes in groundwater levels over time, multiple measurements taken over a period of time in a single well (time-series measurements) are compared to their simulated equivalents. The wells used for comparison in specific areas (figs. 32–39) were selected to represent temporal variations (groundwater-level trends, seasonal fluctuations, and vertical gradients) and to optimize spatial coverage. Hydrographs for wells open to multiple model layers show simulated groundwater levels from all layers penetrated by the well in addition to the groundwater-level measurements. The simulated groundwater levels indicate that the model simulates

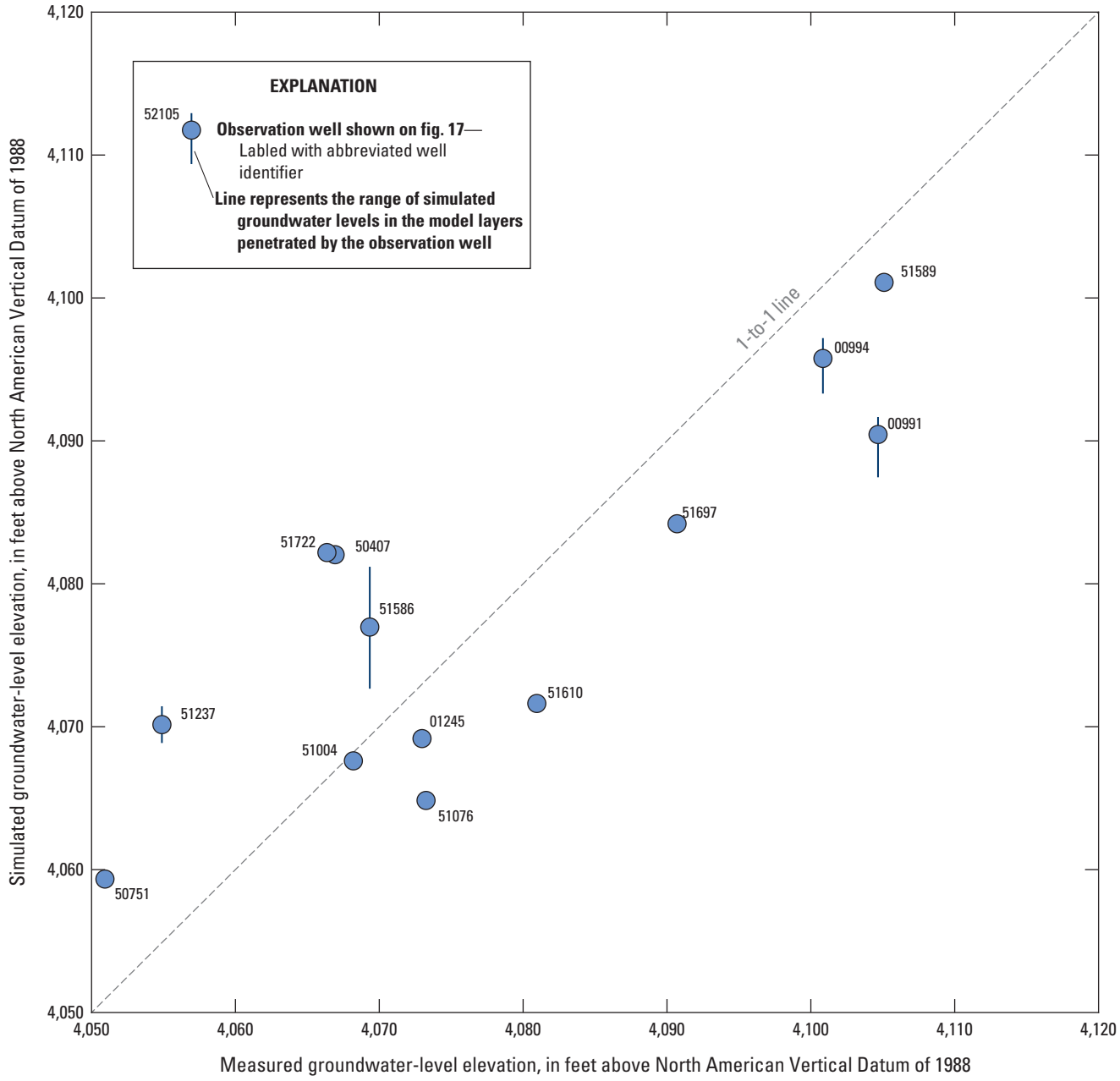

Figure 26. Measured and simulated groundwater-level elevations during February–March 2018 for wells in the Crane area in the Harney Basin Groundwater Model (Gingerich, 2024), Harney Basin, southeastern Oregon. Well locations shown on figure 17.

the timing and magnitude of groundwater-level changes in the Harney Basin to both climatic and pumpage stresses reasonably well.

The largest difference between measured and simulated groundwater levels is in the uplands (fig. 32). The discrepancies in the upland parts of the basin can be attributed to the inherent limitations of model discretization when generalizing complex geologic heterogeneity and large topographic relief into discrete homogeneous model cells. The largest discrepancy is for Well HARN0000782, which is along the southern margin of the model and outside the Harney Basin boundary (figs. 14, 32*C*). Here, the discrepancy is attributed to uncertainty regarding the proximity of several high-capacity irrigation wells to a no-flow boundary along the model edge coupled with a paucity of hydrogeologic information in this area.

In the lowland areas, mismatches between measured and simulated groundwater levels are attributed, at least in part, to uncertainty in the estimated distribution and magnitude of pumpage during 1930–2018. Estimates of the spatial and temporal distribution of pumpage could result in excess or insufficient pumpage being simulated in some locations, causing an overestimation or an underestimation, respectively, of simulated groundwater levels. Local variabilities in the

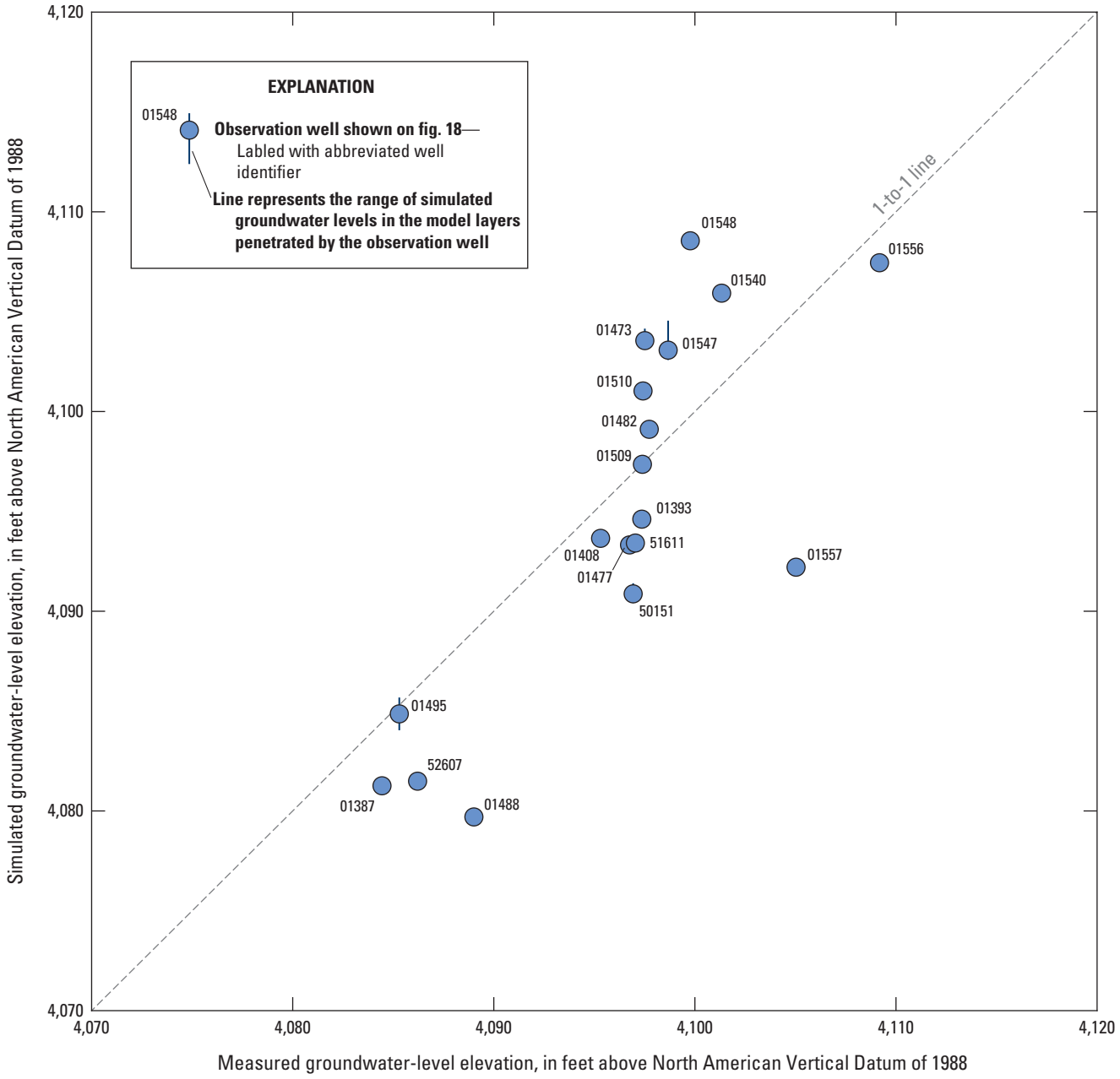

Figure 27. Measured and simulated groundwater-level elevations during February–March 2018 for wells in the Virginia Valley area in the Harney Basin Groundwater Model (Gingerich, 2024), Harney Basin, southeastern Oregon. Well locations shown on figure 18.

hydraulic properties of the geologic materials may not be adequately represented within the layers of lowland geologic deposits, which also would contribute to the overestimation or underestimation of the groundwater levels especially in areas of substantial groundwater-level decline in the few decades prior to 2018.

The HBGM was used to evaluate the long-term declines in groundwater levels in the basin lowlands. For this report, declines are described as the relative difference between the groundwater levels from January 1990 and the end of the transient-state simulation (December 2018). The plots of transient groundwater-level variations (figs. 32–39) show that many of the areas monitored began experiencing substantial groundwater-level declines after 1990, following the wet period of the 1980s and during the period when pumping rates began to increase across the basin. Negative values represent decreases in groundwater level compared to the reference value from January 1990 values in the simulation. The decline data in the lowlands are presented for all 10 model layers (fig. 40*A–J*).

At the end of the model simulation period (2018), the declines in the lowlands generally are largest near the areas of most irrigation pumpage (fig. 13) but vary by area depending on the predominant depth of irrigation wells in each area. The

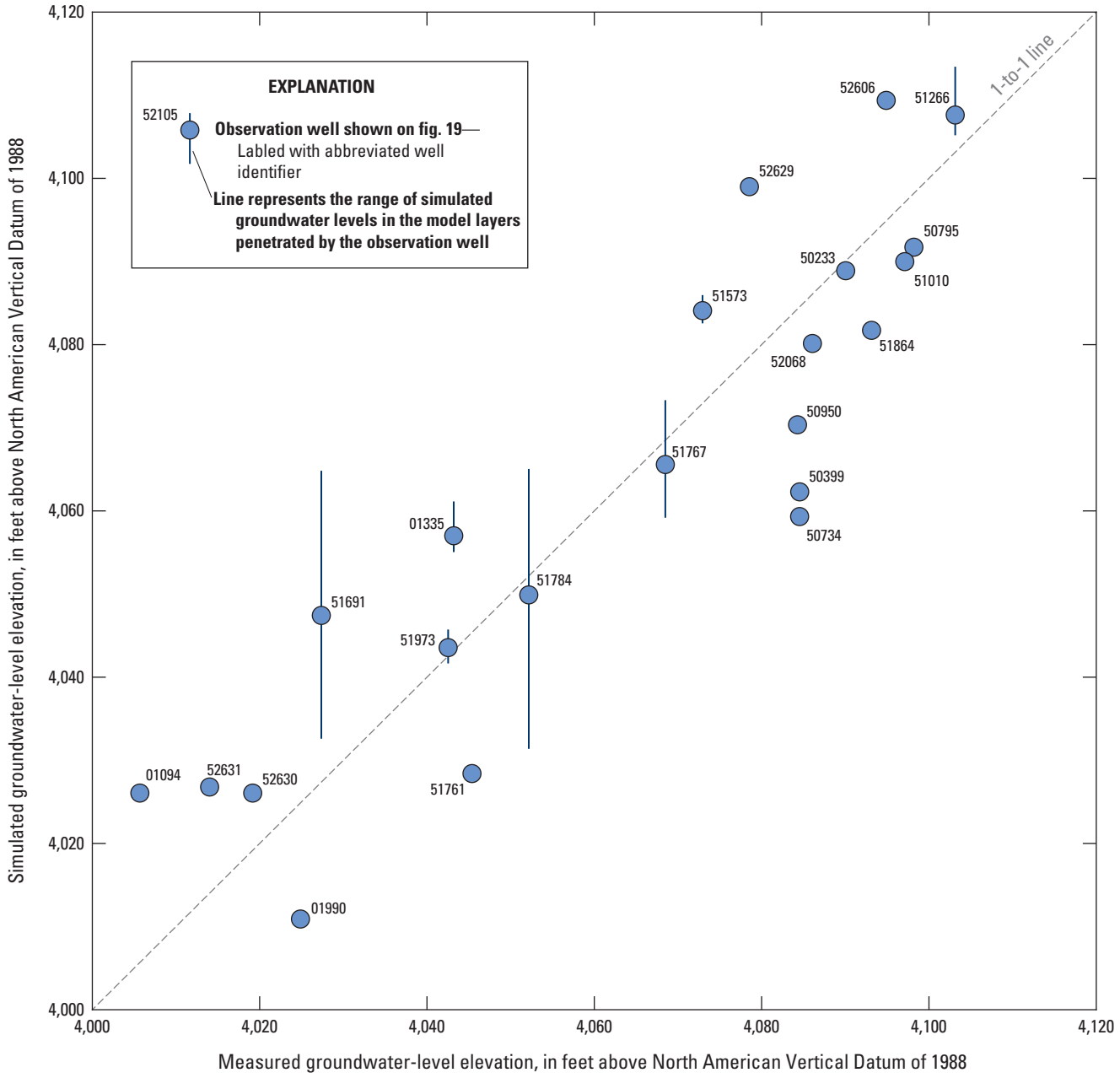

Figure 28. Measured and simulated groundwater-level elevations during February–March 2018 for wells in the Weaver Spring area in the Harney Basin Groundwater Model (Gingerich, 2024), Harney Basin, southeastern Oregon. Well locations shown on figure 19.

simulated decline in the Weaver Spring area is greater than 90 ft in layers 1–6 and diminishes to less than 30 ft in layer 10. The area having groundwater-level declines of at least 40 ft in layer 1 covers about 37 mi^2. The depth and extent of the simulated declines closely match groundwater-level observations from many wells in the Weaver Spring area (figs. 28, 37).

The simulated groundwater-level declines in the Northern lowlands area (north of Highway 20) are greater than 50 ft in layer 1 and increasingly higher in layers 2–5, reaching a maximum greater than 100 ft in layer 5. The declines decrease with depth below layer 5 and diminish to less than 30 ft in layer 10. The area having declines of at least 40 ft in layer 5 covers about 7 mi^2. The simulated decline in this area also matches measured groundwater-level declines in observation wells closely (figs. 25, 34).

In the Crane area, the simulated decline is greater than 40 ft in layers 1–6 and greater than 30 ft in all layers in the relatively small valley of the Crane Creek Gap but less, west of the gap in the broader part of the lowlands. Here, declines are more than 30 ft in layers 5–6 but mostly 20–30 ft across a large area in all 10 layers. The area having at least 20 ft of decline increases with depth; in layer 4 and deeper, the regions of decline in the Northern lowlands area and near Crane area

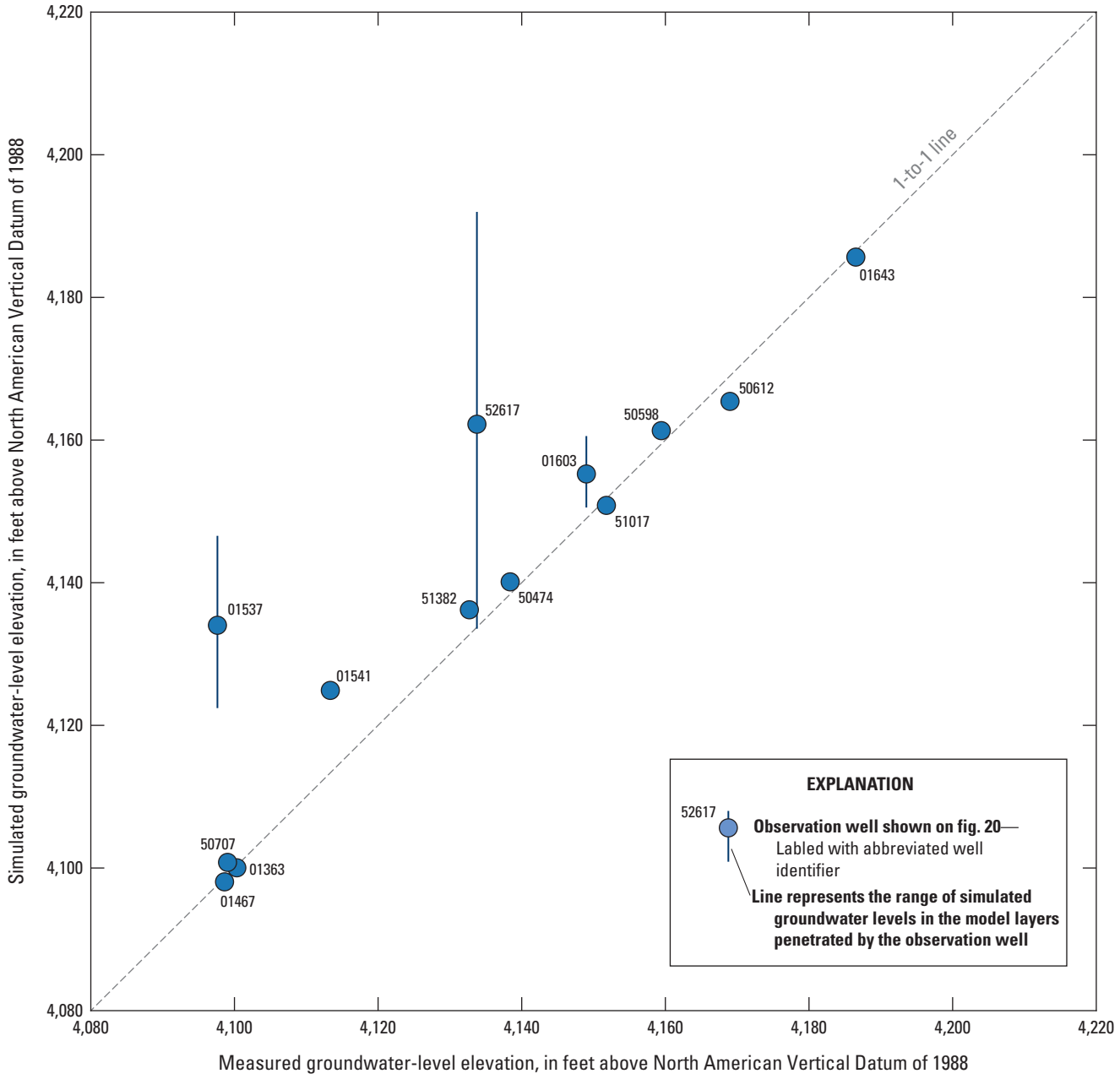

Figure 29. Measured and simulated groundwater-level elevations during February–March 2018 for wells in the Donner und Blitzen River floodplain area in the Harney Basin Groundwater Model (Gingerich, 2024), Harney Basin, southeastern Oregon. Well locations shown on figure 20.

coalesce (fig. 40*D*). No Crane Creek Gap observation wells are available to compare with simulated declines. West of Crane, simulated declines compare reasonably well with measured groundwater levels (figs. 26, 35).

Three areas of decline between Burns and Lawen are related to individual deep irrigation wells that penetrate into depths represented by layers 6–8 in the HBGM (fig. 4*F–H*). The relatively lower hydraulic conductivity of these layers generally leads to areas having large simulated declines but limited extent around irrigation wells. However, no observation wells are deep enough to penetrate into layers deeper than layer 5 in or near these areas of simulated decline; therefore, the existence and extent of these areas of steep declines are uncertain.

In Virginia Valley area, simulated declines are generally 20–30 ft throughout all 10 layers of the HBGM (fig. 40*A–J*). Although the model closely matches groundwater levels at the end of 2018 in wells HARN0052607 and HARN0052608, no measured groundwater levels are available prior to 2016 to evaluate the extent of declines since 1990 in Virginia Valley. Declines along the Silvies and Donner und Blitzen River floodplains are generally less than 10 ft everywhere except for

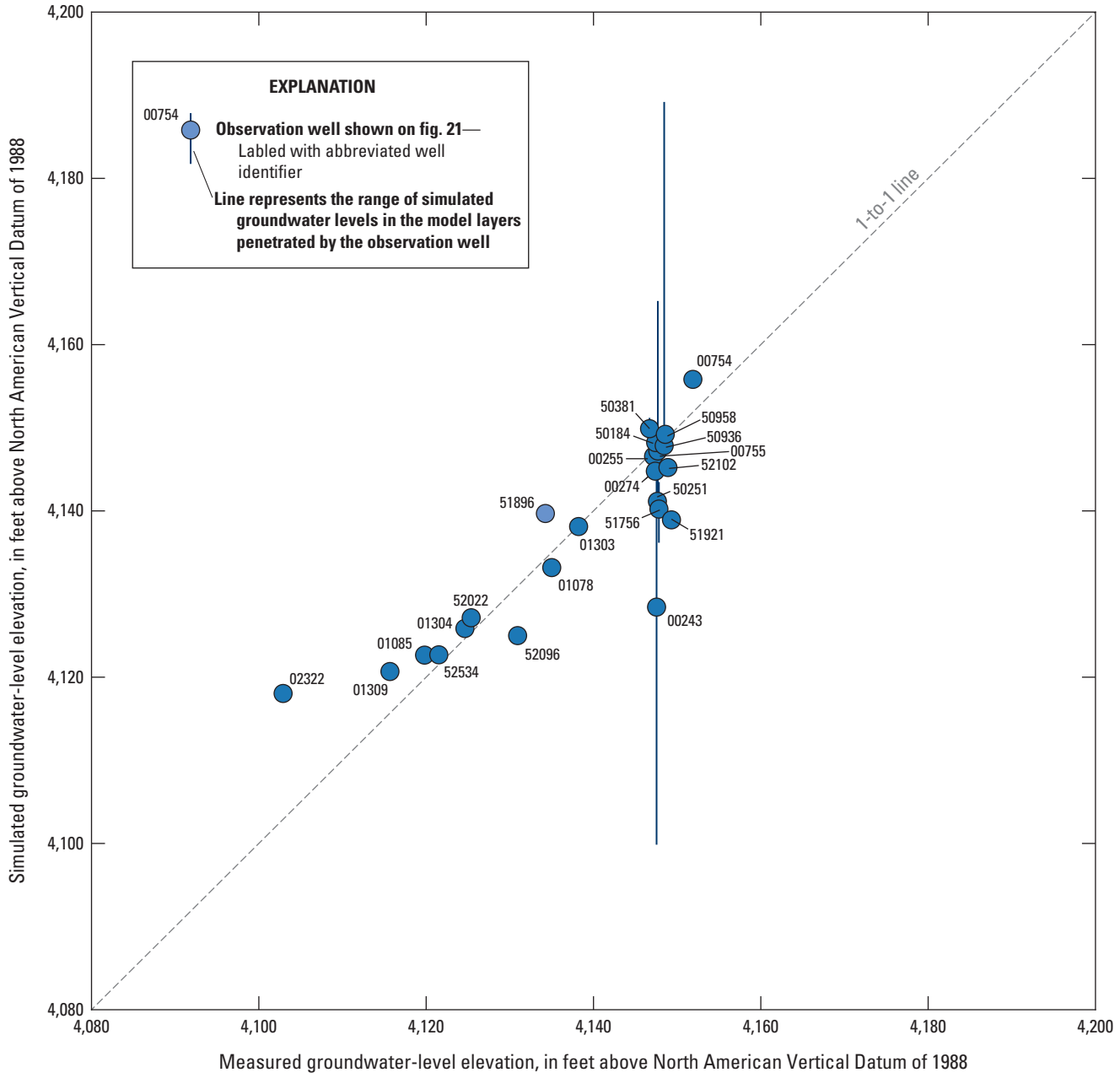

Figure 30. Measured and simulated groundwater-level elevations during February–March 2018 for wells in the Silver Creek floodplain area in the Harney Basin Groundwater Model (Gingerich, 2024), Harney Basin, southeastern Oregon. Well locations shown on figure 21.

a small strip along the extreme southern end of the lowlands near Frenchglen (fig. 40*A*). This area of simulated decline is likely due to differences between 1990 and 2018 in the amount of inflow from the uplands to the south due to the influences of changing recharge and not due to the effects of groundwater pumpage. The only pumpage in this area is from domestic and livestock withdrawals. The simulated declines along the river floodplains generally match the long-term groundwater-level observations available for comparison in these areas (fig. 40*A*).

In the upper Silver Creek floodplain, some areas having 20–30 ft of decline are simulated in layers 1–2; layers with low hydraulic conductivity overlying the western permeable zone (fig. 4*C–F*). Otherwise, the upper floodplain has less than 20 ft of decline in layers 3–10, and the Warm Springs Valley area has less than 10 ft of decline in layers 1–10 (fig. 40*A–J*), likely due to less pumpage in this area.

No groundwater-level observations are available at depths below the level of layer 6 throughout the model, so the simulated declines in deeper layers cannot be verified with measurements.

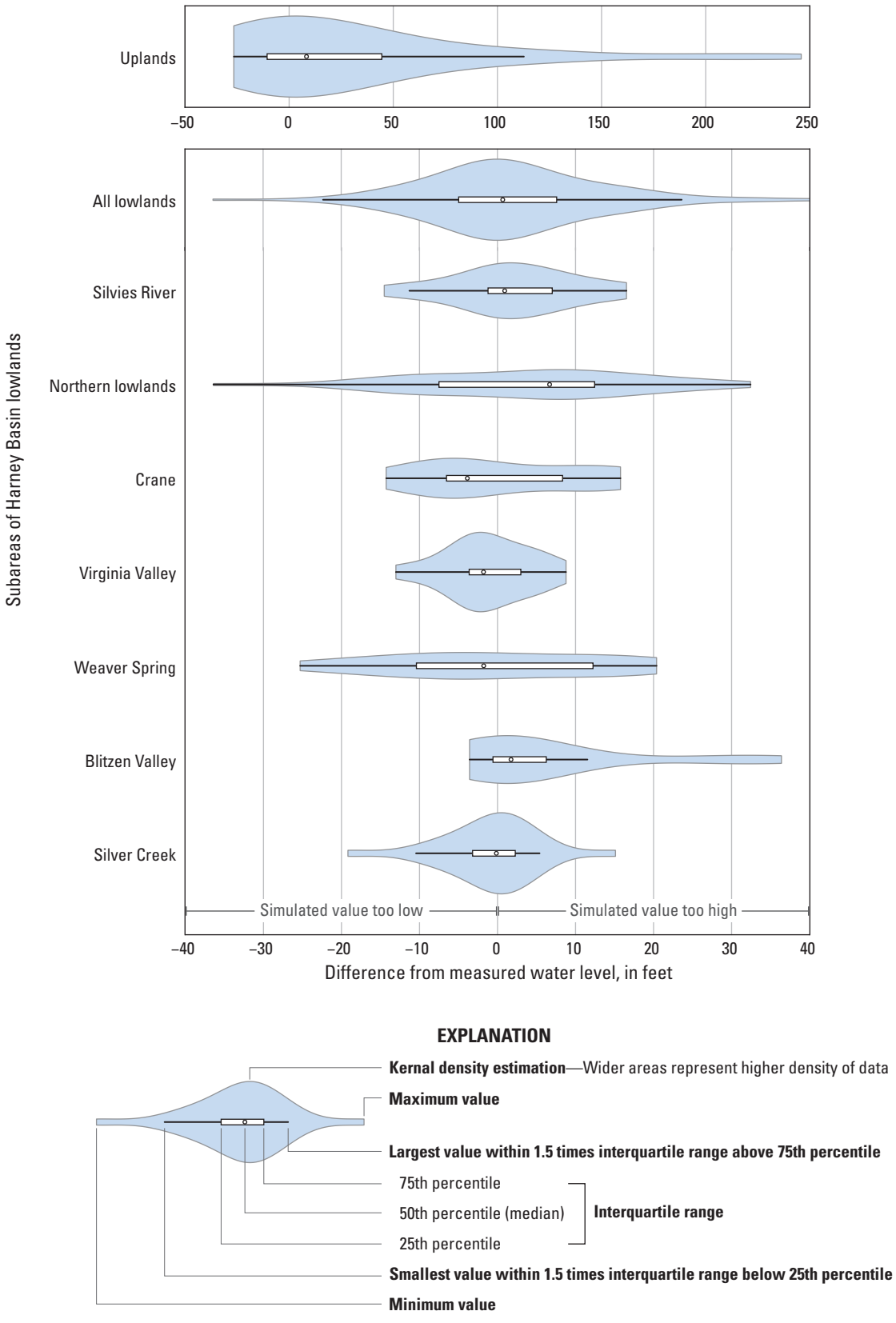

Figure 31. Violin plots of the difference between measured and simulated groundwater-level elevations during February–March 2018 for the Harney Basin Groundwater Model (Gingerich, 2024), Harney Basin, southeastern Oregon.

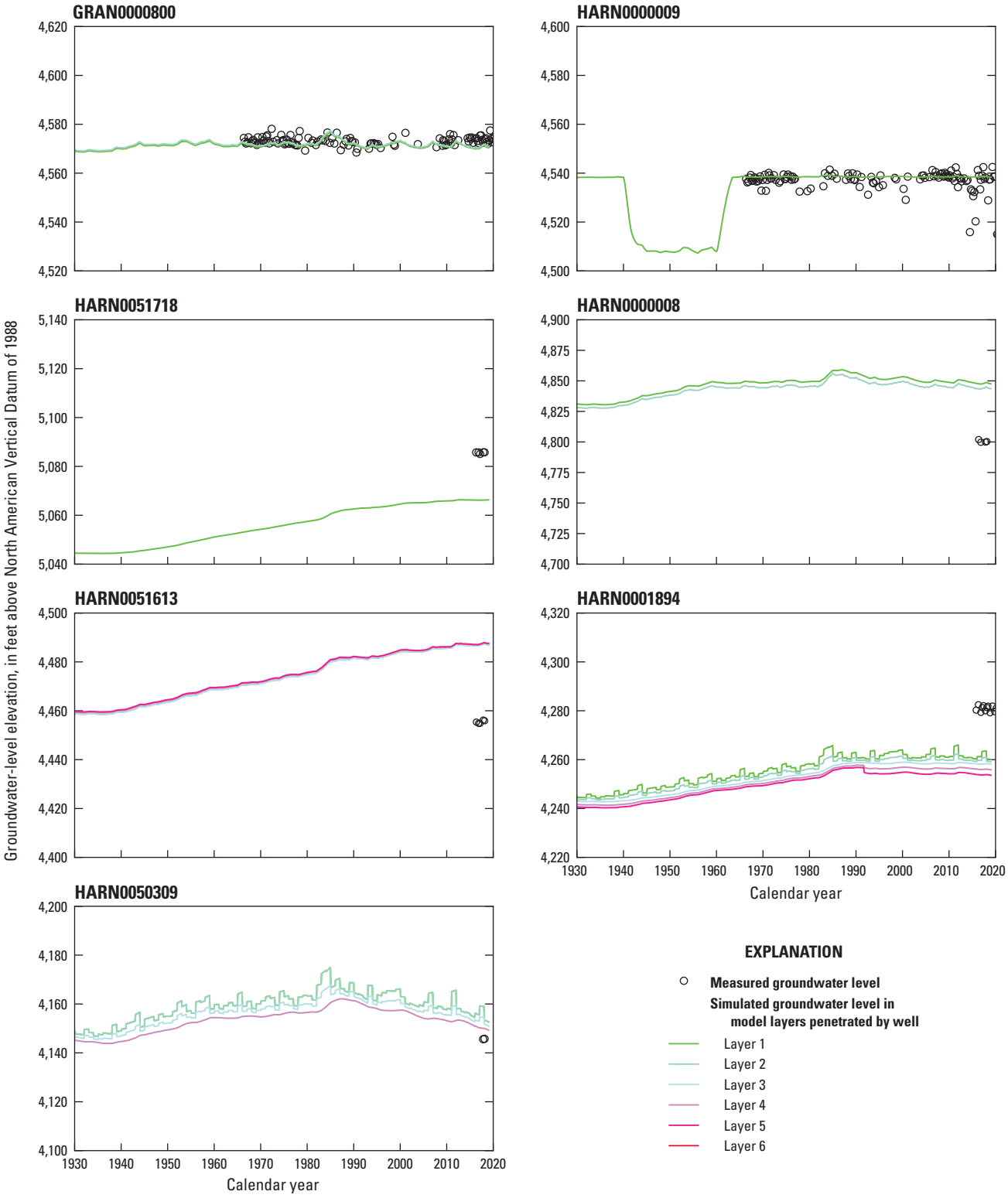

Figure 32. Measured and simulated groundwater-level elevations for Upland wells during 1930–2018 in the Harney Basin Groundwater Model (Gingerich, 2024), Harney Basin, southeastern Oregon.

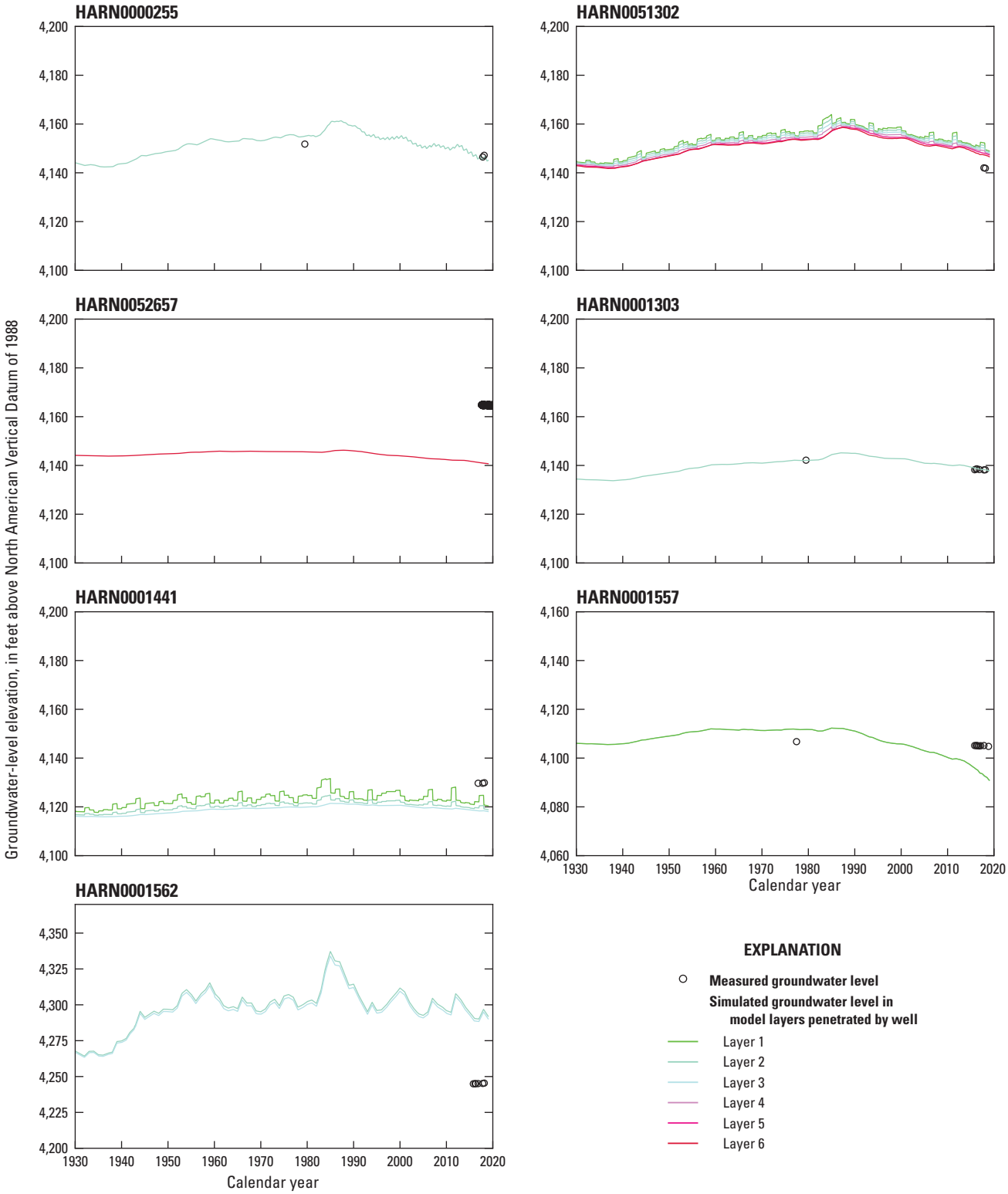

Figure 32.—Continued

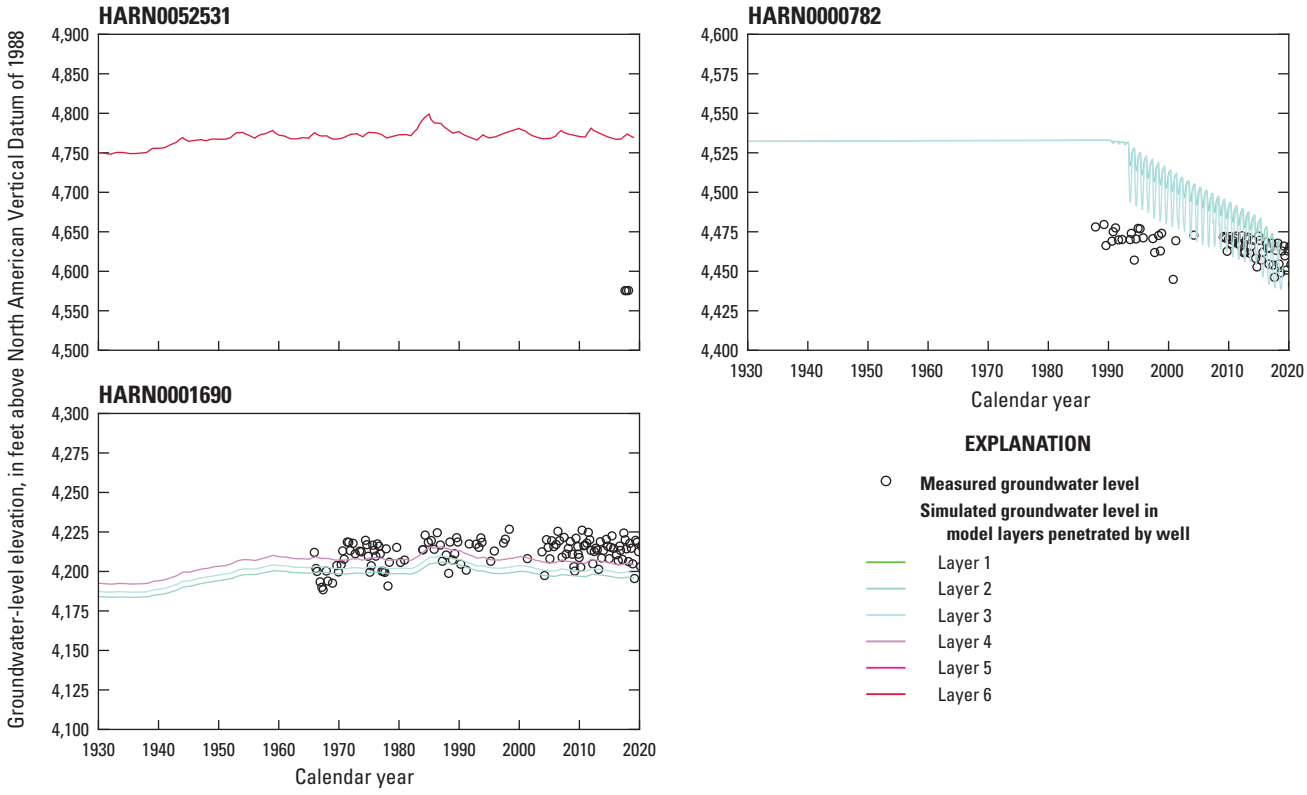

Figure 32.—Continued

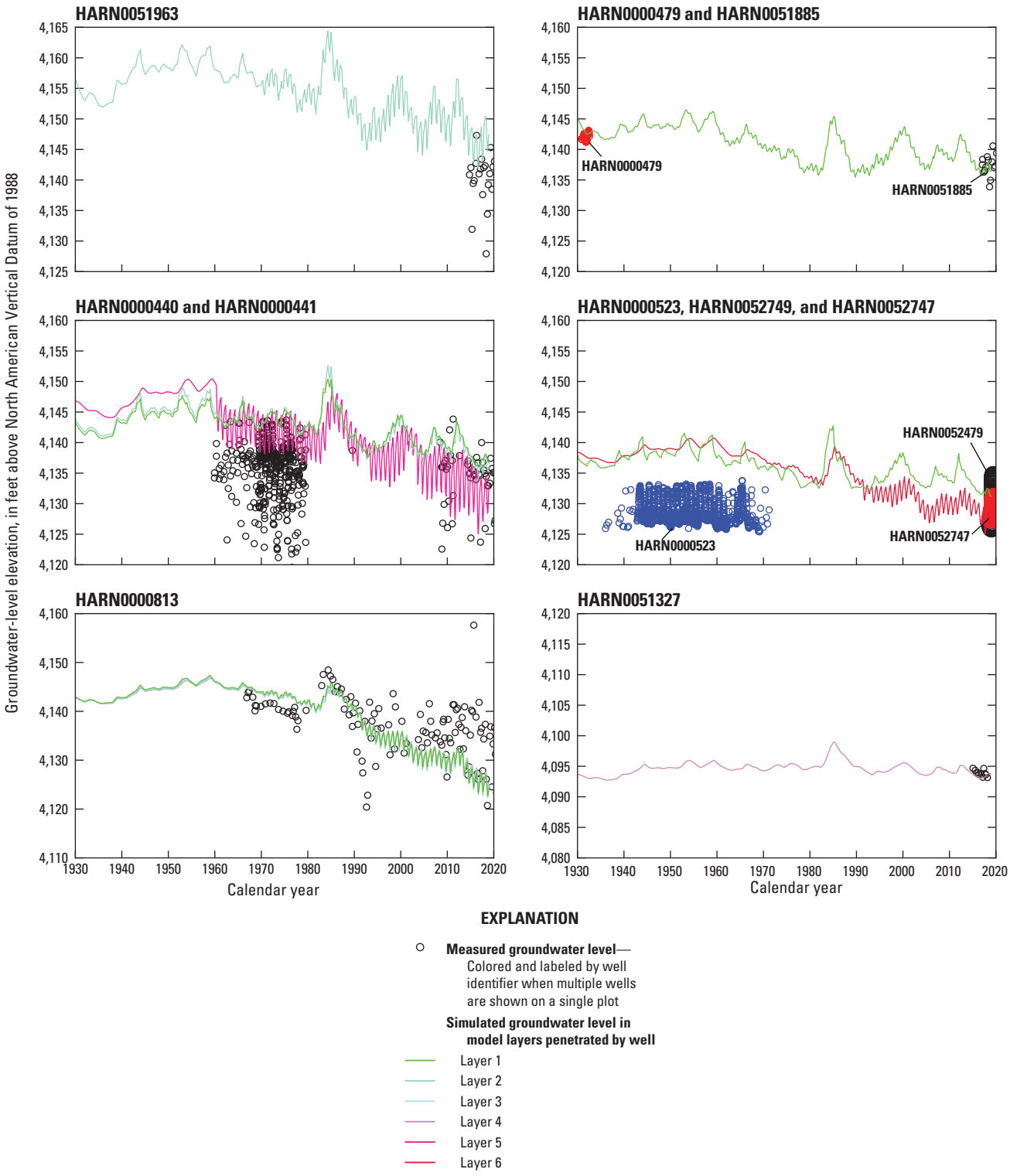

Figure 33. Measured and simulated groundwater-level elevations for Silvies River area wells during 1930–2018 in the Harney Basin Groundwater Model (Gingerich, 2024), Harney Basin, southeastern Oregon.

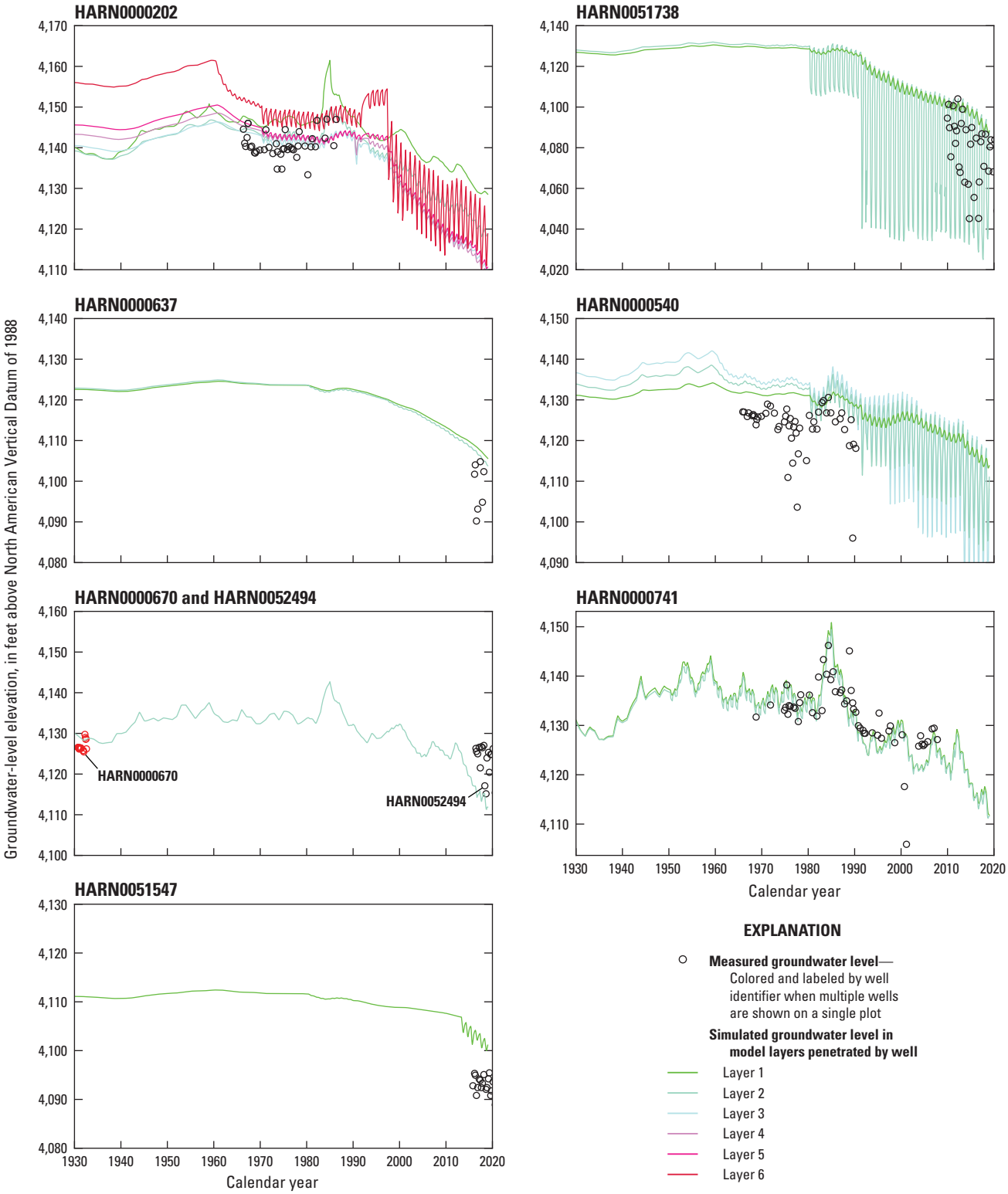

Figure 34. Measured and simulated groundwater-level elevations for Northern Lowlands area wells during 1930–2018 in the Harney Basin Groundwater Model (Gingerich, 2024), Harney Basin, southeastern Oregon.

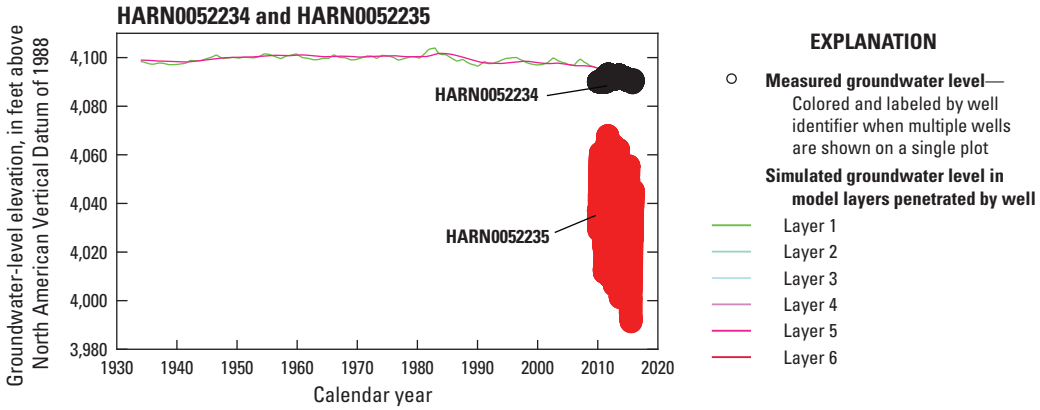

Figure 34.—Continued

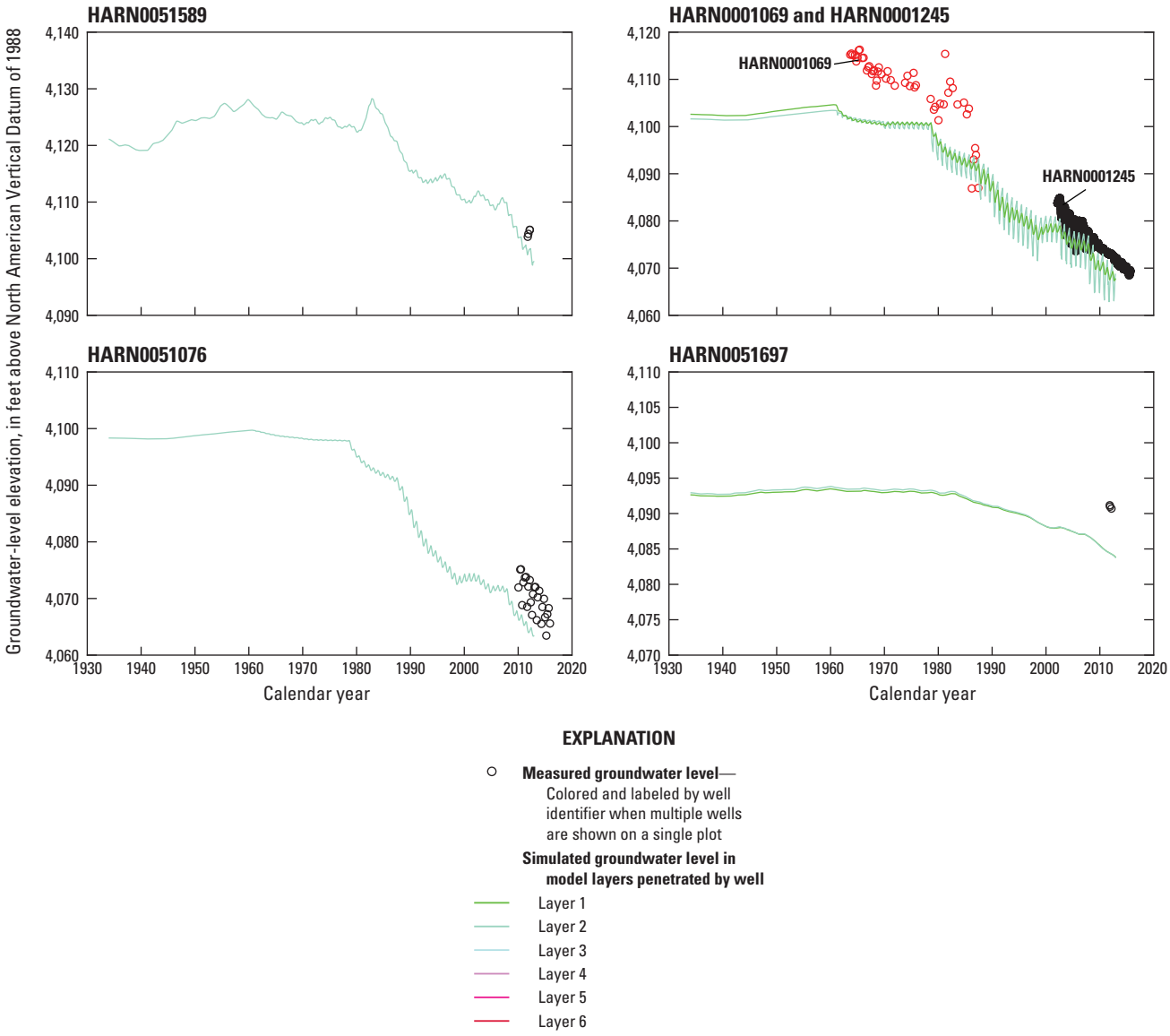

Figure 35. Measured and simulated groundwater-level elevations for Crane area wells during 1930–2018 in the Harney Basin Groundwater Model (Gingerich, 2024), Harney Basin, southeastern Oregon.

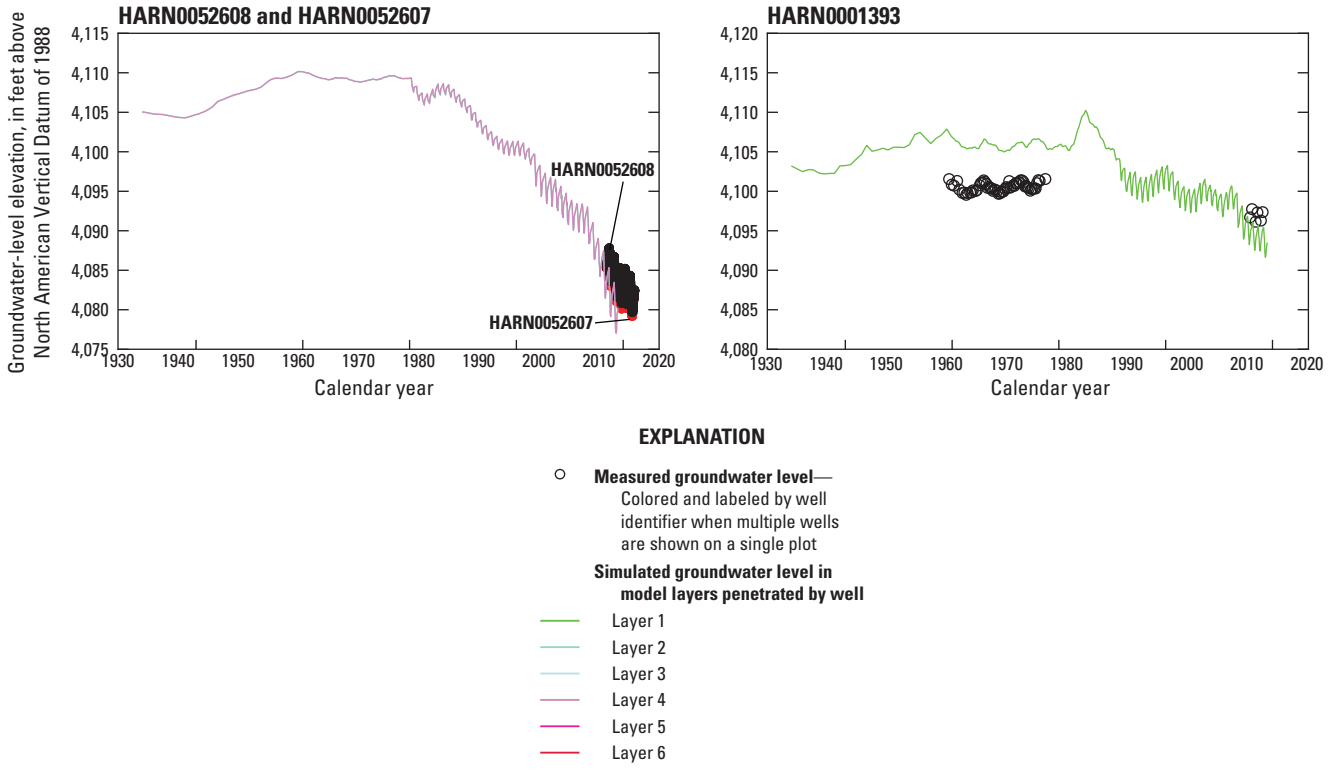

Figure 36. Measured and simulated groundwater-level elevations for Virginia Valley area wells during 1930–2018 in the Harney Basin Groundwater Model (Gingerich, 2024), Harney Basin, southeastern Oregon.

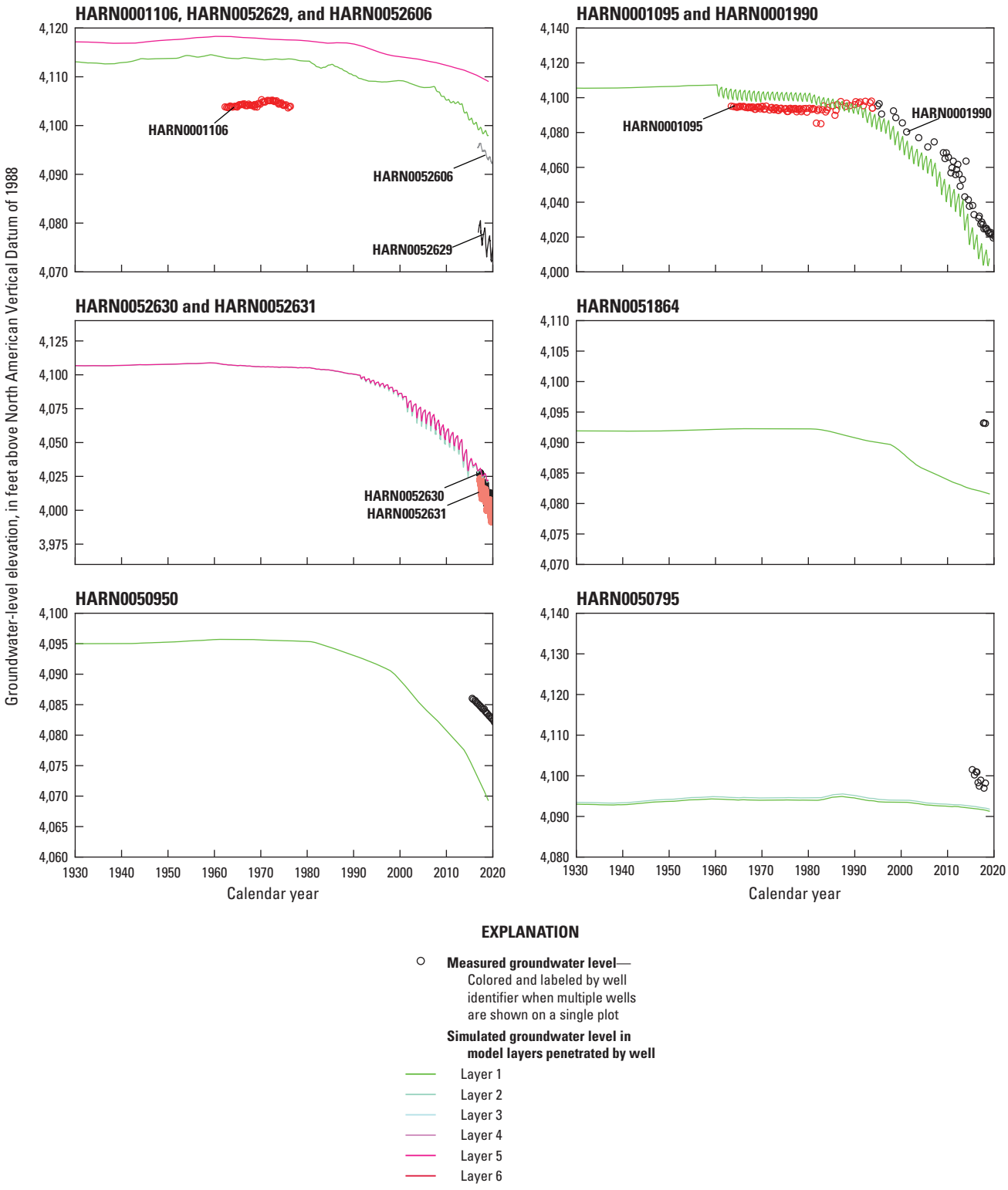

Figure 37. Measured and simulated groundwater-level elevations for Weaver Spring area wells during 1930–2018 in the Harney Basin Groundwater Model (Gingerich, 2024), Harney Basin, southeastern Oregon.

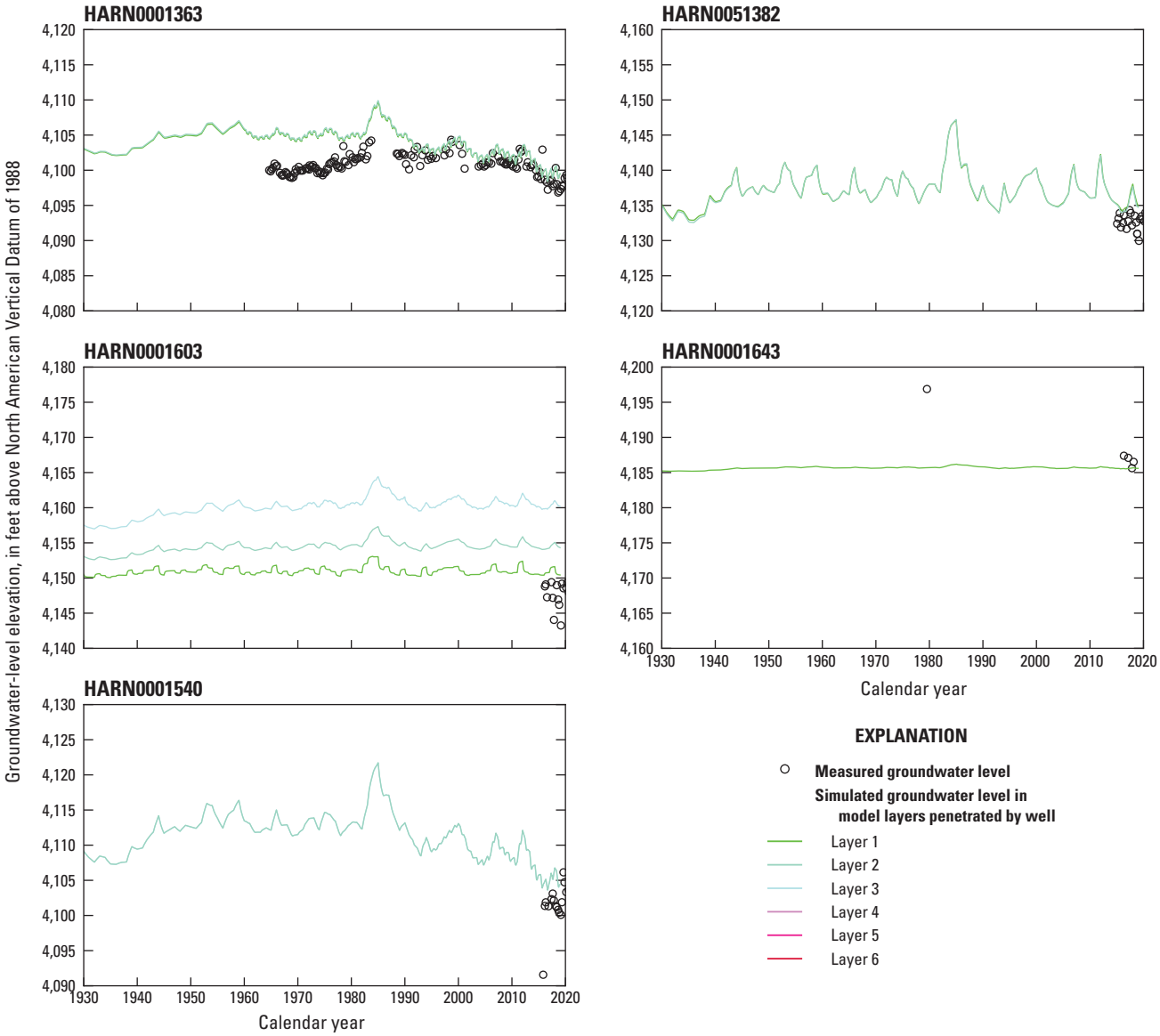

Figure 38. Measured and simulated groundwater-level elevations for Donner und Blitzen River area wells during 1930–2018 in the Harney Basin Groundwater Model (Gingerich, 2024), Harney Basin, southeastern Oregon.

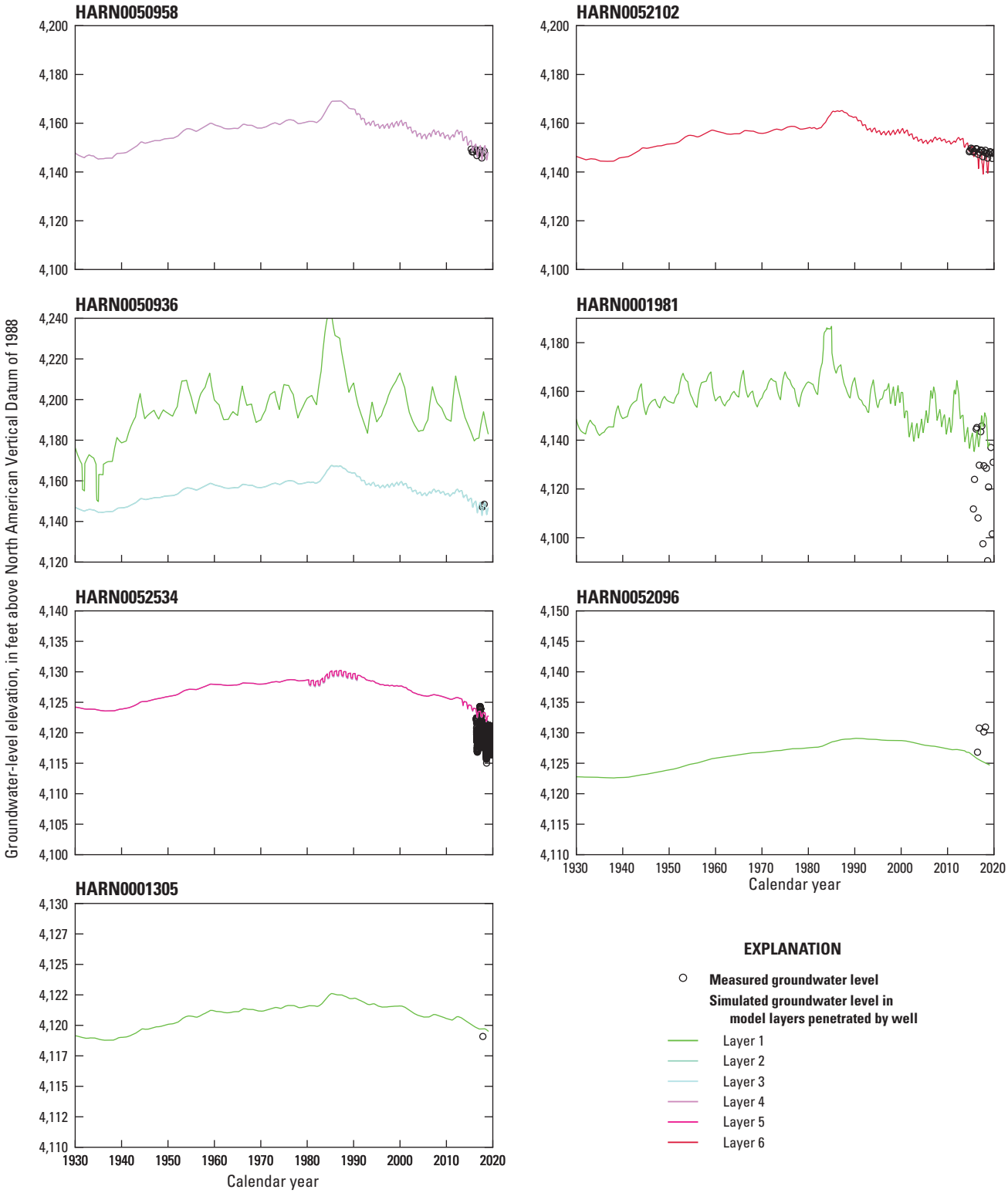

Figure 39. Measured and simulated groundwater-level elevations for Silver Creek area wells during 1930–2018 in the Harney Basin Groundwater Model (Gingerich, 2024), Harney Basin, southeastern Oregon.

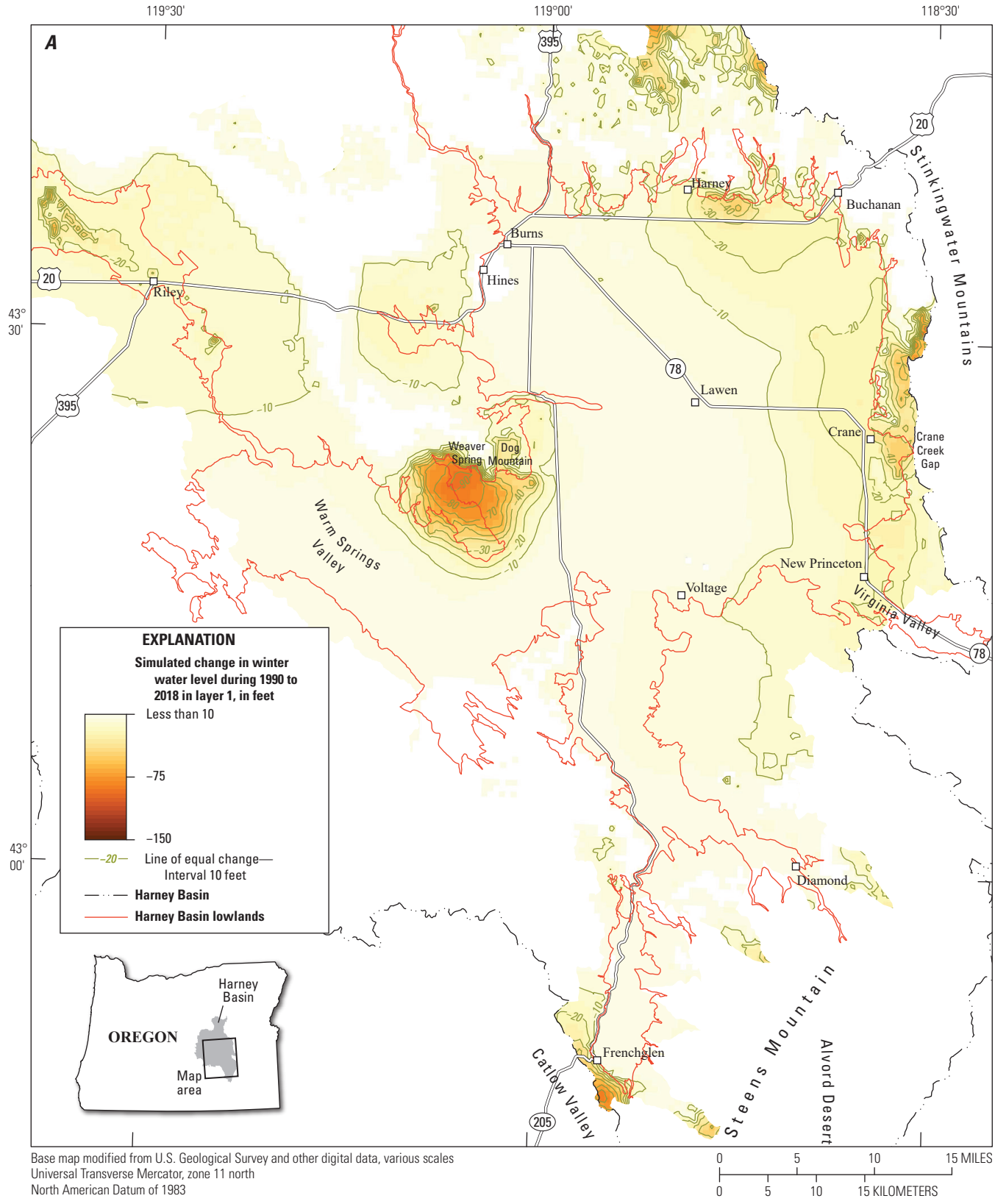

Figure 40. Simulated changes in lowland winter groundwater levels for the period 1990–2018 from the Harney Basin Groundwater Model (Gingerich, 2024) for (*A*) layer 1, (*B*) layer 2, (*C*) layer 3, (*D*) layer 4, (*E*) layer 5, (*F*) layer 6, (*G*) layer 7, (*H*) layer 8, (*I*) layer 9, and (*J*) layer 10, Harney Basin, southeastern Oregon.

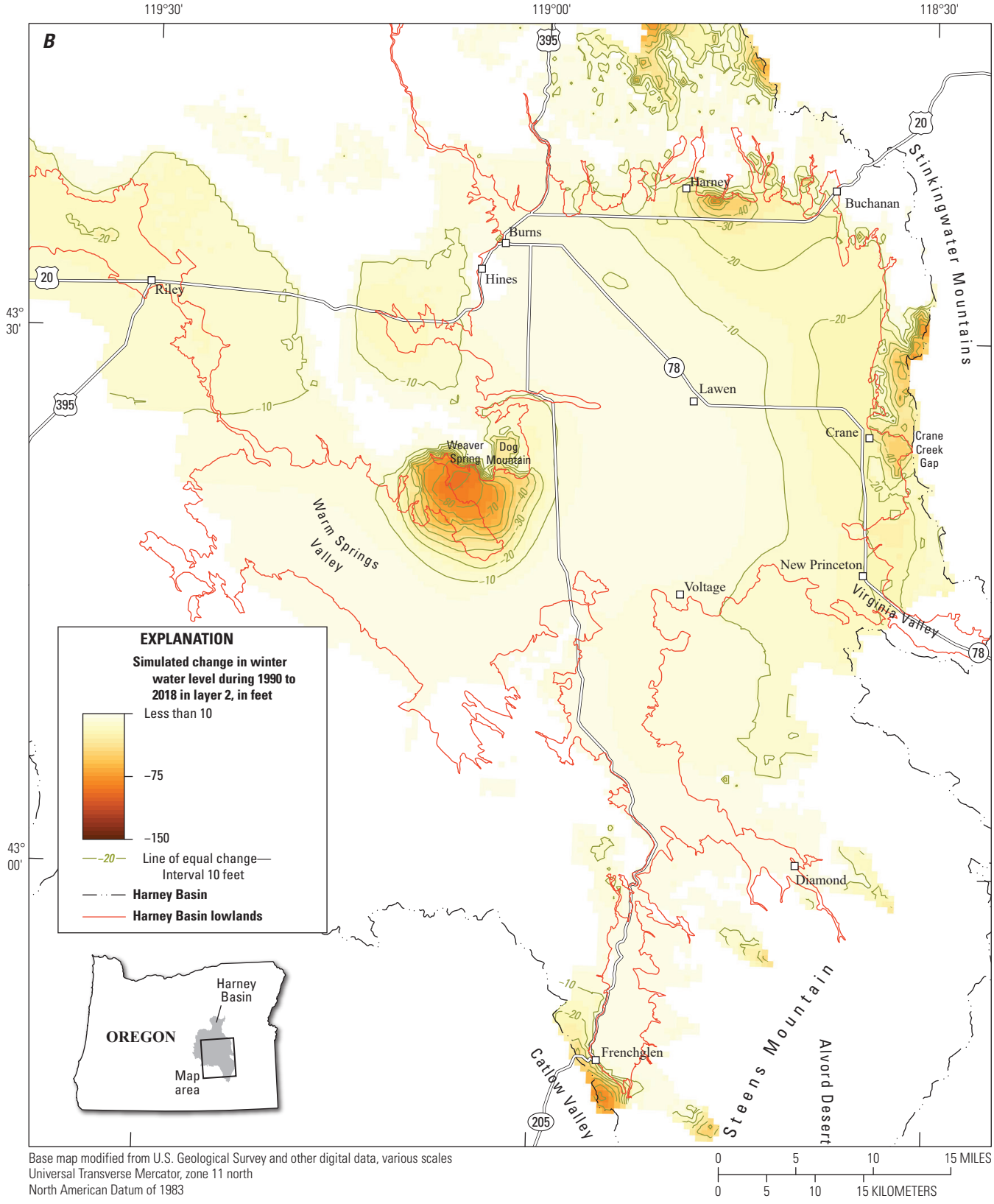

Figure 40.—Continued

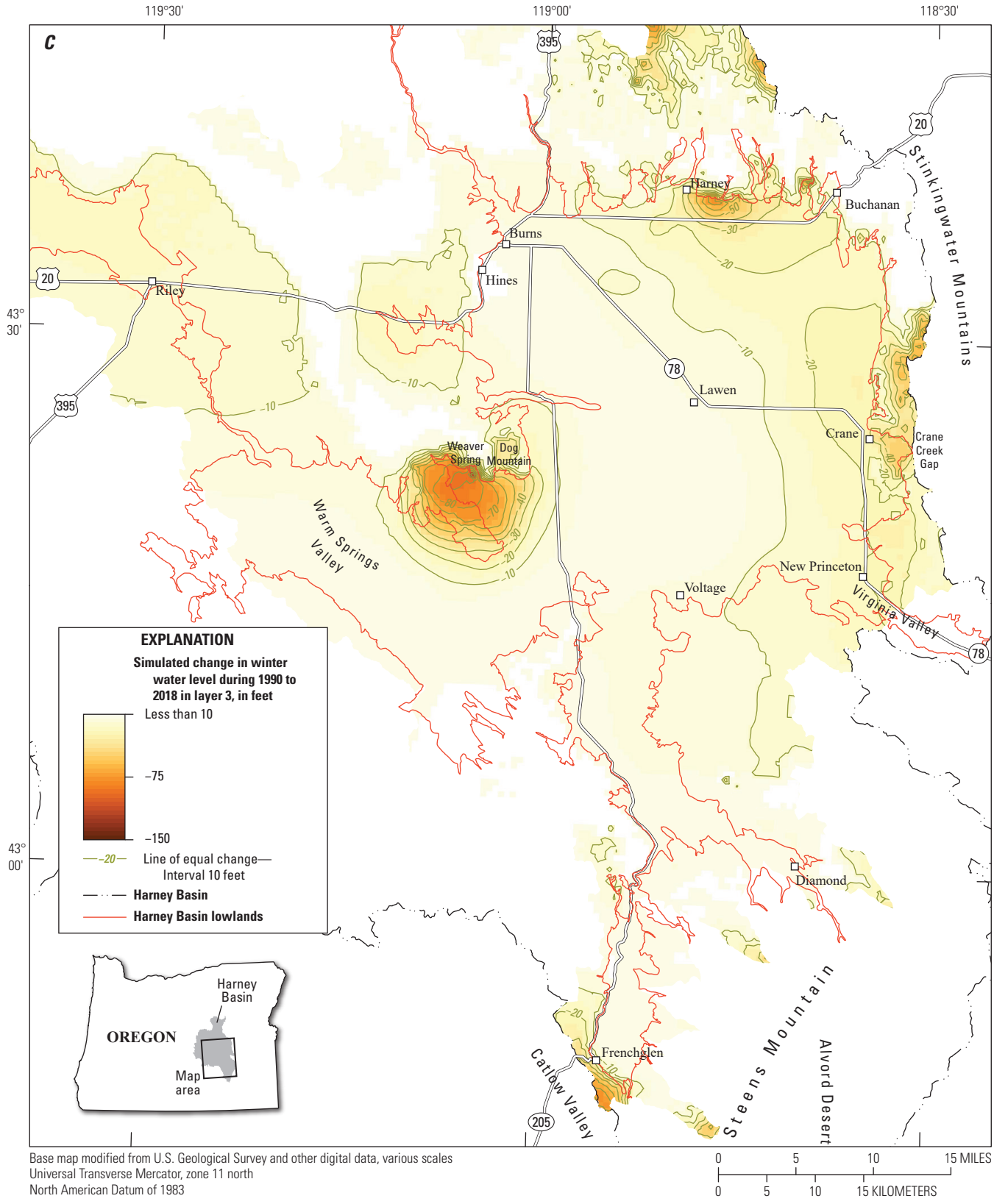

Figure 40.—Continued

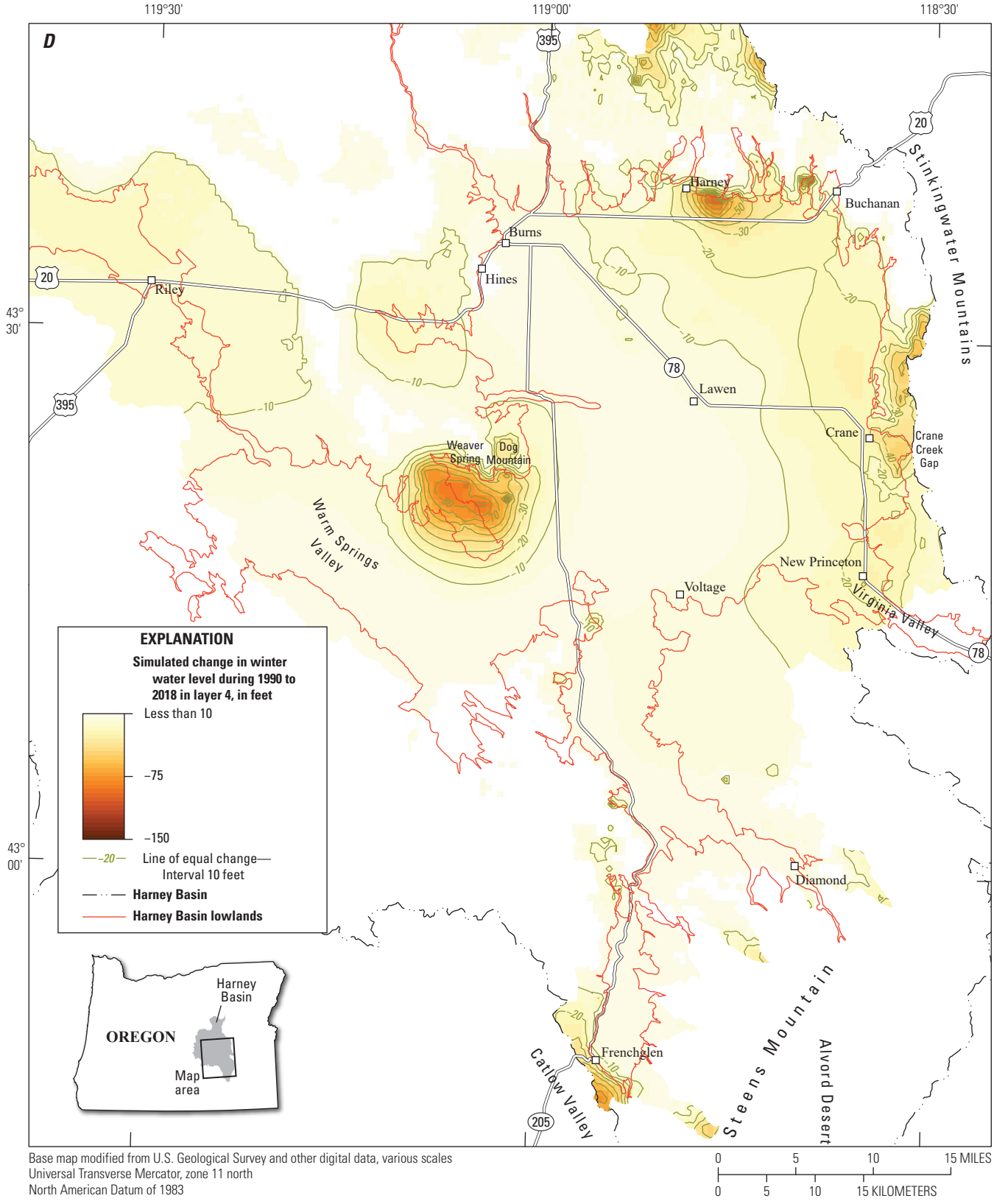

Figure 40.—Continued

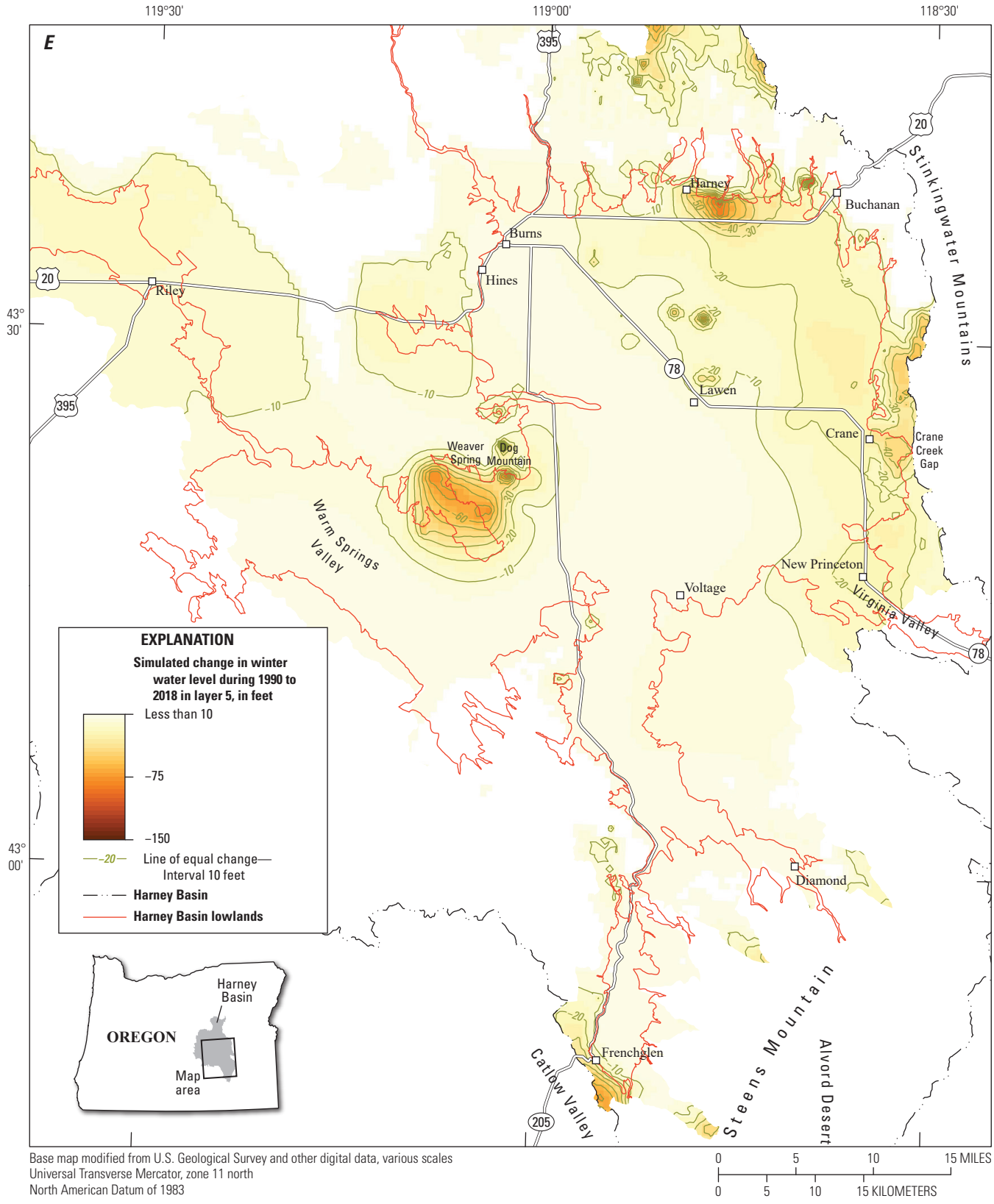

Figure 40.—Continued

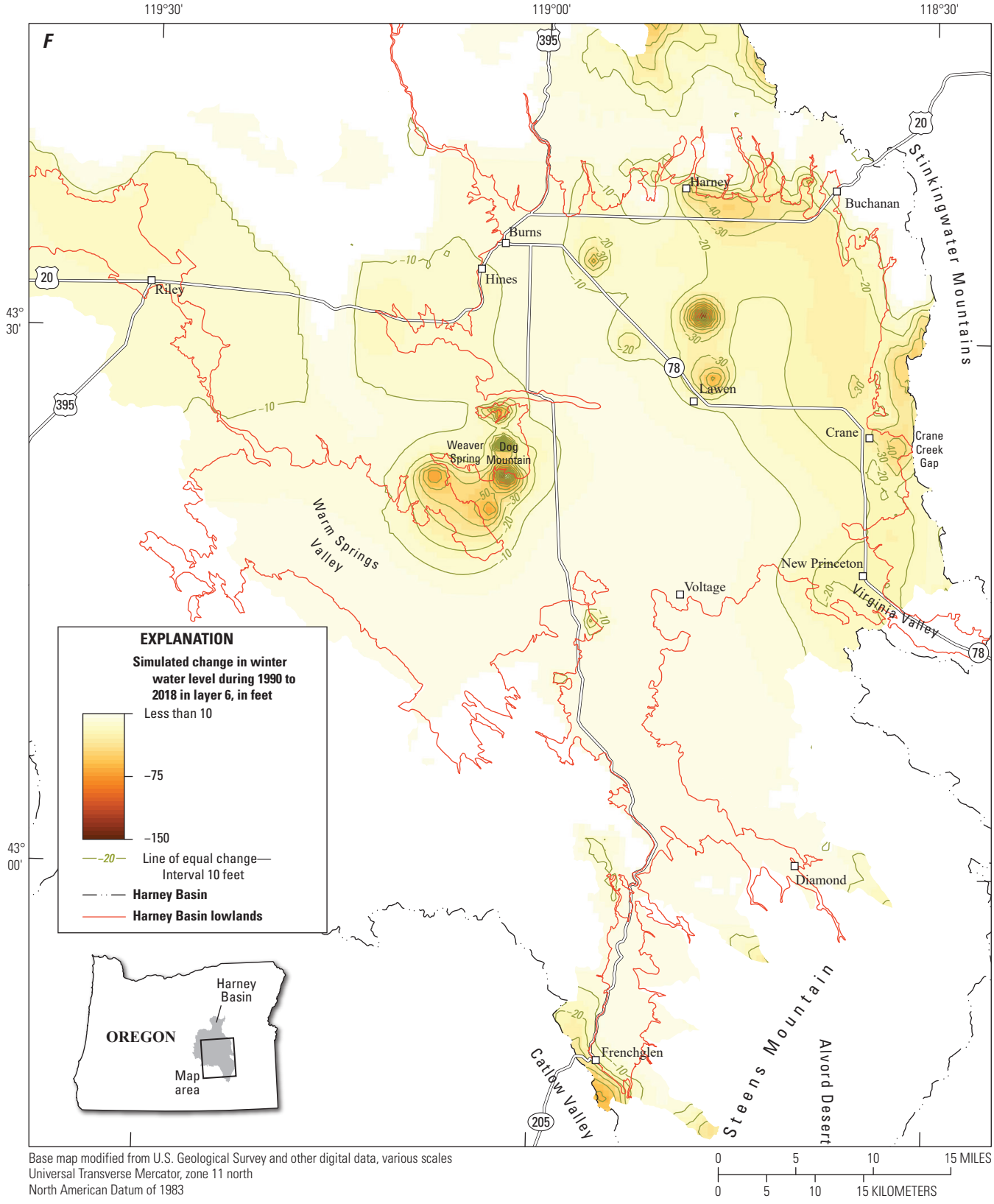

Figure 40.—Continued

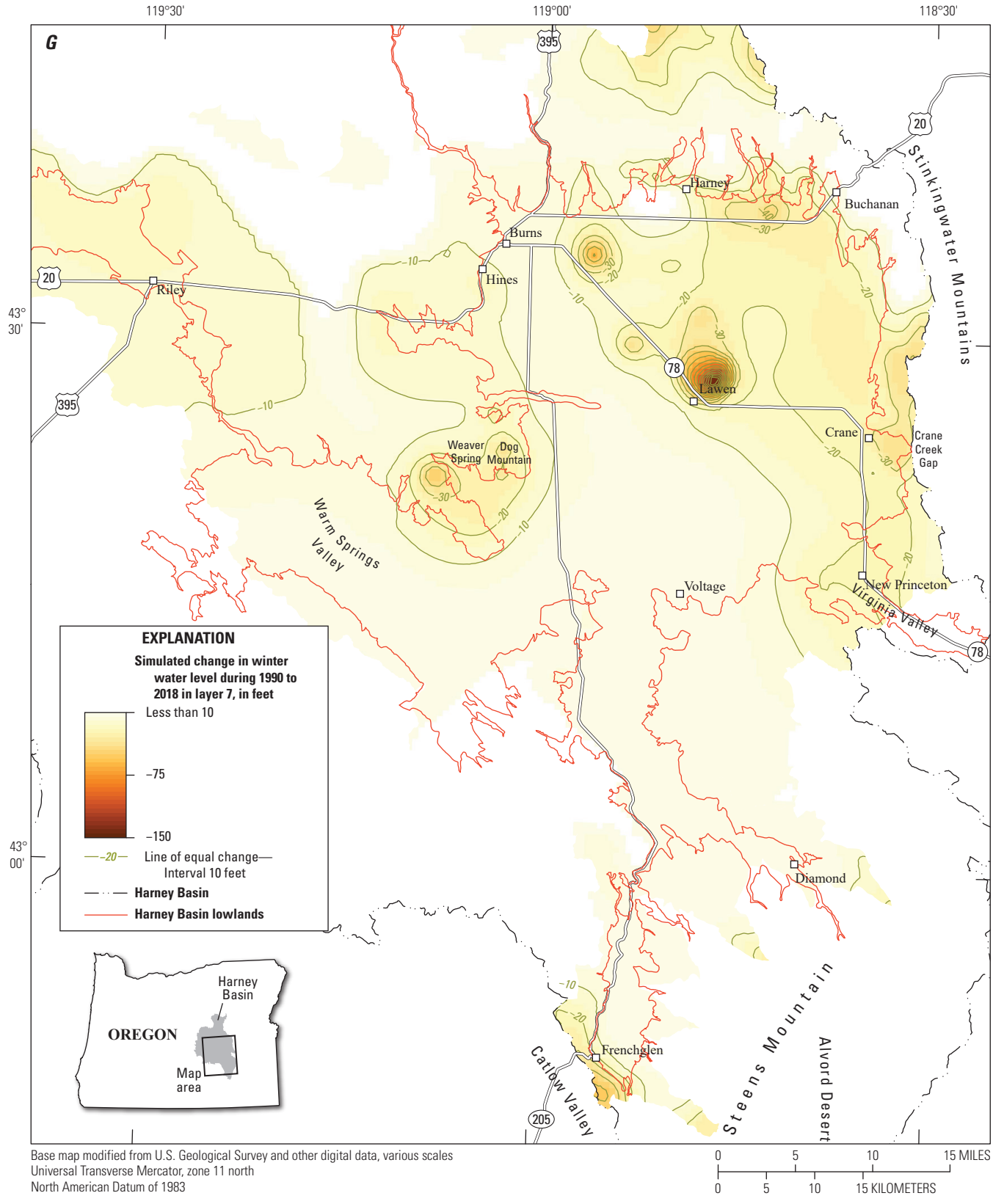

Figure 40.—Continued

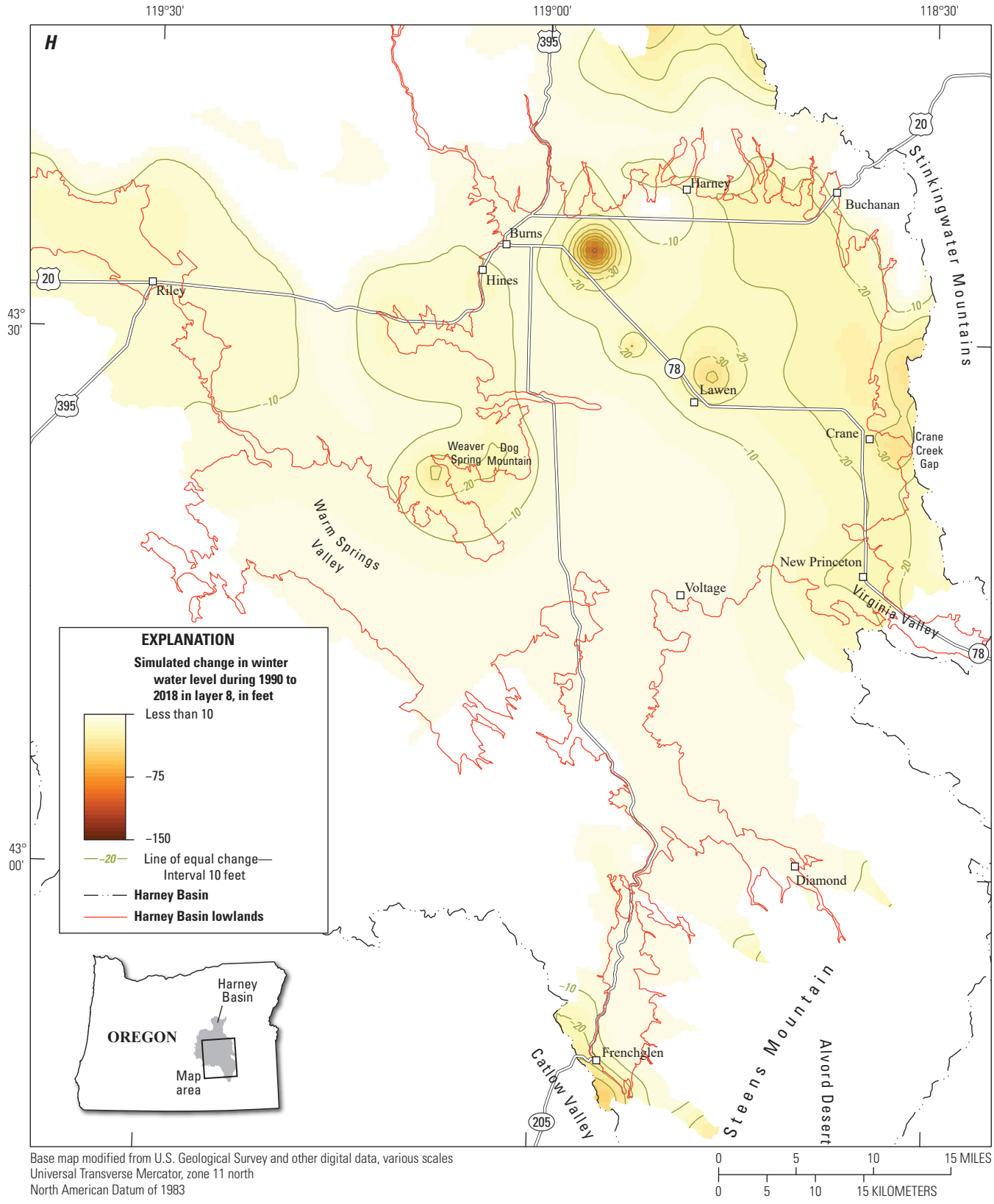

Figure 40.—Continued

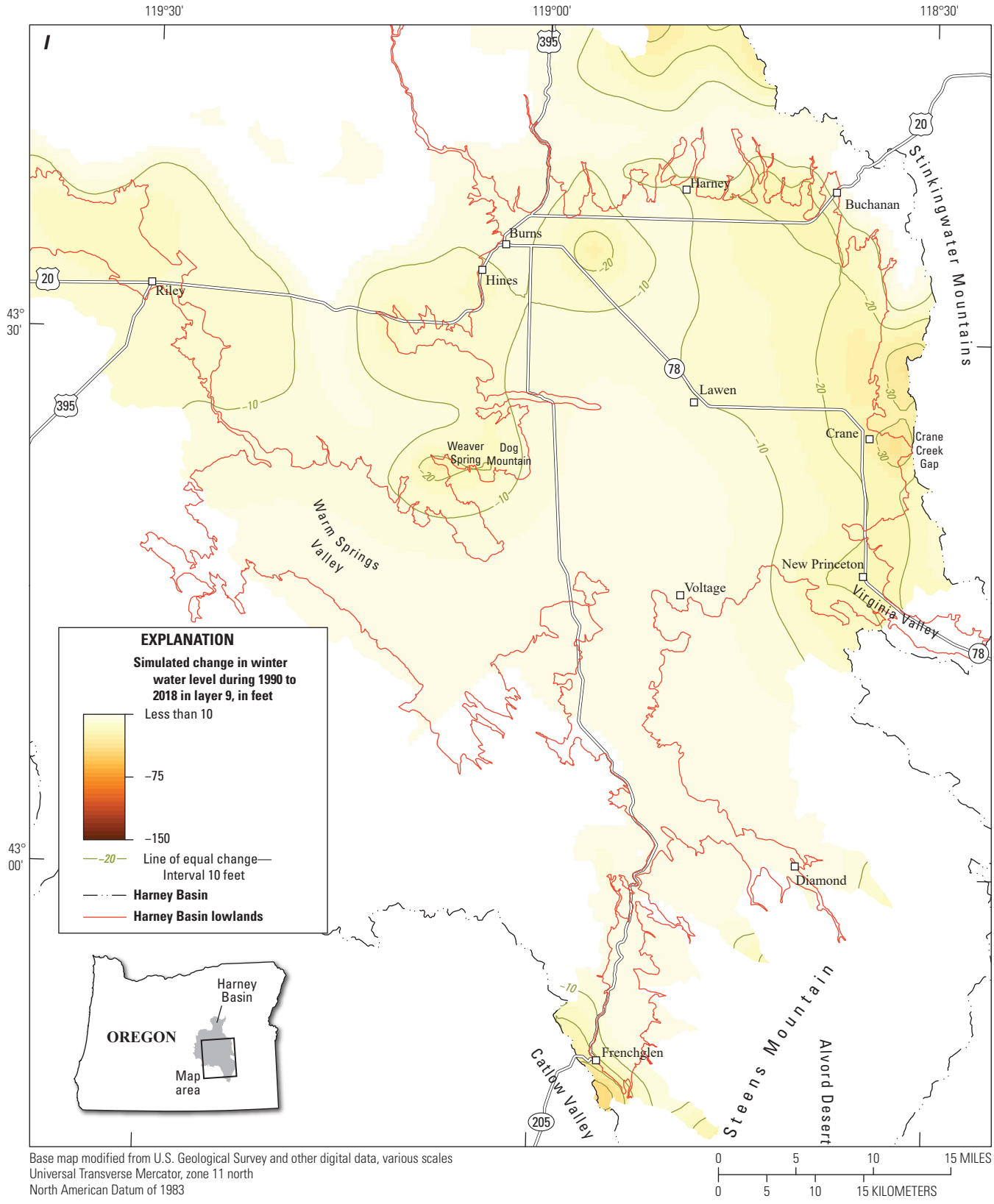

Figure 40.—Continued

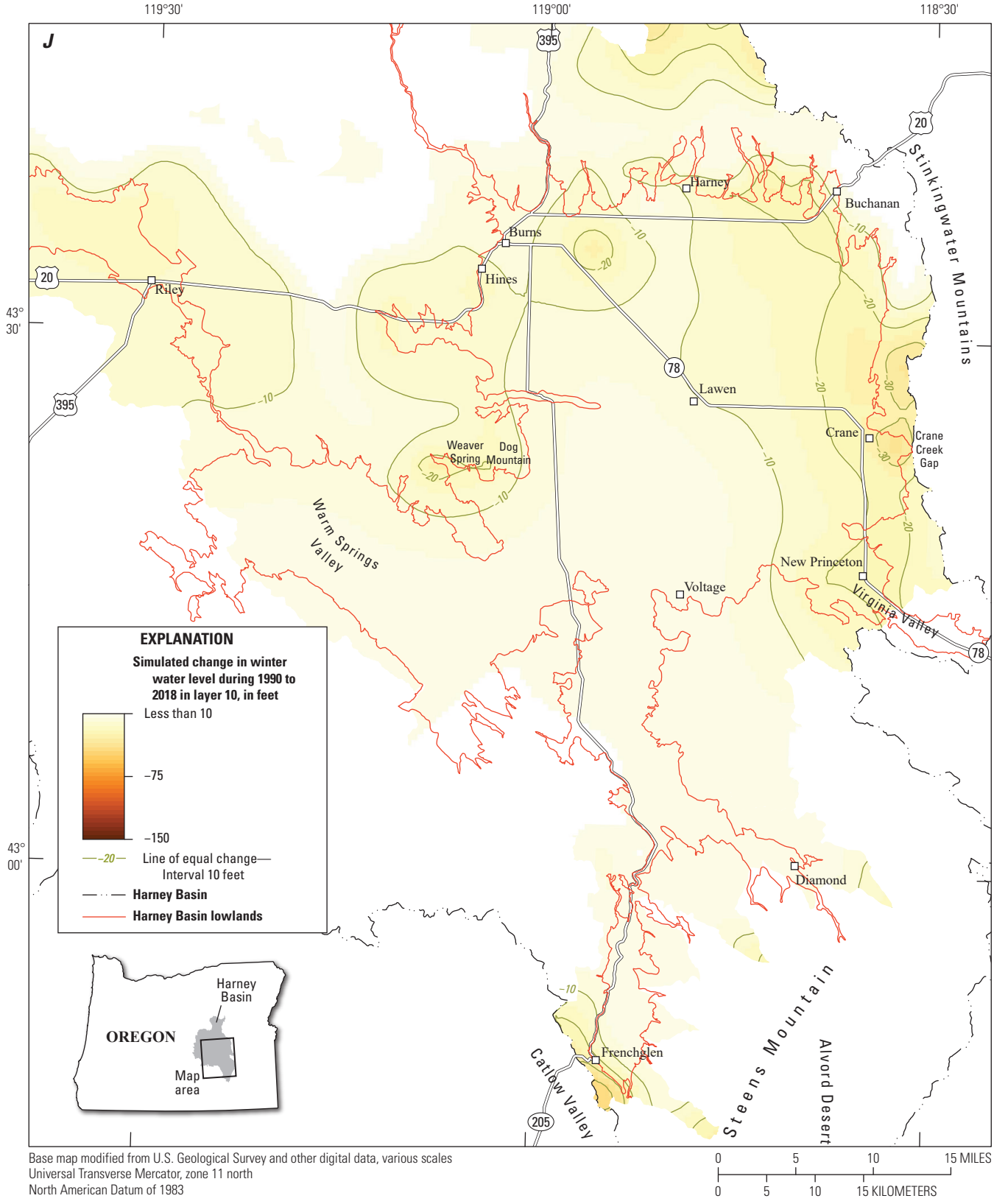

Figure 40.—Continued

Comparison of Estimated Base Flow to Simulated Stream Discharge

The calibration target for upland discharge was specified to adequately represent the total volume of water discharging as base flow so that the volume of water remaining in the upland groundwater-flow system to flow into the lowlands is accurately represented. To determine how well the HBGM results reflect the measured base-flow estimates, one measure of model fit compares base flows estimated for water years 1982–2016 to the simulated groundwater discharge to streams during the same time on a graph; an exact match would cause all observations to lie on the one-to-one (1:1) correlation line. The simulated groundwater discharge to streams in the HBGM are plotted relative to the estimated stream base flow for various streamgaged watersheds throughout the basin (fig. 41). Simulated drain discharges that are above the 1:1 correlation line indicate that the model overestimates the discharge; conversely, simulated discharges that are below the line indicate the model underestimates the discharge.

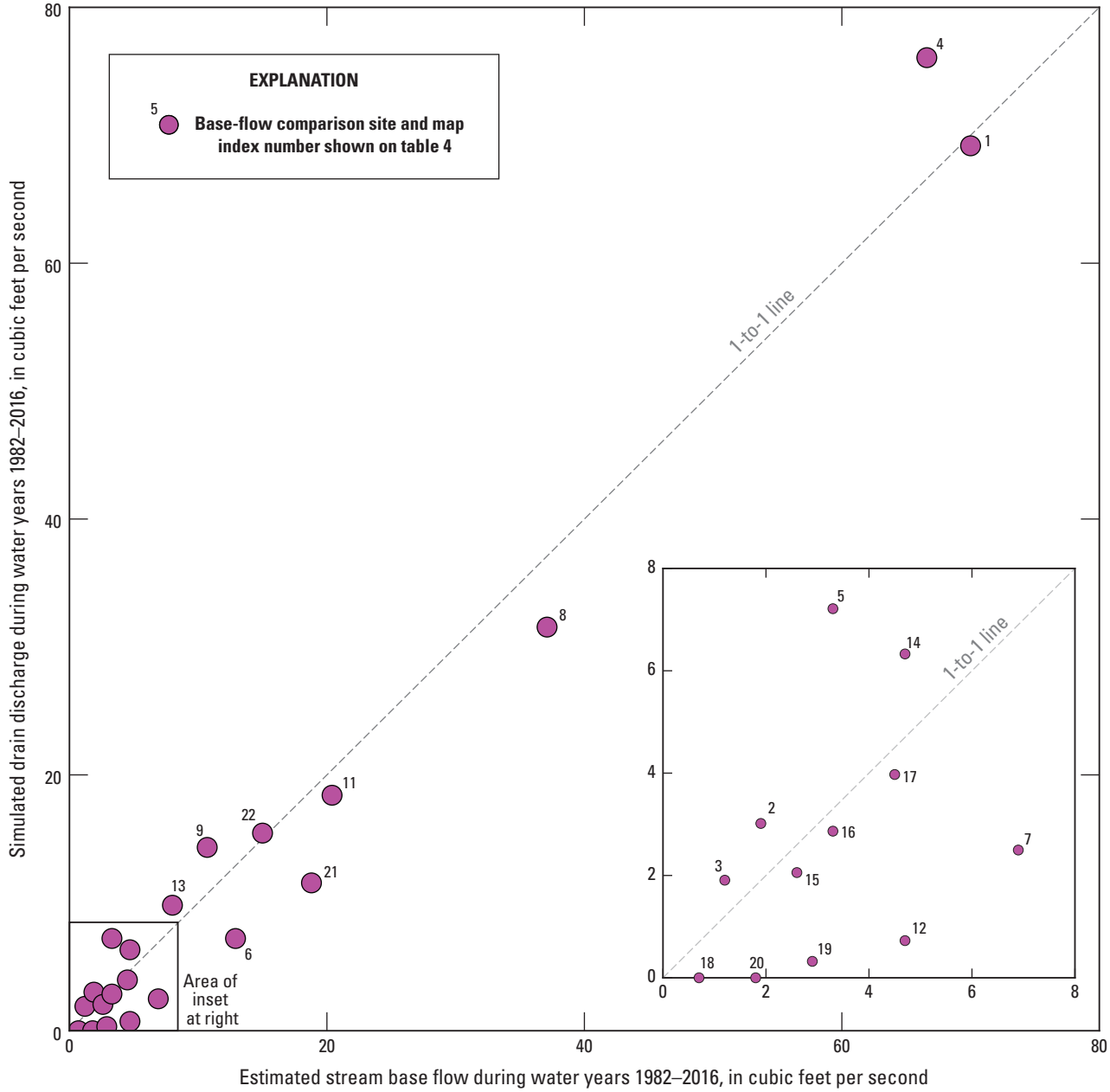

Figure 41. Simulated stream discharge compared to estimated base flow during water years 1982–2016 (from Garcia and others [2022]) in the Harney Basin Groundwater Model (Gingerich, 2024), Harney Basin, southeastern Oregon. Numbers correspond to subbasin numbering on figure 22 and table 4.

The simulated stream discharge matches stream base-flow estimates within about 5 percent over the entirety of the HBGM (table 4). The Northern region has the closest match followed by the Southern region and the Western region. The sum of simulated Northern region discharge is 111.3 cubic feet per second (ft^3/s), an excellent match with the estimated base flow of 111.4 ft^3/s. The sum of the simulated Southern region discharge is 154.5 ft^3/s, a 4-percent underestimate of the base flow. The Western region simulated discharge is underestimated at 18.7 ft^3/s, a relative error of −27 percent. For each region, the largest discharge estimates for the Silvies River, Donner und Blitzen River, and Silver Creek watersheds are the closest to the target values. The comparisons for the smaller watersheds are more variable. Due to the size of the model cells, stream-bottom and spring elevations were highly generalized depending on topography; therefore, larger watersheds tend to have better matches as overestimates and underestimates of individual drain cells offset each other along the course of the streams.

Table 4. Summary of comparisons between simulated drain discharge and estimated base flow (Garcia and others, 2022) for the transient-state simulation, Harney Basin Groundwater Model (Gingerich, 2024), 1982–2016, southeastern Oregon.

[Map index number: Locations of streamgaged and ungaged watersheds are shown on figure 22. Estimated base flow scaled to 1982–2016 from Garcia and others (2022). **Abbreviations**: USGS, U.S. Geological Survey; OWRD, Oregon Water Resources Department; ft^3/s, cubic feet per second; NA, not applicable]

Site name	USGS/OWRD site number (other site number)	Map index number	Region	Estimated base flow scaled to 1982–2016 (ft^3/s)	Model-simulated drain discharge during 1982–2016 (ft^3/s)	Relative error (percent)	MODFLOW 6 drain observation files representing watershed
Silvies River near Burns, OR	10393500	1	Northern	70.0	69.2	–1	L_Silvies.drn, L_Silvies2.drn, CricketCrk.drn, Emigrant_Crk.drn, Emigrant_Crk2.drn, Trout_Crk.drn, Silvies_SodaSpr.drn,
Rattlesnake Creek near Harney, OR	10394600	2	Northern	1.9	3.0	59	Rattlesnake_Crk.drn
Rock Creek near Burns, OR	10395600	3	Northern	1.2	1.9	59	Rock_Crk.drn
Sagehen Creek at Silvies River	31200202	12	Northern	4.7	0.7	–85	SageHen_Crk.drn, WillowCrk.drn
Poison Creek Slough at Ninemile Slough	31200106	13	Northern	8.0	9.8	23	Poison_Crk.drn
Malheur Slough above Ninemile Slough	31200107	14	Northern	4.7	6.3	35	Cow_Crk.drn, Rock_Crk.drn, LittleRockCrk.drn
Hot Springs Slough at Malheur Slough	31200102	15	Northern	2.6	2.1	–21	Curtis_Crk.drn, Mahon_Crk.drn, Crowcamp_Crk.drn
Soldier Creek at Poison Creek Slough	31200105	16	Northern	3.3	2.9	−13	Soldier_Crk.drn, Prater_Crk.drn
Silvies River below Soda Spring near Seneca, OR	10392400	22	Northern	15.0	15.4	3	Silvies_SodaSpr.drn, Bear_Crk.drn
Total for Northern Region				111.4	111.3	0	
Donner und Blitzen River near Frenchglen, OR	10396000 (357010)	4	Southern	66.6	76.1	14	Blitzen.drn
Mud Creek near Diamond, OR	10396500	5	Southern	3.3	7.2	118	Mud_Crk.drn
Bridge Creek near Frenchglen, OR	10397000 (357004)	6	Southern	12.9	7.2	−44	Bridge_Crk.drn
Krumbo Creek, below Krumbo Reservoir	357009	7	Southern	6.9	2.5	−64	Krumbo_Crk.drn
Kiger Creek near Diamond, OR	10399000	8	Southern	37.1	31.6	−15	Kiger.drn
Mccoy Creek near Diamond, OR	10400000 (357007)	9	Southern	10.7	14.3	34	McCoy_Crk.drn
Cucamonga Creek at Kiger Creek	31200303	17	Southern	4.5	4.0	−12	Cucamonga.drn
Riddle Creek area	NA	21	Southern	18.8	11.6	−39	Happy_Vly.drn

Table 4. Summary of comparisons between simulated drain discharge and estimated base flow (Garcia and others, 2022) for the transient-state simulation, Harney Basin Groundwater Model (Gingerich, 2024), 1982–2016, southeastern Oregon.—Continued

[Map index number: Locations of streamgaged and ungaged watersheds are shown on figure 22. Estimated base flow scaled to 1982–2016 from Garcia and others (2022). **Abbreviations**: USGS, U.S. Geological Survey; OWRD, Oregon Water Resources Department; ft^3/s, cubic feet per second; NA, not applicable]

Site name	USGS/OWRD site number (other site number)	Map index number	Region	Estimated base flow scaled to 1982–2016 (ft^3/s)	Model-simulated drain discharge during 1982–2016 (ft^3/s)	Relative error (percent)	MODFLOW 6 drain observation files representing watershed
Total for Southern Region				160.8	154.4	−4	
Silver Creek below Nicoll Creek near Riley, OR	10403400	11	Western	20.4	18.4	−10	Silver_Nicholl.drn, Silver_Nicholl2.drn, NicollCrk.drn, Claw_Crk.drn
Chickahominy Creek at Silver Creek	31200402	18	Western	0.7	0.0	−100	Chickahominy.drn
Miller Canyon Creek at Silver Creek	31200404	19	Western	2.9	0.3	−89	Miller_Can.drn
Virginia Creek at Silver Creek	31200403	20	Western	1.8	0.0	−100	RockQuarry_Crk.drn, Pine_Springs_Crk.drn
Total for Western Region				25.8	18.7	−27	
Total for Harney Basin Groundwater Model				298.0	284.4	–5	

Model Sensitivity to Parameters

The variety of parameter values in the model was kept to a minimum to avoid creating an overly complex model that could not be justified on the basis of existing information. Hydrologic data do not exist to parameterize local heterogeneity. Through the calibration process, several hydrologic properties stood out as having the most influence on the model and on affecting the fit between measured and simulated groundwater levels and flows in various areas. Hydraulic conductivities of HUs underlying the uplands were the key parameters for matching upland groundwater levels and stream discharge (base flow) but these parameters had minimal direct effect on lowland groundwater levels. The main goal for calibrating groundwater levels and discharge in the uplands was having the HBGM calculate a reasonable representation of the amount and distribution of groundwater leaving the uplands and entering the lowland groundwater-flow system. Where different combinations of parameter values gave similarly reasonable results, the parameters were set at reasonable values and kept constant for the remaining simulations to keep the model as simple as possible. In the lowlands, the horizontal hydraulic conductivity of the Younger basin fill and Older basin fill HUs controlled the groundwater levels (including the magnitude and extent of declines), especially in layers 1–5. These two HUs were lumped together in the lowlands and modifications were made to the kriged surfaces for each layer to obtain better matches to measured groundwater levels. Modifications were deliberately kept to broad areas to avoid placing too much weight on matching groundwater levels at individual wells.

Simulated Groundwater Budget

The lowland groundwater budget components (fig. 42) were extracted from the model budget output file using Zonebudget for MODFLOW 6 (Langevin and others, 2022) with delineated zones for the uplands and lowlands and the regions (Northern, Southern, Western) that were presented in Garcia and others (2022). The simulation shows fluctuations in recharge to the lowlands coincide with the substantial variations in streamflow infiltration and varied yearly (due to scaled precipitation; fig. 8) and monthly (due to irrigation pumping cycles). Direct groundwater inflow from the uplands to the lowlands (recharge by underflow on fig. 42)

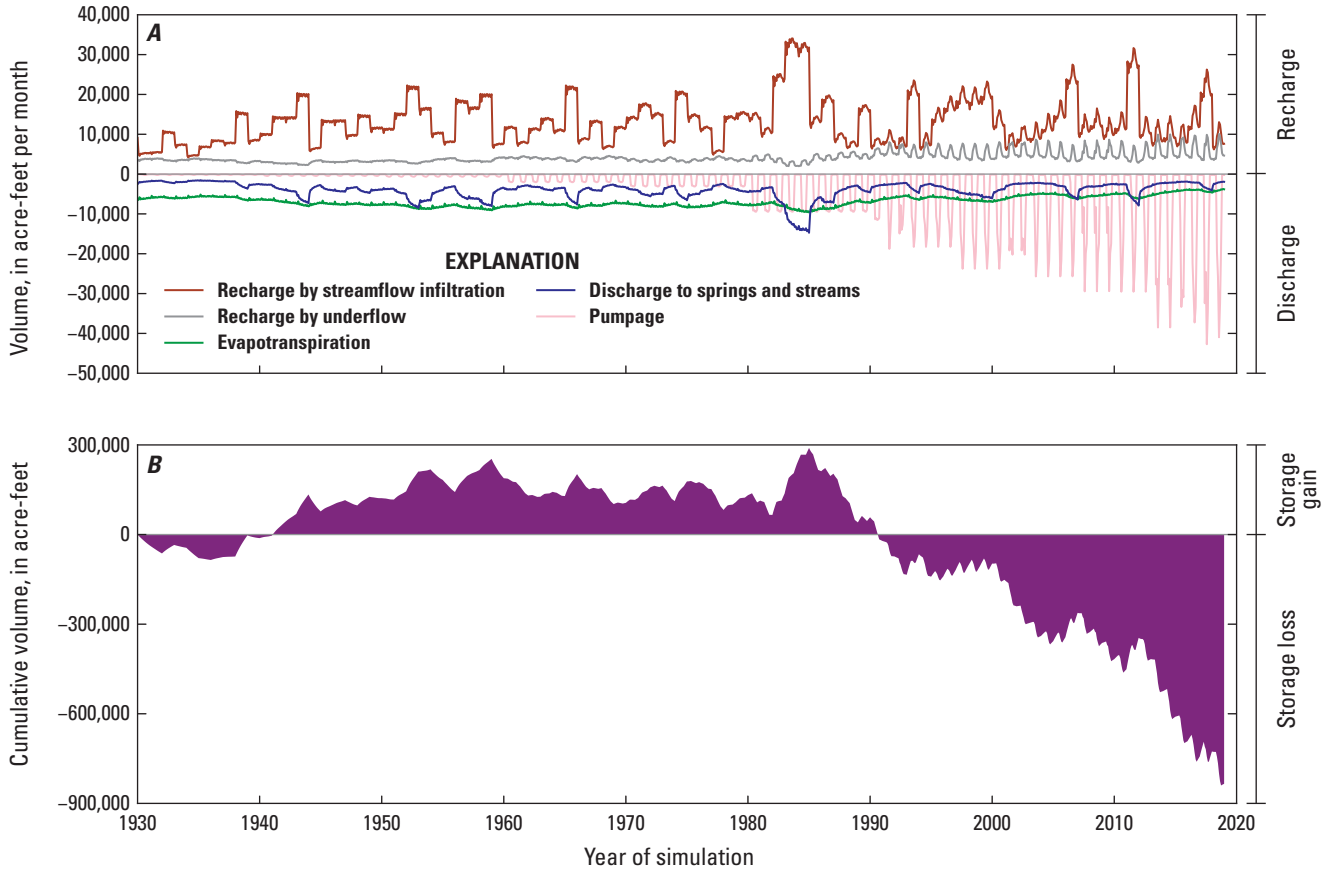

Figure 42. Simulated lowland (*A*) groundwater-budget components and (*B*) cumulative change in groundwater storage, 1930–2018, in the Harney Basin Groundwater Model (Gingerich, 2024), Harney Basin, southeastern Oregon.

remained relatively steady until about 1980 when groundwater pumpage began to induce additional flow from the uplands by increasing the groundwater gradient toward the pumping locations. In the mid-1980s, groundwater inflow decreased slightly for several years, likely due to the higher groundwater levels in the lowlands created during the wettest period of the transient simulation. As groundwater pumpage increased after 1990, the volume of groundwater inflow increased and followed the seasonal pumping patterns.

Prior to the mid-1980s, monthly groundwater inflow from uplands to lowlands ranged from about 3,500 to 4,200 acre-ft, totaling about 42,000 acre-ft annually. By 2018, a year with lower-than-average recharge but substantial pumpage, monthly fluctuations in groundwater inflow from the uplands ranged from 3,500 acre-ft in February to 10,000 acre-ft in July, totaling about 60,000 acre-ft annually. In the HBGM, these seasonal fluctuations are due to the steep gradients between the lowlands and uplands created during the height of the irrigation season when groundwater withdrawal rates are largest. The seasonal fluctuations in inflow from the uplands displayed in the HBGM may be an artifact of how the uplands and lowlands are defined, especially in the upper Silver Creek floodplain, where the fluctuations are largest. In places, the lowlands form a thin band with uplands on either side. Wells in this area penetrate the highly permeable zone at depth, which stretches beneath the uplands and lowlands in this area and provides a conduit for relatively easy movement of water back and forth between the two zones as pumping cycles on and off annually. No measurements or observations are available anywhere in the Harney Basin to confirm or refute whether these seasonal fluctuations actually occur in the groundwater-flow system.

Prior to 1980, groundwater discharge was dominated by ET, with discharge to streams occasionally increasing to about the same rates as those of ET in the wetter years (fig. 42*A*). After 1980, the increased pumpage coincided with decreases in simulated ET and discharge to streams. The monthly volume of simulated ET averaged about 7,400 acre-ft (about 89,000 acre-ft annually) prior to 1980, but with the exception of a few wet periods, declined relatively steadily after that, so that by 2018 the monthly simulated ET was about 4,100 acre-ft (about 49,000 acre-ft annually). Simulated discharge to streams averaged about 3,800 acre-ft per month (about 46,000 acre-ft annually) prior to 1980 but was only about 2,200 acre-ft per month (about 26,000 acre-ft annually) in 2018. Simulated outflow to the adjacent Malheur River Basin through Virginia Valley followed a similar pattern of decline after 1980 and by 2018 had been reduced to zero flow during the months of highest pumpage (fig. 43).

The HBGM simulated water budget is compared with the water-budget components estimated for the lowlands during 1982–2016 (Garcia and others, 2022) to demonstrate how reasonably HBGM represents the overall groundwater-flow system (table 5). As expected, the simulated surface inflow from streams and irrigation closely matches the estimated value because this component of recharge is assigned to recharge cells in the HBGM. The value for groundwater inflow from the uplands is calculated by the HBGM and depends on designated upland recharge and the gradient between the uplands and the lowlands where inflow takes place. During 1982–2016, lowland recharge by groundwater inflow from uplands totaled about 49,000 acre-ft/yr and was estimated by subtracting upland base flow and spring discharge from upland recharge estimates (Garcia and others, 2022). The simulated groundwater inflow from the uplands for the same period was about 60,000 acre-ft/yr, a relative difference of about 22 percent (table 5). As noted previously, prior to 1980 when pumpage was much less, the simulated groundwater inflow from the uplands averaged about 45,000 acre-ft/yr, a value much closer to the inflow estimate.

Some accounting details must be considered when comparing the ET and surface-water discharge of Garcia and others (2022) to water budget components of the HBGM. The estimated mean annual volume of ET from natural, non-irrigated areas across the Harney Basin lowlands of Garcia and others (2022), which totaled 119,000 acre-ft, includes discharge from most lowlands springs. This includes the large volume of spring discharge in Warm Springs Valley, which is accounted for as ET from irrigated and non-irrigated vegetation and (or) evaporation from open water. The remaining volume of discharge to lowland springs was estimated at 8,900 acre-ft. Many of the springs included in the ET estimate of Garcia and others (2022) are simulated separately in the HBGM, so simulated spring discharge is larger and simulated ET is smaller than their respective estimates. The proper way to compare these estimated and simulated budget components is to compare sums of ET and discharge to springs and streams. Together ET and spring discharge were estimated by Garcia and others (2022) as 127,900 acre-ft/yr. The sum of the simulated ET and spring discharge in the HBGM is about 124,000 ac-ft/yr, a relative difference of about −3 percent when compared to the water-budget estimate (table 5).

Lowland spring discharge simulated by the HBGM can also be compared to field measurements. Comparing the simulated lowland spring discharge to measured values is, however, problematic, as few individual measurements are available. Measured discharge from lowland springs totaled about 34,000 acre-ft/yr, mostly from Warm Springs Valley and Sodhouse Spring, with a springflow measurement accuracy of about 15 percent (Garcia and others, 2022). Total lowland springflow simulated in the HBGM is about 51,000 acre-ft/yr, or about 50 percent higher than the estimated value. This difference could be due to the uncertainty in springflow measurements and the lack of available estimates of springflow or base flow in most of the Southern region and large expanses of the Western region to compare with the HBGM.

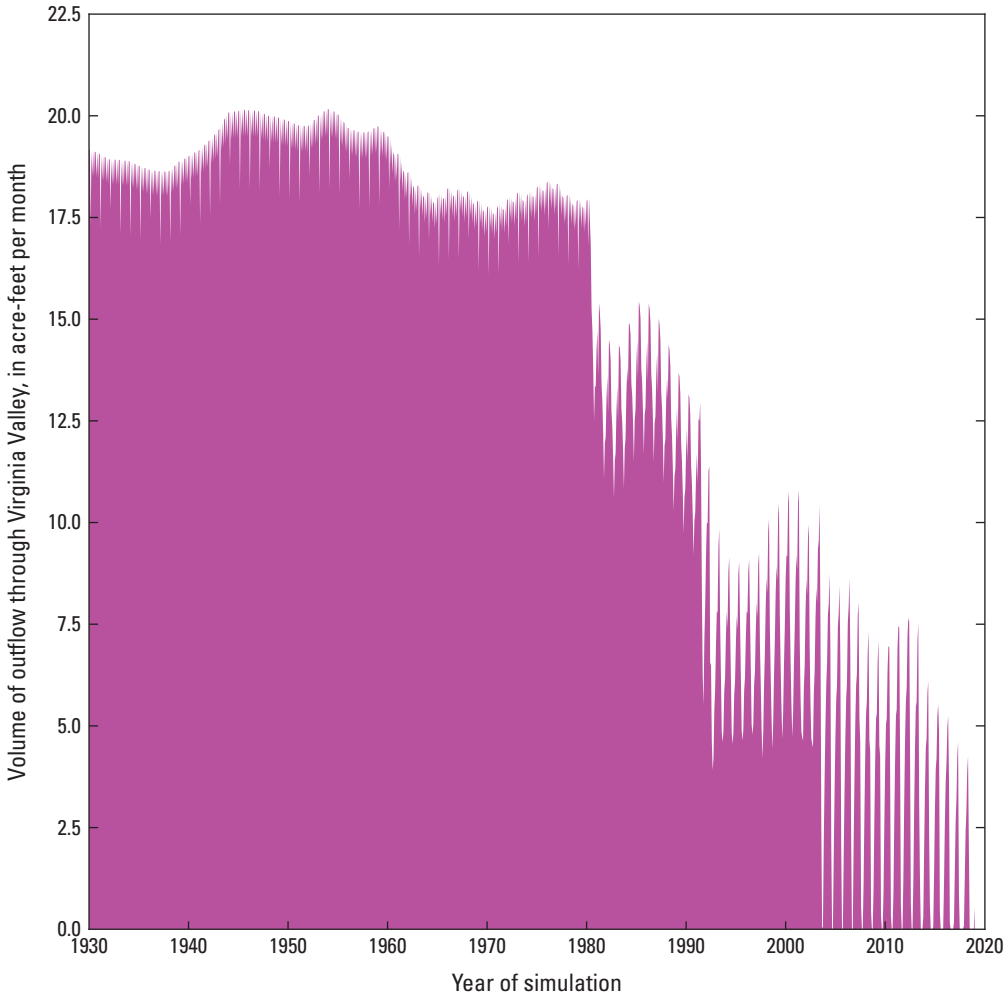

Figure 43. Simulated discharge to the Malheur River Basin through Virginia Valley, 1930–2018, in the Harney Basin Groundwater Model (Gingerich, 2024), Harney Basin, southeastern Oregon.

Table 5. Summary of comparisons between estimated lowland water-budget components (Garcia and others, 2022) and lowland water-budget components for the transient-state simulation, Harney Basin Groundwater Model (Gingerich, 2024), 1982–2016, Harney Basin, southeastern Oregon.

[Estimated values from Garcia and others (2022). **Abbreviation**: acre-feet per year, ac-ft/yr]

Lowland water budget component	Estimated (ac-ft/yr)	Simulated (ac-ft/yr)	Relative difference (percent)
Groundwater inflow from uplands	49,000	59,956	−22
Surface inflow from streams and irrigation	116,000	117,687	−1
Discharge to springs and surface water	8,900	50,330	−466
Discharge through evapotranspiration	119,000	73,932	38
Combined spring and evapotranspiration	127,900	124,262	3
Discharge to adjacent basins	3,100	87	97

Groundwater Storage

Simulated lowland groundwater storage in the HBGM was characterized by gains during periods of above-average recharge and minimal pumpage followed by losses as pumpage increased and recharge decreased (fig. 42*B*). During 1930–40, the groundwater reservoir had a small cumulative net loss relative to the pre-1930 condition, totaling about −85,000 acre-ft. During 1940–89, the lowland system gained groundwater, peaking in 1985 after several very wet years at around 290,000 acre-ft more than the pre-1930 condition. As groundwater pumpage increased from 1990 onward, losses in cumulative groundwater storage increased and the simulated deficit in groundwater storage, compared with the pre-1930 condition, totaled about −840,000 acre-ft by 2018.

To better understand the effects of pumpage on the lowland groundwater budget, a comparison was made between the calibrated transient simulation and an equivalent simulation for the same time period, but with all pumpage turned off. Cumulative pumpage in the transient simulation during 1930–2018 totaled about 3.4×10^6 acre-ft. In the non-pumpage simulation, cumulative lowland evapotranspiration totaled about 1.2×10^6 acre-ft higher, cumulative drain discharge totaled about 1.1×10^6 acre-ft higher, and the cumulative surplus in groundwater storage totaled about 1.1×10^6 acre-ft larger. As expected, the cumulative difference in lowland ET, drainage, and storage between the two simulations was nearly equivalent to the cumulative lowland pumpage used in the calibrated transient simulation. This total volume of pumped water in the HBGM by the end of 2018 was supplied relatively equally by decreased lowland ET (35 percent), decreased lowland spring and stream discharge (32 percent), and the deficit in lowland groundwater storage (32 percent).

Future Scenarios

The HBGM was used to quantify changes in groundwater level and storage under two future hypothetical withdrawal scenarios. These were selected to better understand potential future conditions under present pumpage rates and to better understand how groundwater might recover under reduced pumpage conditions. In scenario 1, all irrigation pumpage for 2018 continues unchanged until 2100 and, in scenario 2, all irrigation pumpage ceases after 2018. These simulations are meant to explore a wide range of possible future conditions and are not meant to recommend any particular management alternatives. Recharge for both scenarios is based on average precipitation and land use during 1982–2016. The simulated initial conditions for the future scenarios are the final conditions (end of 2018) from the calibrated transient simulation.

Scenario 1—2018 Withdrawal Rates and Locations With Average Recharge

In scenario 1, average 1982–2016 recharge and the most recent withdrawals are used to simulate the effects on the lowland groundwater-flow system by continuing the 2018 groundwater-use conditions through 2100. At the end of the 82-year simulation, the areas of decline deepened and expanded due to continued pumpage and the subsequent removal of water from groundwater storage (figs. 44–45). The areas with the largest groundwater-level declines are the Weaver Spring area with more than 210 ft, and the northern lowland area with more than 170 ft by 2100. Although the rate of decline in some areas decreased, most areas were still declining at the end of the simulation.

Because some model cells experienced more than 100 ft of groundwater-level decline, they became dewatered during certain months of the simulation. Pumping wells in these dewatered cells are subsequently unable to remove water so the model code reduces groundwater withdrawal from these cells to zero. At the end of scenario 1, the model-adjusted monthly pumpage was as much as 1.7-percent lower relative to the starting 2018 rates.

Overall, simulated groundwater discharge to springs and streams continued to decline throughout scenario 1, almost exclusively due to the decreases in the Western region of the study area (fig. 46). Groundwater discharge in the Western region during the first year of the simulation averaged about 1,100 acre-ft per month (totaling about 14,000 acre-ft per year) but decreased to about 550 acre-ft per month (totaling 6,700 acre-ft) during the final year of the simulation. For comparison, groundwater discharge in the Western region during 1990 totaled 19,400 acre-ft. Groundwater discharge to springs and streams in the Northern and Southern regions increases for the initial several years of the simulation because the 1982–2016 recharge used for scenario 1 is higher than the recharge during the final few years of the calibration simulation. By the last year of the simulation, total groundwater discharge in the Northern region was about 3,400 acre-ft; total discharge during 1990 was 3,300 acre-ft. In the Southern region total groundwater discharge was about 13,000 acre-ft in the final year of scenario 1 compared with about 13,700 acre-ft during 1990.

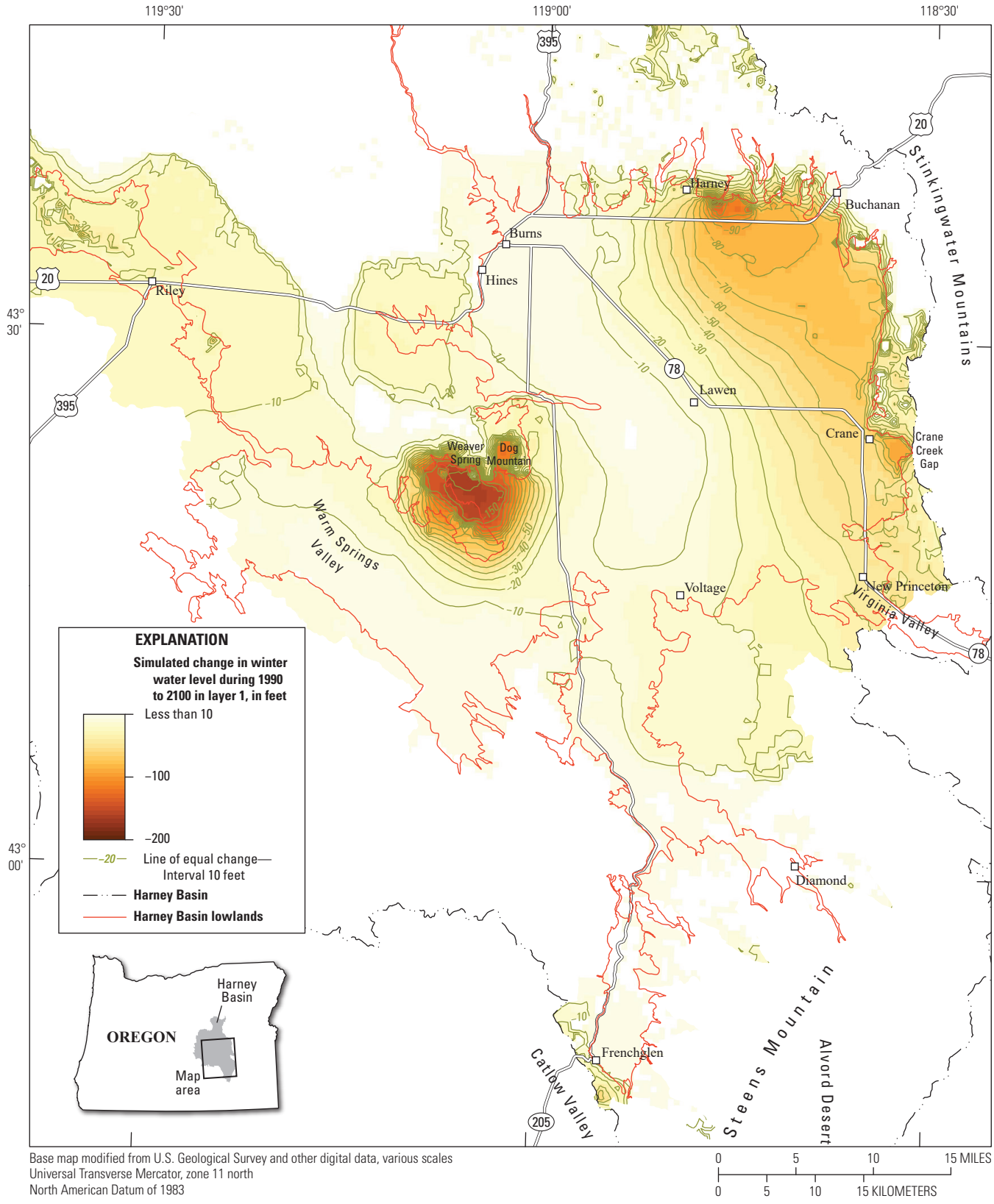

Figure 44. Simulated total lowland groundwater-level declines during 1990–2100 in layer 1 for scenario 1 (2018 pumpage continued during 2019-2100) in the Harney Basin Groundwater Model (Gingerich, 2024), Harney Basin, southeastern Oregon.

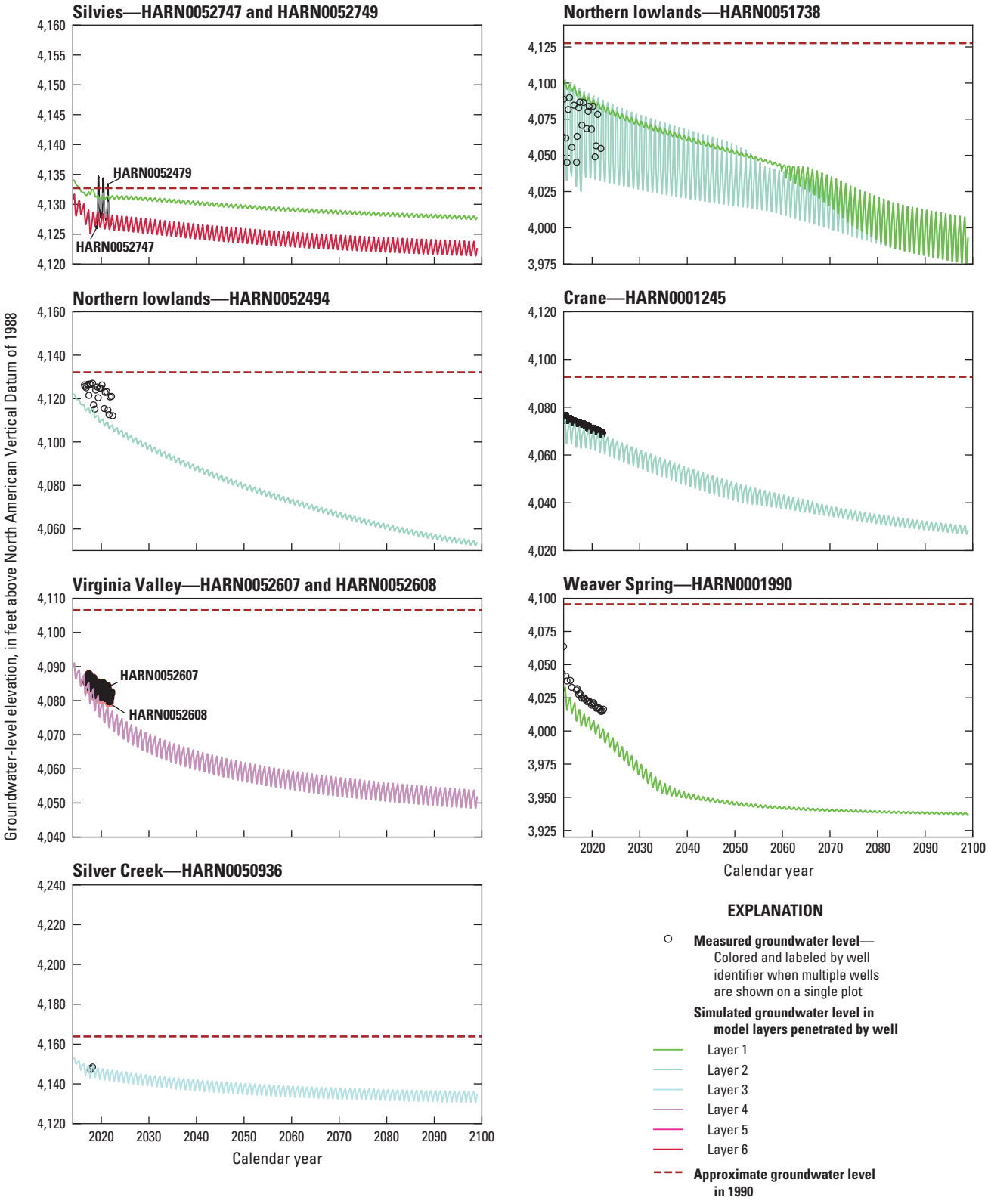

Figure 45. Simulated groundwater levels at selected lowland wells for scenario 1 (2018 pumpage continued during 2019–2100) in the Harney Basin Groundwater Model (Gingerich, 2024), Harney Basin, southeastern Oregon.

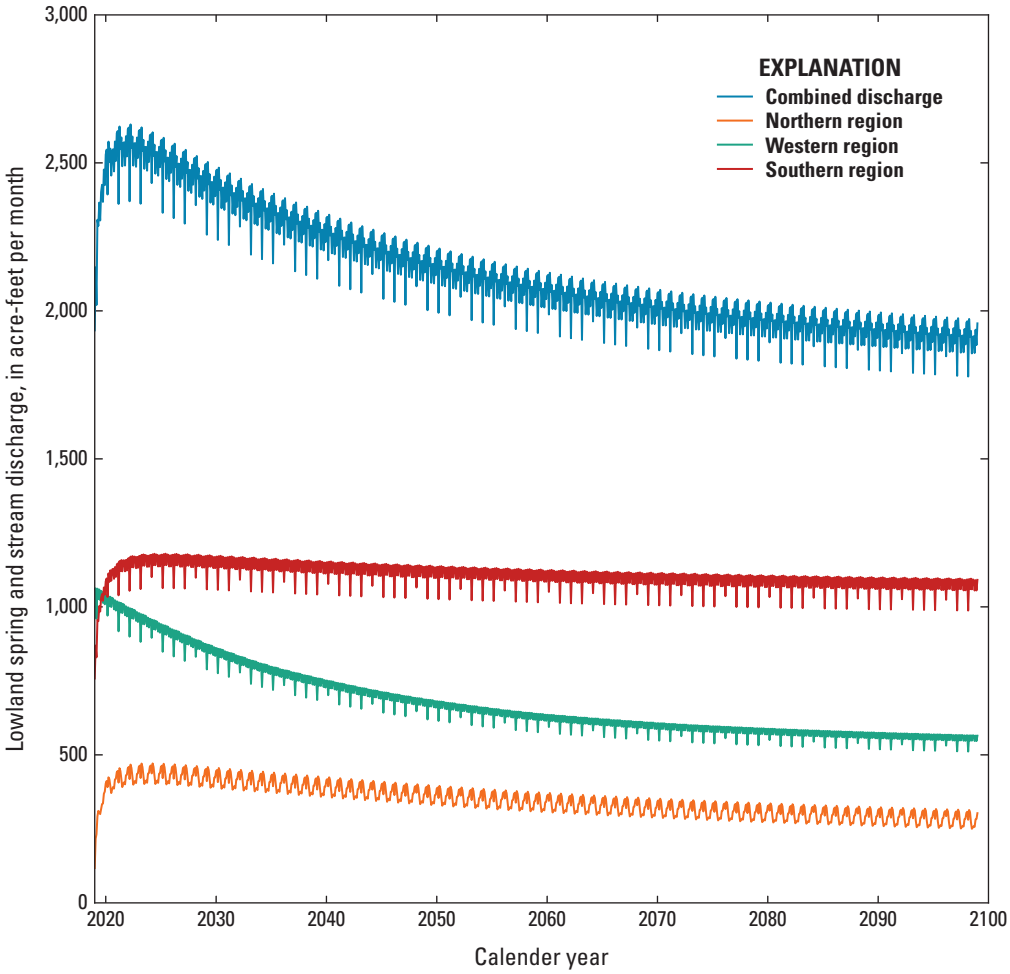

Figure 46. Simulated groundwater discharge to springs and streams for scenario 1 (2018 pumpage continued during 2019–2100) in the Harney Basin Groundwater Model (Gingerich, 2024), Harney Basin, southeastern Oregon.

Scenario 2—Zero Irrigation Pumpage With Average Recharge

In scenario 2, the simulation uses average 1982–2016 recharge and zero withdrawals after 2018 to evaluate the rate at which the lowland groundwater-flow system would return to groundwater-level conditions within 5 ft of 1990 conditions (fig. 47), a time prior to the subsequent decades having substantial pumpage. In this scenario the alluvial areas of the upper Silver Creek floodplain and the Weaver Spring area take the longest to recover to conditions similar (within 5 ft) to 1990 groundwater-level conditions (fig. 48). In both areas, groundwater levels take more than 60 years to recover to within 5 ft of 1990 levels. Parts of the Crane area take more than 40 years to recover, but most of the Crane area and the northeast part of the lowlands recovers in 20–30 years. Groundwater levels in most of the Virginia Valley area recover within 20 years. The areas that recover the fastest are along the Silvies and Donner und Blitzen River floodplains, where groundwater levels return to within 5 ft of 1990 levels in less than 10 years. Assuming all other simulated factors stay the same, future recharge lower than the 1982–2016 average would extend these durations and future recharge higher than the average would shorten the duration of recovery.

Groundwater discharge to springs and streams increases throughout the lowlands during scenario 2 (fig. 49). The largest increase is for springs and streams in the Northern region, with yearly totals increasing from about 4,000 acre-ft per year to about 22,000 acre-ft per year by the end of the simulation. The Southern region increases from about 12,000 acre-ft per year to about 19,000 acre-ft per year and the region is also the fastest to recover to a condition of steady discharge. The Western region takes the longest to recover and the discharge is still increasing at the end of the scenario. Here, the discharge increases from about 14,700 acre-ft per month to about 20,000 acre-ft per month by 2100.

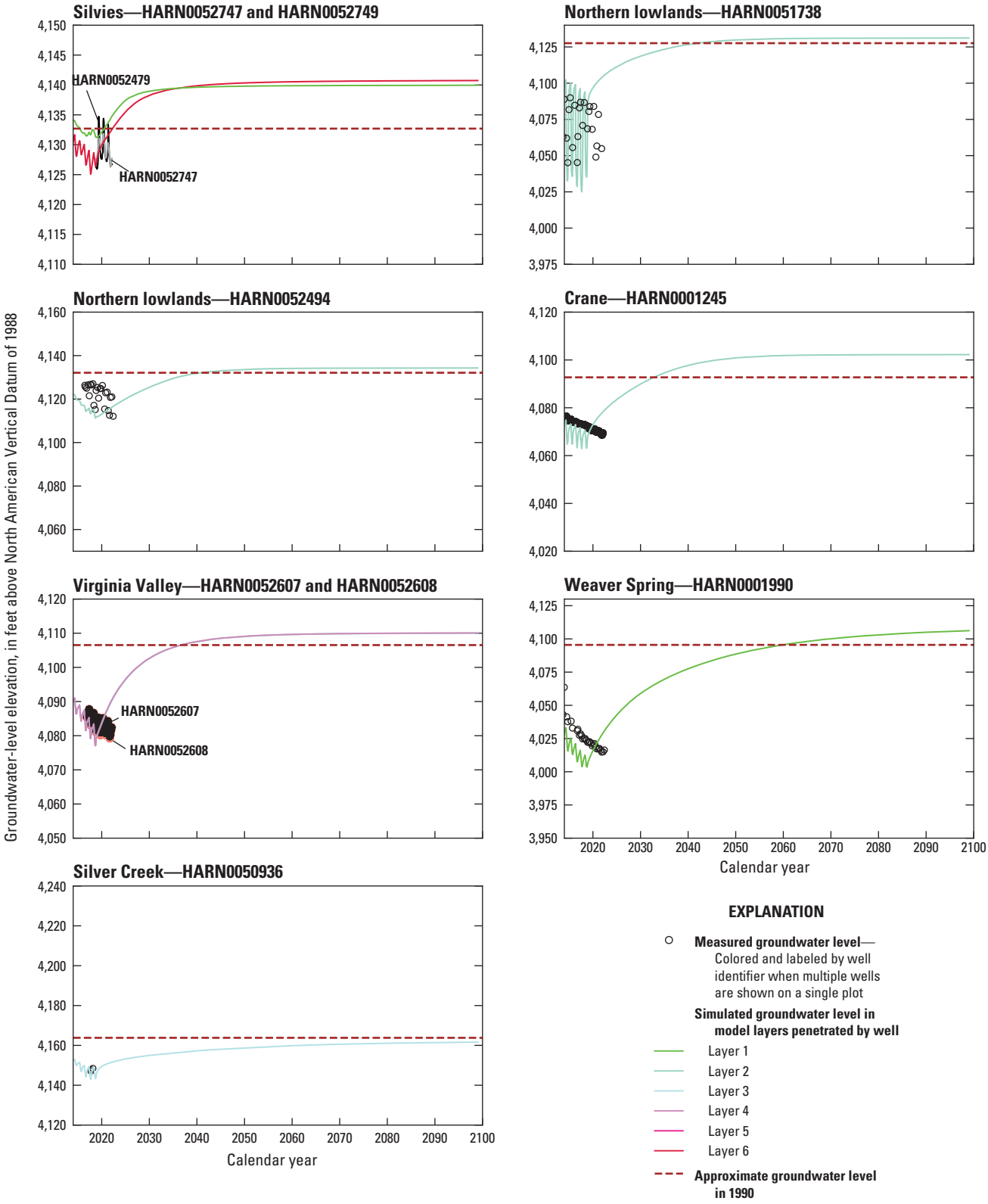

Figure 47. Simulated groundwater levels at selected lowland wells for scenario 2 (no irrigation pumpage during 2019–2100) in the Harney Basin Groundwater Model (Gingerich, 2024), Harney Basin, southeastern Oregon.

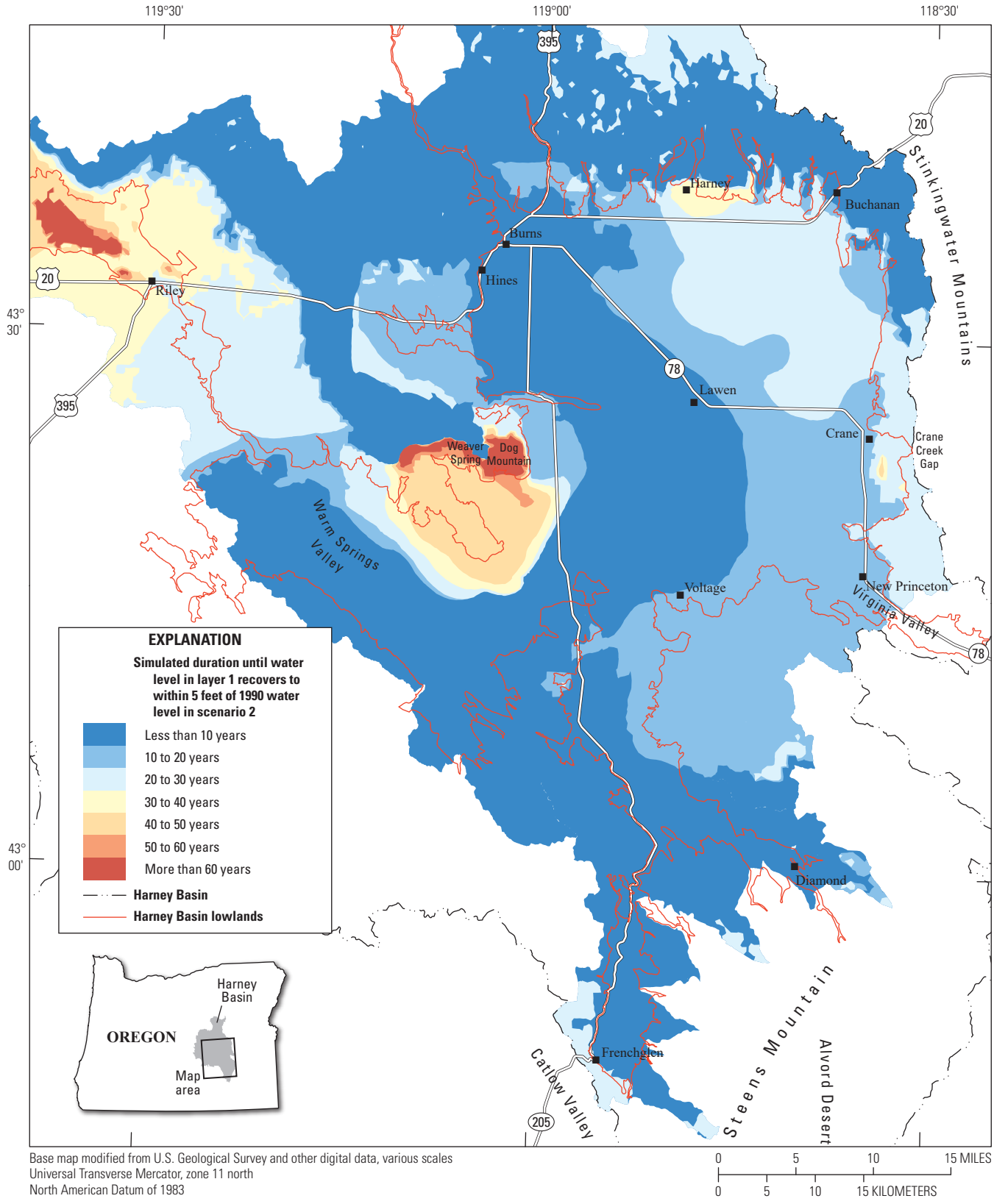

Figure 48. Simulated duration of recovery in layer 1 for scenario 2 (no irrigation pumpage during 2019–2100) in the Harney Basin Groundwater Model (Gingerich, 2024), Harney Basin, southeastern Oregon.

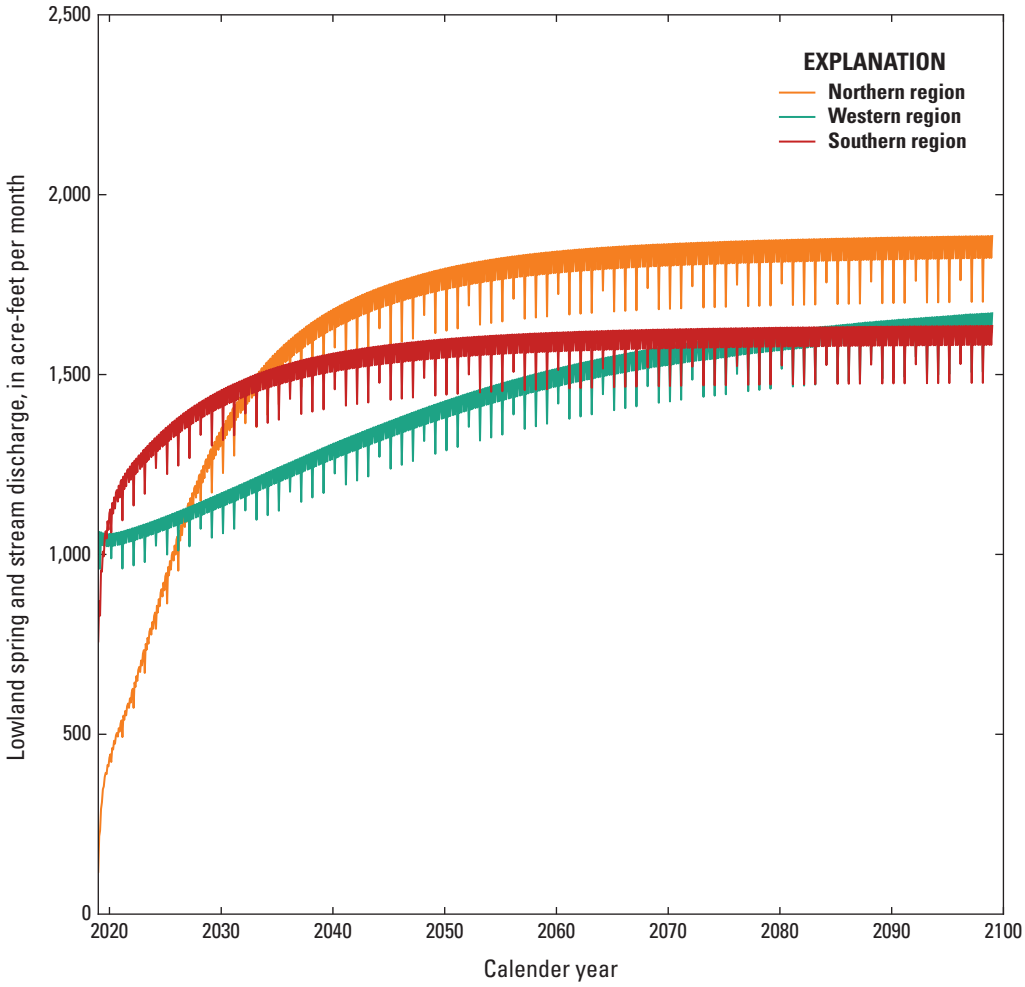

Figure 49. Simulated groundwater discharge to springs and streams for scenario 2 (zero irrigation pumpage continued during 2019–2100) in the Harney Basin Groundwater Model (Gingerich, 2024), Harney Basin, southeastern Oregon.

Model Uncertainty, Limitations, and Improvements

The HBGM documented in this report and provided in Gingerich (2024) is a mathematical simplification of a complex natural system and thus has inherent error and uncertainty. Model discretization, in space and time, can be a source of error. Geologic and hydrologic properties are assumed uniform within a model cell; however, variations in properties at scales smaller than that used for discretization can affect results in ways that are not represented by the model. The model solves for average conditions within each 92-acre cell for each time step with the parameters interpolated or extrapolated from measurements or estimated during calibration. In model cells containing more than one pumping well, the well locations and withdrawal rates are aggregated and generalized. The model cannot be used to differentiate water levels or effects on wells at scales smaller than the extent of a model cell. Likewise, simulated stress periods are discretized to a monthly time scale. Hydrologic conditions that occur at shorter time scales may not be accurately represented.

Differences between measured and simulated groundwater levels and groundwater discharge are greater in some areas than others, which may reflect uncertainties in the recharge or withdrawal estimates, boundary conditions, assigned parameter values in the model, or representations of the different hydrogeological features in the model. The recharge estimates are based on water-budget computations and assumptions about recharge mechanisms that could be improved with a better understanding of the spatial distributions of evapotranspiration, streamflow infiltration, and land-cover characteristics. Withdrawals represented in the model were based on the latest available information, much of which was estimated using remote sensing and incomplete water-use records. Unreported withdrawals and uncertainties in reported withdrawals that cannot be quantified also affect the model accuracy.

Because of the uncertainty in some parameters used in the model (especially hydraulic properties in the lowlands) and in some components of the model structure (such as the estimated pumpage), the model is not ideally suited for predicting actual groundwater levels at any specific location. The model overpredicts in some areas and underpredicts in others. Results are more reliable in areas where data (such as water levels, well logs, and pumpage estimates) are abundant and less reliable in areas with little or no data constraining the results. The most appropriate application of the model is comparing the relative effects of different water-management scenarios on the entire groundwater-flow system.

Despite these potential limitations, the HBGM is the most realistic, accurate, and reliable means, at present, for understanding many aspects of the hydrogeologic system of the Harney Basin. When used correctly, the HBGM can contribute to a better understanding of the hydrogeologic system. As more data become available and more modeling capabilities are developed, the HBGM can provide a foundation for updates and refinements to improve its usefulness as a tool for the management of water resources in the Harney Basin. Future refinements and improvements to the model should be driven by (and targeted to) specific questions or issues about the groundwater-flow system in the basin.

Summary and Conclusions

A numerical groundwater-flow model of the Harney Basin was developed to gain a better understanding of the hydrologic conditions within the basin and to provide a management tool that can provide insight into the effects of future stresses within the groundwater basin. The Harney Basin Groundwater Model (HBGM) was developed with the finite-difference groundwater modeling software MODFLOW 6. The HBGM incorporates current understanding of the hydrologic, climatic, geologic, and landscape conditions of the Harney Basin. The model has the capability to simulate hydraulic heads (groundwater levels in wells), groundwater discharge to springs and streams, and evapotranspiration (ET) from the groundwater-flow system under a variety of pumpage and/or climate scenarios.

The HBGM was calibrated to measured and estimated hydrologic conditions during 1930–2018. Model fit was evaluated using base-flow estimates at 21 streamgaging sites and groundwater-level observations at 186 wells. The simulated base flow basin-wide is within 5 percent of the best available base-flow estimates. A reasonable match between the measured and simulated groundwater levels was achieved throughout the 1,300-foot (ft) range of measured groundwater-level elevations in the basin.

The median of the residuals for 33 wells representing the uplands is 8.4 ft when comparing groundwater levels in early 2018, indicating that the model simulates upland groundwater levels that are slightly higher than measured but the model fit is considered acceptable for representing the upland groundwater-flow processes especially considering the upland topographic variability. The median of the residuals for 153 wells representing the lowlands is 0.7 ft, with some areas having groundwater levels higher than measured (Northern lowlands, Donner und Blitzen River, Silvies River floodplain) and some lower than measured (Crane area, Virginia Valley, Weaver Spring area, Silver Creek floodplain). The areas with the most pumping wells (Weaver Spring, the Northern lowlands, and Crane areas) generally were the most difficult to match.

Plots of transient groundwater-level variations show that many of the lowland areas monitored began experiencing substantial declines after 1990, following the wet period of the 1980s and during the period when pumpage began to increase across the basin. Simulated groundwater-level declines (compared to the reference groundwater levels from January 1990) match the areas of largest measured declines in the lowlands near the areas of most irrigation pumpage. The simulated decline in the Weaver Spring area is greater than 90 ft and the area having declines of at least 40 ft in layer 1 cover about 37 square miles (mi^2). The simulated groundwater-level declines in the Northern lowlands are greater than 100 ft in layer 5 and the area having simulated declines of at least 40 ft in layer 5 cover about 7 mi^2. In the Crane area, the simulated decline is greater than 40 ft but mostly 20–30 ft across a large region in all 10 layers.

The major groundwater budget components for the HBGM include precipitation, ET, spring and stream discharge, and groundwater pumpage. Recharge from precipitation and streamflow infiltration and discharge through pumpage were inputs to the model and the model calculates ET and spring and stream discharge. Total annual upland recharge in the study area from precipitation and snowmelt during 1982–2016 averaged about 294,000 acre-ft per year, and surface-water infiltration in the lowlands averaged about 158,000 acre-ft per year. Groundwater pumpage, based on published estimates, increased substantially during the transient simulation, and peaked in 2017, totaling about 149,000 acre-ft. Simulated ET averaged about 89,000 acre-ft annually prior to 1980, but declined with the increase in pumpage, so that by 2018 the simulated annual ET was about 49,000 acre-ft. Simulated groundwater discharge to streams averaged about 46,000 acre-ft annually prior to 1980 but was only about 26,000 acre-ft in 2018. Discharge to the adjacent Malheur River Basin through Virginia Valley was a minor part of the water budget. The groundwater pumped from the lowland system during 1982–2016 was supplied relatively equally by decreased lowland ET (35 percent), decreased lowland spring and stream discharge (32 percent), and the deficit in lowland groundwater storage (30 percent).

Two scenarios were used to investigate (1) the effects of continued 2018 groundwater withdrawals and (2) the capacity of the groundwater-flow system to recover under reduced irrigation pumpage. Both scenarios include the assumption that future recharge will be the same as it was

during 1982–2016. These scenarios are not intended to represent any proposed management scenarios. When 2018 pumpage is continued unchanged until 2100 (scenario 1), the areas of decline expand and declines increase; total decline in the Weaver Spring area is more than 210 ft. Groundwater levels in most areas were continuing to decline at the end of the simulation, indicating that the areas of decline were continuing to expand, and a new steady-state condition had not yet been reached. For scenario 2, irrigation pumpage was set to zero after 2018. In that scenario, the alluvial areas of the upper Silver Creek floodplain and the Weaver Spring area take the longest to recover, needing more than 60 years to recover to 1990 levels. Most of the groundwater levels in the Crane area and the northeast part of the lowlands recover in 20 to 30 years.

Generally, increased withdrawal will result in lower groundwater levels in nearby and downgradient wells. However, the extent of these effects for withdrawal rates greater than presented in this report has not been evaluated. The numerical model developed for this study simulates groundwater levels on a regional scale and thus may not accurately predict the pumped groundwater level at an individual well, but the simulated values are still indicative of expected regional trends in groundwater levels. The model has several other limitations for predictive purposes because of the various assumptions used and overall model uncertainties. Model uncertainty can be reduced, and usefulness increased, as the understanding of groundwater recharge, the distribution of hydraulic properties of the various geologic units, and the geometry of the hydrologic features become better known through additional data collection.

Generally, groundwater levels and budgets simulated using the HBGM indicate the importance of climate stresses (precipitation and evapotranspiration) and groundwater pumpage to the overall groundwater-flow system. The developed HBGM can be used to improve understanding of the hydrologic processes in the Harney Basin and to simulate future management scenarios with different climatic and anthropogenic changes.

References Cited

Bakker, M., Post, V., Hughes, J.D., Langevin, C.D., White, J.T., Leaf, A.T., Paulinski, S.R., Bellino, J.C., Morway, E.D., Toews, M.W., Larsen, J.D., Fienen, M.N., Starn, J.J., and Brakenhoff, D., 2022, FloPy v3.3.6: U.S. Geological Survey Software Release, accessed December 15, 2022, at https://doi.org/https://doi.org/10.5066/F7BK19FH.

Beamer, J.P., and Hoskinson, M.D., 2021, Historical irrigation water use and groundwater pumpage estimates in the Harney Basin, Oregon, 1991–2018: Oregon Water Resources Department Open File Report 2021–02, 53 p. [Also available at https://www.oregon.gov/owrd/wrdreports/OWRD_OFR_2021-02_Harney_Basin_METRIC_Irrigation_Use_Report.pdf.]

Boschmann, D.E., 2021, Generalized geologic compilation map of the Harney Basin: Oregon Water Resources Department Open-File Report 2021-01, 57 p. [Also available at https://www.oregon.gov/owrd/wrdreports/OFR_2021-01_report.pdf.]

Brown, C.E., and Thayer, T.P., 1966, Geologic map of the Mount Vernon Quadrangle, Grant County, Oregon: U.S. Geological Survey Geologic Quadrangle Map GQ-548, scale 1:62,500. [Also available at https://doi.org/10.3133/gq548.]

Corson-Dosch, N.T., and Garcia, C.A., 2022, Soil-Water-Balance (SWB) model archive used to simulate mean annual upland recharge from infiltration of precipitation and snowmelt in Harney Basin, Oregon, 1982–2016: U.S. Geological Survey data release, accessed October 16, 2022, at https://doi.org/10.5066/P94NH4D8.

Freeze, R.A., and Cherry, J.A., 1979, Groundwater: Englewood Cliffs, New Jersey, Prentice-Hall, Inc., 604 p.

Gannett, M.W., and Lite, K.E., Jr., 2004, Simulation of regional ground-water flow in the Upper Deschutes Basin, Oregon: U.S. Geological Survey Water-Resources Investigations Report 2003–4195, 95 p. [Also available at https://doi.org/10.3133/wri034195.]

Gannett, M.W., Lite, K.E., Jr., Risley, J.C., Pischel, E.M., and La Marche, J.L., 2017, Simulation of groundwater and surface-water flow in the upper Deschutes Basin, Oregon: U.S. Geological Survey Scientific Investigations Report 2017–5097, 80 p. [Also available at https://doi.org/10.3133/sir20175097.]

Gannett, M.W., Wagner, B.J., and Lite, K.E., Jr., 2012, Groundwater simulation and management models for the upper Klamath Basin, Oregon and California: U.S. Geological Survey Scientific Investigations Report 2012–5062, 92 p. [Also available at https://doi.org/10.3133/sir20125062.]

Garcia, C.A., Corson-Dosch, N.T., Beamer, J.P., Gingerich, S.B., Grondin, G.H., Overstreet, B.T., Haynes, J.V., and Hoskinson, M.D., 2022, Hydrologic budget of the Harney Basin groundwater system, southeastern Oregon: U.S. Geological Survey Scientific Investigations Report 2021–5128, 144 p. [Also available at https://doi.org/10.3133/sir20215128.]

Gingerich, S.B., 2024, MODFLOW model used to simulate groundwater flow in the Harney Basin, southeastern Oregon: U.S. Geological Survey data release, https://doi.org/10.5066/P9OEKEIO.

Gingerich, S.B., Johnson, H.M., Boschmann, D.E., Grondin, G.H., and Garcia, C.A., 2021, Contour dataset of the potentiometric surfaces of shallow and deep groundwater-level altitudes in Harney Basin, Oregon, February–March 2018: U.S. Geological Survey data release, https://doi.org/10.5066/P9ZJTZUV.

Gingerich, S.B., Johnson, H.M., Boschmann, D.E., Grondin, G.H., and Garcia, C.A., 2022, Groundwater resources of the Harney Basin, southeastern Oregon: U.S. Geological Survey Scientific Investigations Report 2021–5103, 118 p. [Also available at https://doi.org/10.3133/sir20215103.]

Greene, R.C., Walker, G.W., and Corcoran, R.E., 1972, Geologic map of the Burns quadrangle, Oregon: U.S. Geological Survey, scale 1:250,000. [Also available at https://doi.org/10.3133/i680.]

Grondin, G.H., 2021, Methods and results for estimating groundwater pumped, returned, and consumed for non-irrigation uses in the Harney Basin, Oregon: Oregon Water Resources Department Open-File Report 2021-03, 28 p. [Also available at https://www.oregon.gov/owrd/wrdreports/OWRD_OFR_2021-003_Harney_Basin_non_irrigation_GW_use_report_stamped.pdf.]

Grondin, G.H., Boschmann, D.E., Barnett, H.J., and Scandella, B.P., 2021, Methods and results for estimating the hydraulic characteristics of the subsurface materials in the Harney Basin, Oregon: Oregon Water Resources Department Open File Report 2021-04, 63 p. [Also available at https://www.oregon.gov/owrd/wrdreports/OFR_2021-04_Harney_Basin_subsurface_hydraulic_properties.pdf.]

Langevin, C.D., Hughes, J.D., Banta, E.R., Niswonger, R.G., Panday, S., and Provost, A.M., 2017, Documentation for the MODFLOW 6 groundwater flow model: U.S. Geological Survey Techniques and Methods, book 6, chap. A55, 197 p. [Also available at https://doi.org/10.3133/tm6A55.]

Langevin, C.D., Hughes, J.D., Provost, A.M., Russcher, M.J., Niswonger, R.G., Panday, S., Merrick, D., Morway, E.D., Reno, M.J., Bonelli, W.P., and Banta, E.R., 2022, MODFLOW 6 modular hydrologic model version 6.3.0: U.S. Geological Survey Software Release, accessed January 8, 2023, at https://doi.org/10.5066/P9FL1JCC.

Lohman, S.W., 1972, Ground-water hydraulics: U.S. Geological Survey Professional Paper 708, 70 p. [Also available at https://doi.org/10.3133/pp708.]

Oregon Water Resources Department, 2019, Well log information system: Salem, Oregon, Oregon Water Resources Department, accessed January 8, 2024, at https://apps.wrd.state.or.us/apps/gw/well_log/Default.aspx.

Oregon Water Resources Department, 2024, SILVIES R NR BURNS, OR: Oregon Water Resources Department, accessed January 8, 2024, at https://apps.wrd.state.or.us/apps/sw/hydro_report/gage_data_request.aspx?station_nbr=10393500.

Piper, A.M., Robinson, T.W., and Park, C.F., 1939, Geology and ground-water resources of the Harney Basin, Oregon, with a statement on Precipitation and tree growth: U.S. Geological Survey Water Supply Paper 841, 189 p. [Also available at https://doi.org/10.3133/wsp841.]

Schibel, H.J., and Grondin, G.H., 2023, Methods and results for estimating 1930–2018 well pumpage in the Harney Basin, Oregon: Oregon Water Resources Department Open-File Report 2023-01, 72 p. [Also available at https://www.oregon.gov/owrd/WRDReports/OWRD_OFR_2023_01.pdf.]

Swanson, D.A., 1969, Reconnaissance geologic map of the east half of the Bend quadrangle, Crook, Wheeler, Jefferson, Wasco, and Deschutes Counties, Oregon: U.S. Geological Survey Open-File Report v, p. 68–266. [Also available at https://doi.org/10.3133/ofr68266.]

U.S. Geological Survey, 2024a, Silvies River Near Burns, OR—10393500: U.S. Geological Survey, accessed January 8, 2024, at https://waterdata.usgs.gov/monitoring-location/10393500/.

U.S. Geological Survey, 2024b, Donner Und Blitzen River NR Frenchglen OR—10396000: U.S. Geological Survey, accessed January 8, 2024, at https://waterdata.usgs.gov/monitoring-location/10396000/.

Walker, G.W., 1963, Reconnaissance geologic map of the eastern half of the Klamath Falls (AMS) quadrangle, Lake and Klamath Counties, Oregon: U.S. Geological Survey Mineral Investigations Field Studies Map MF-260, scale 1:250,000. [Also available at https://doi.org/10.3133/mf260.]

Walker, G.W., Peterson, N.V., and Greene, R.C., 1967, Reconnaissance geologic map of the east half of the Crescent quadrangle, Lake, Deschutes, and Crook Counties, Oregon: U.S. Geological Survey Miscellaneous Investigations Series Map I-493, scale 1:125,000. [Also available at https://doi.org/10.3133/i493.]

Walker, G.W., and Repenning, C.A., 1965, Reconnaissance geologic map of the Adel quadrangle, Lake, Harney, and Malheur counties v. I-446: Oregon, U.S. Geological Survey Miscellaneous Geologic Investigations Map. [Also available at https://doi.org/10.3133/i446.]

Appendix 1. Hydrostratigraphic Units in the Harney Basin Groundwater Model

Appendix 1 shows the distribution of hydrostratigraphic units in layers 1–10 of the Harney Basin Groundwater Model (fig. 1.1).

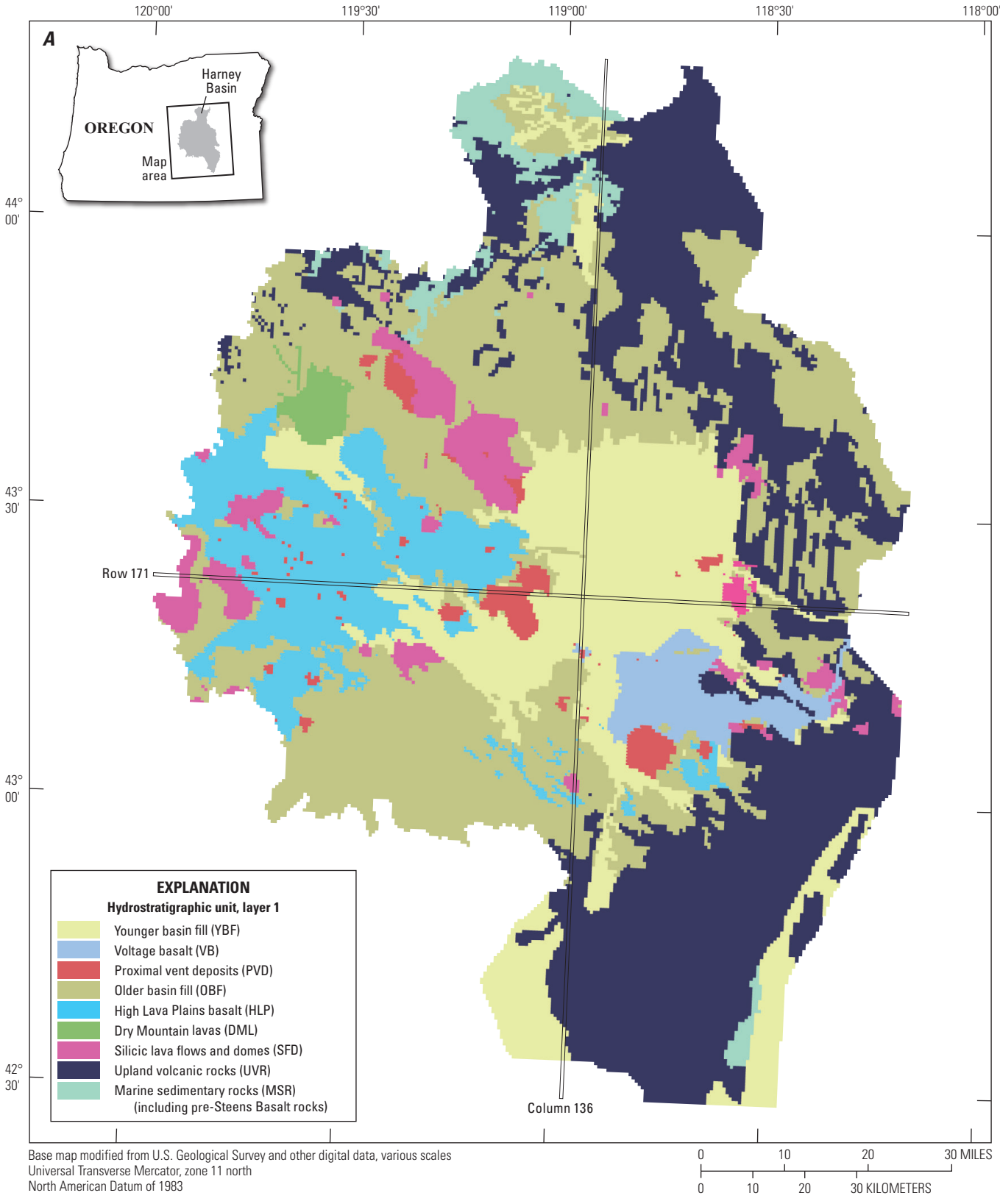

Figure 1.1. Distribution of the hydrostratigraphic units in layers 1–10, Harney Basin, southeastern Oregon. Hydrostratigraphic units described in Gingerich and others (2022).

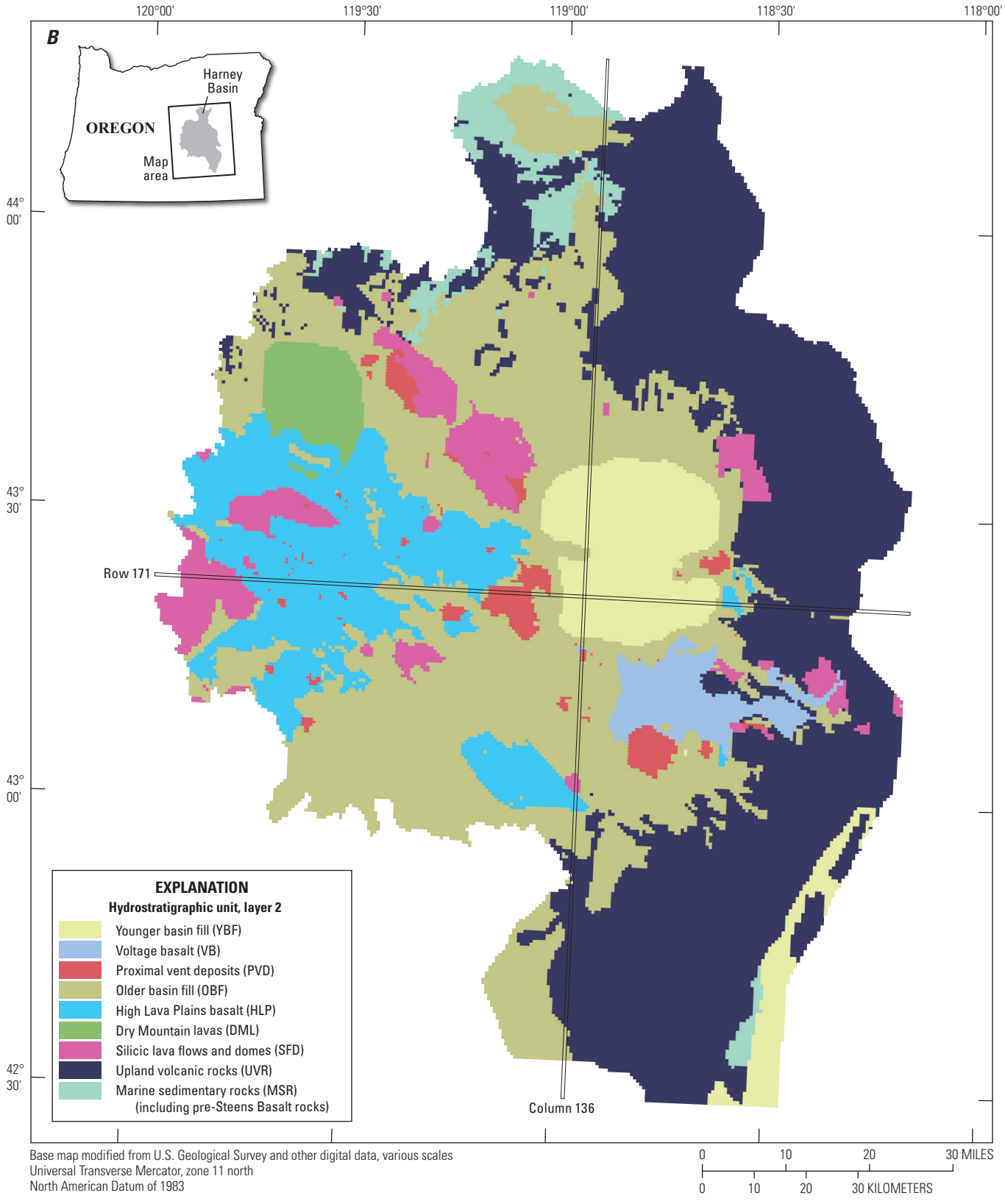

Figure 1.1.—Continued

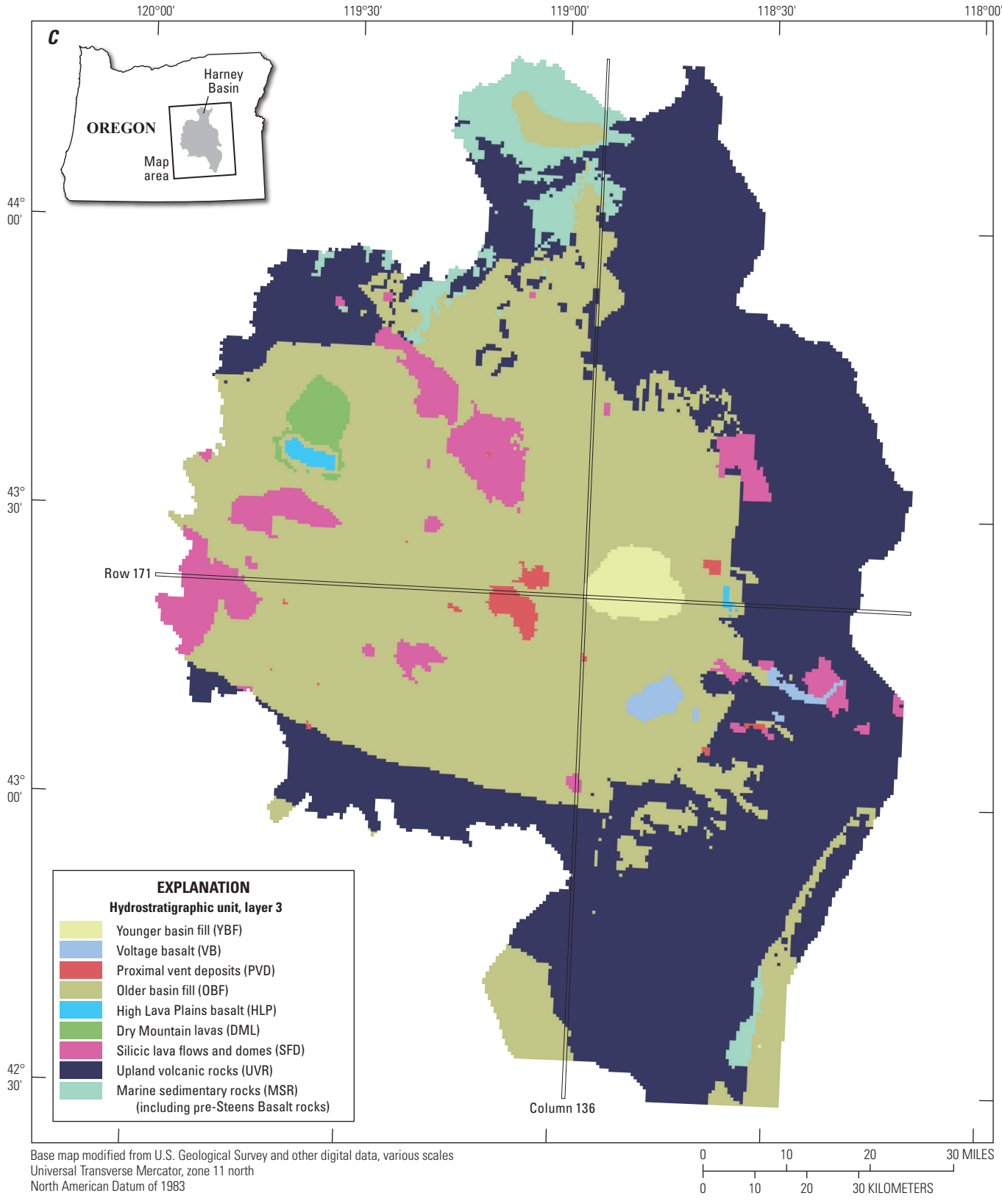

Figure 1.1.—Continued

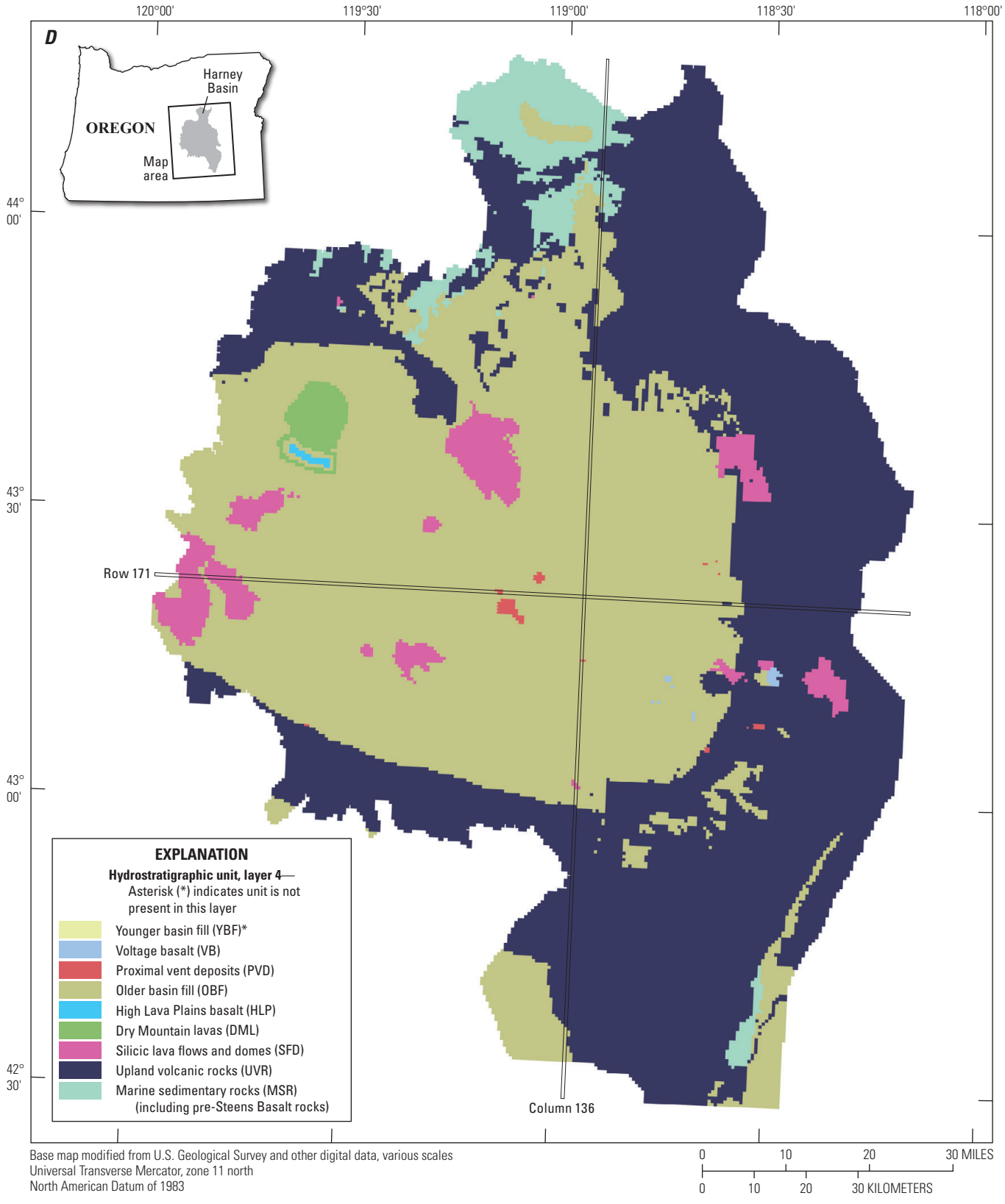

Figure 1.1.—Continued

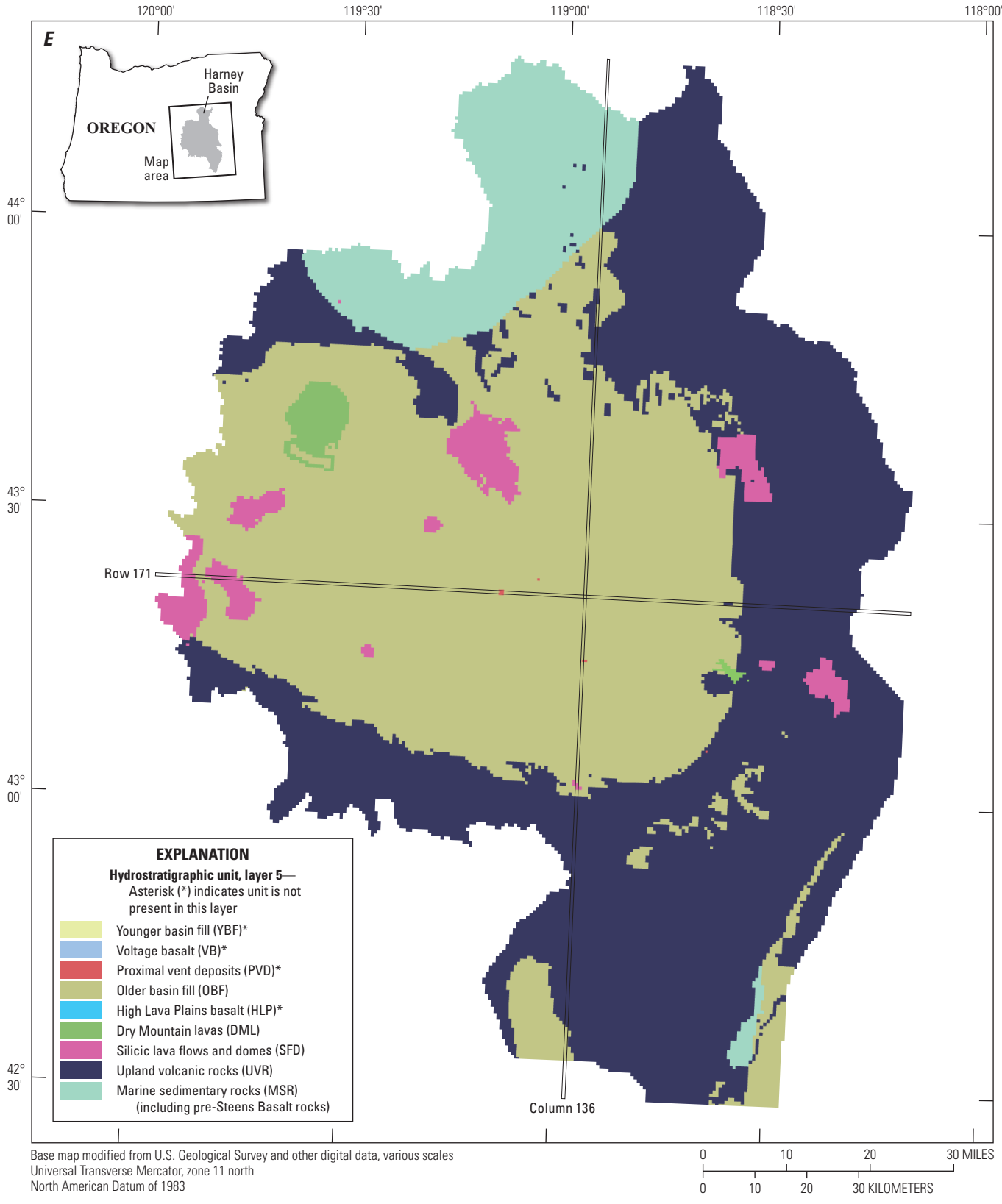

Figure 1.1.—Continued

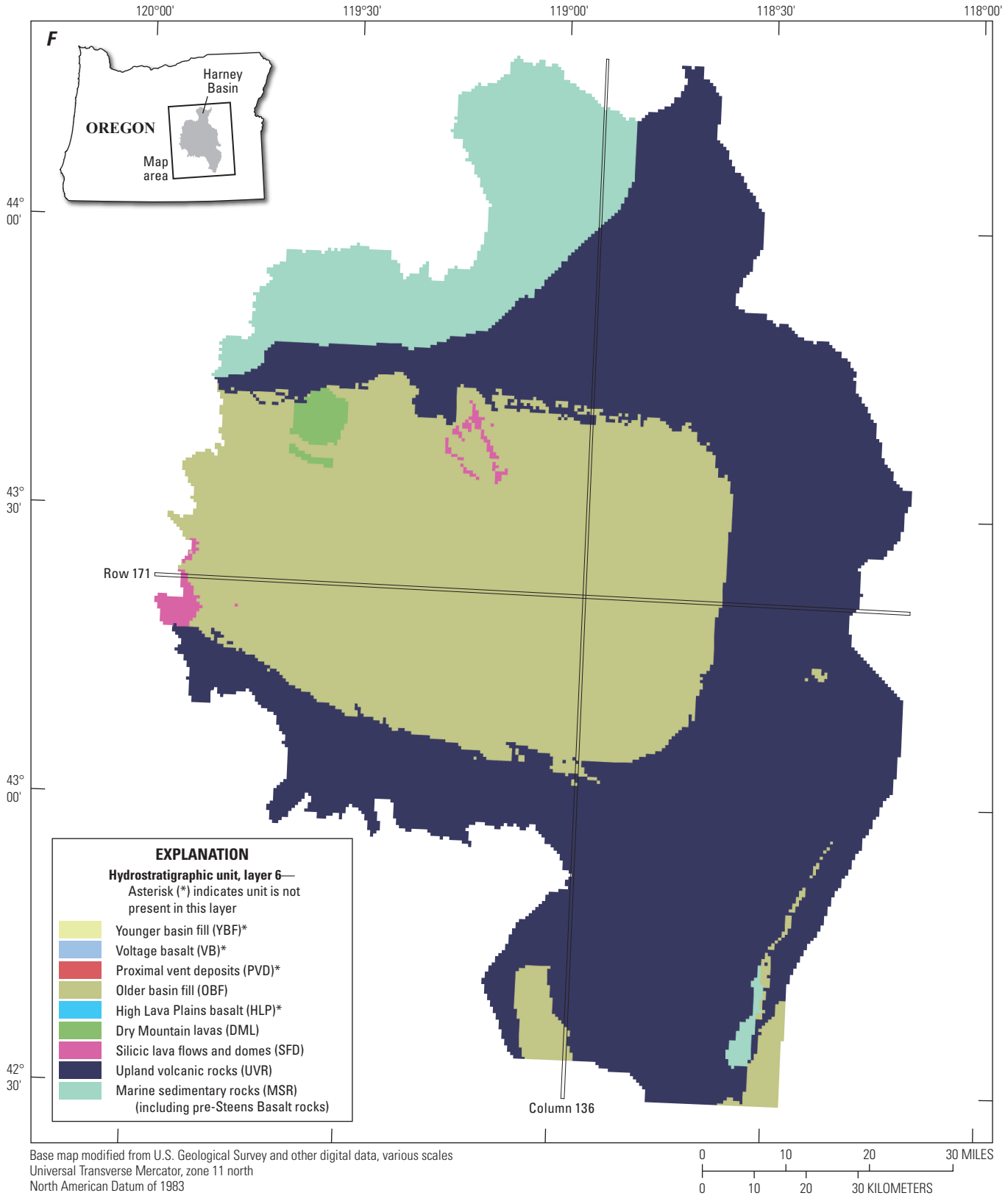

Figure 1.1.—Continued

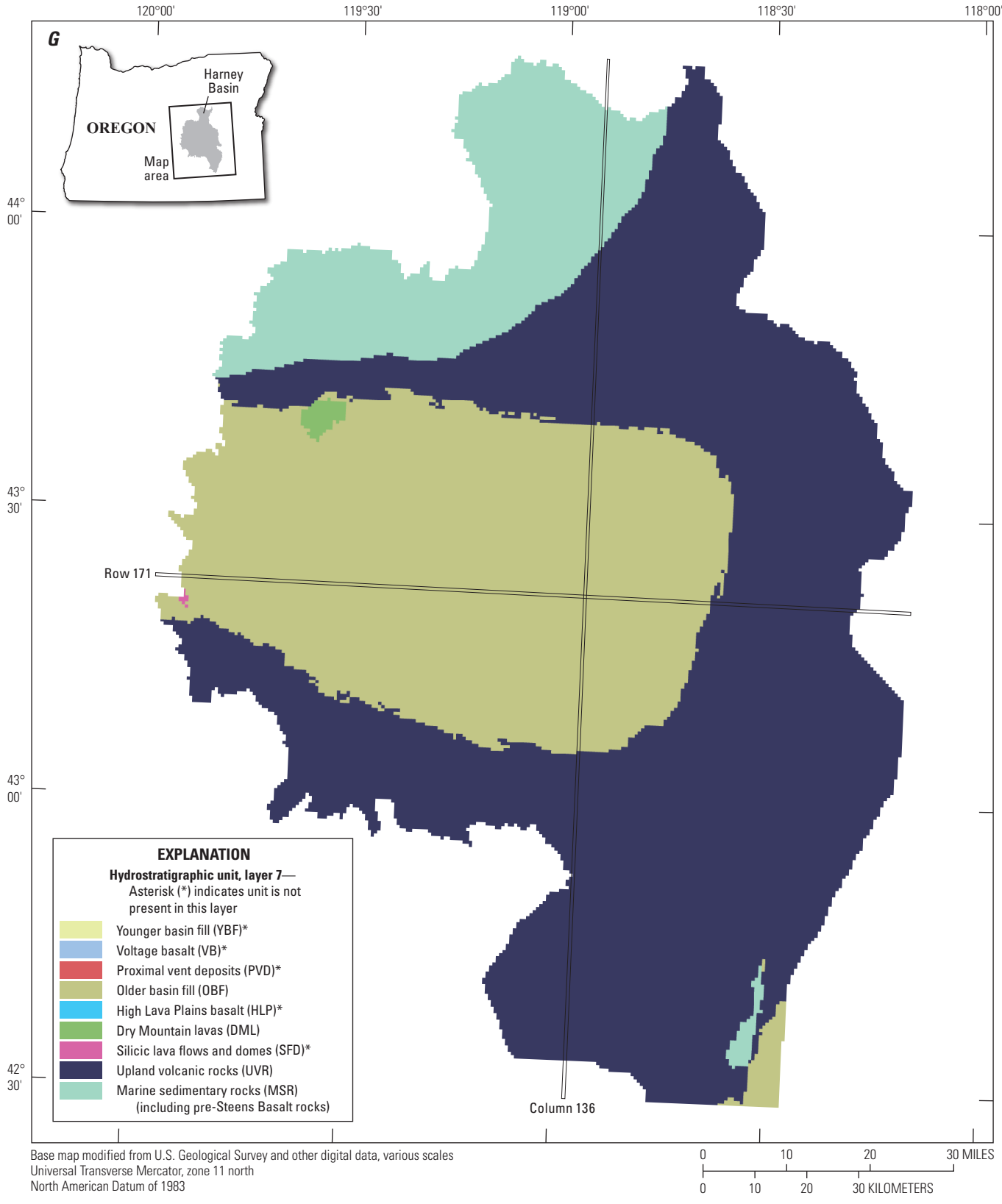

Figure 1.1.—Continued

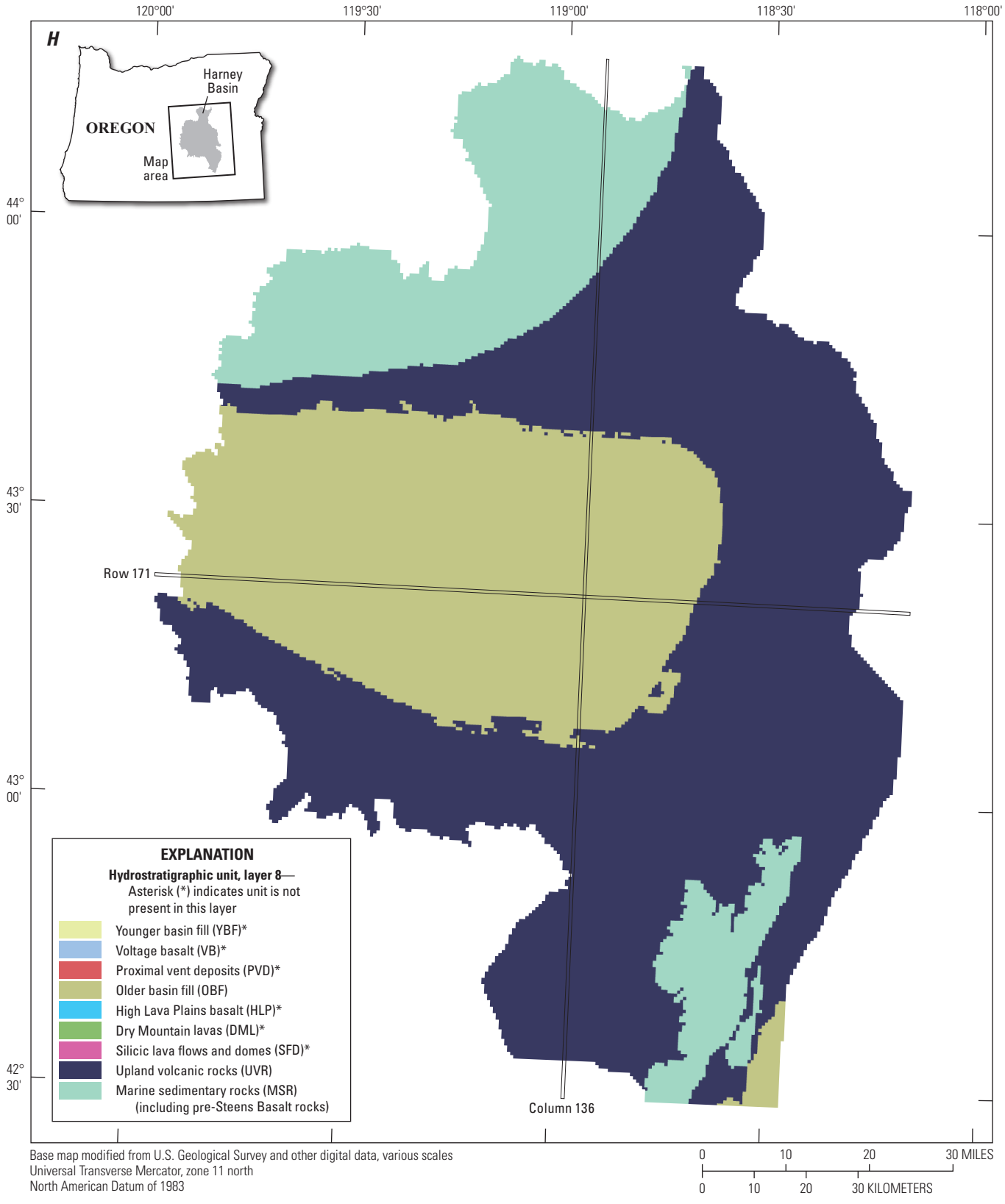

Figure 1.1.—Continued

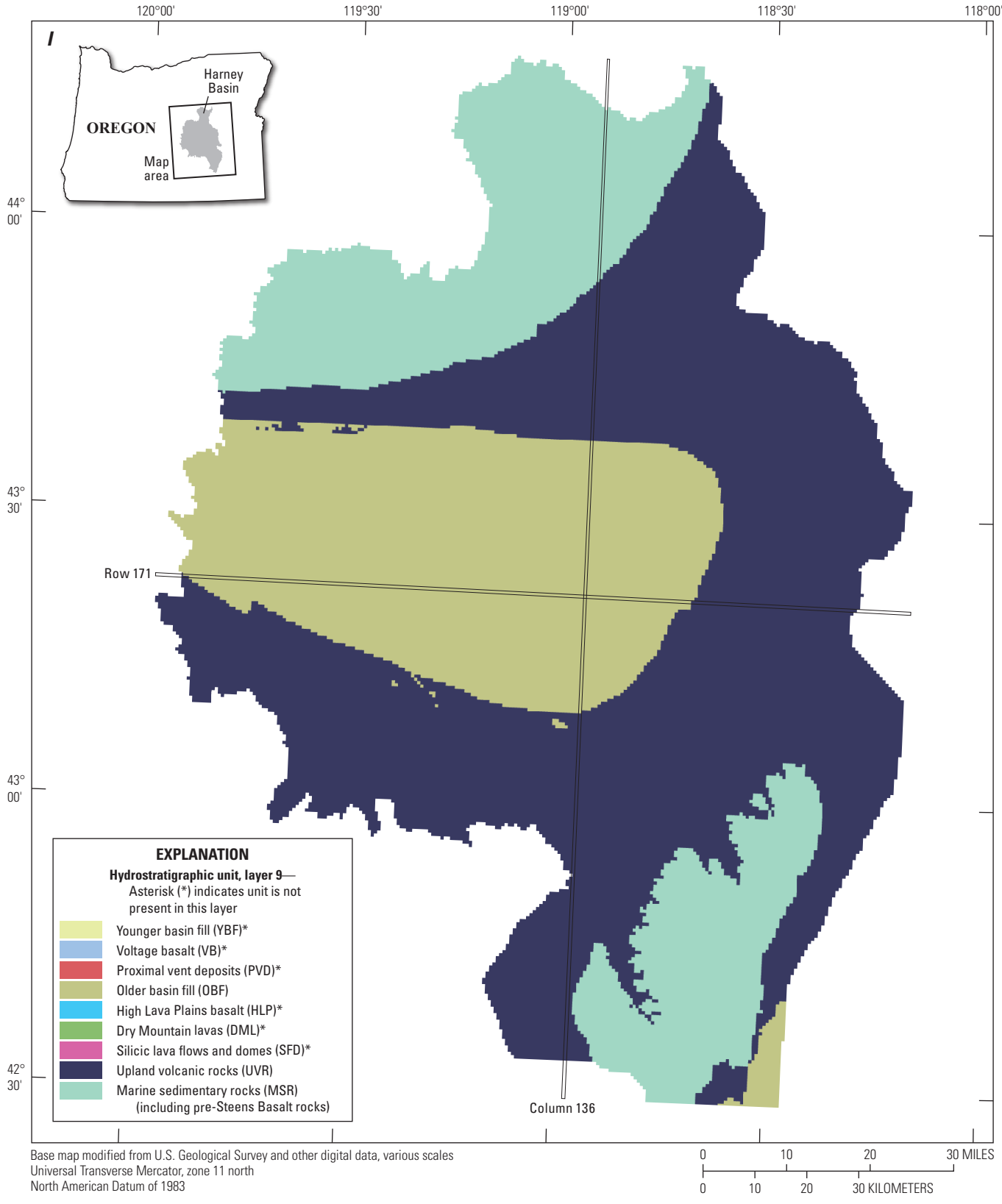

Figure 1.1.—Continued

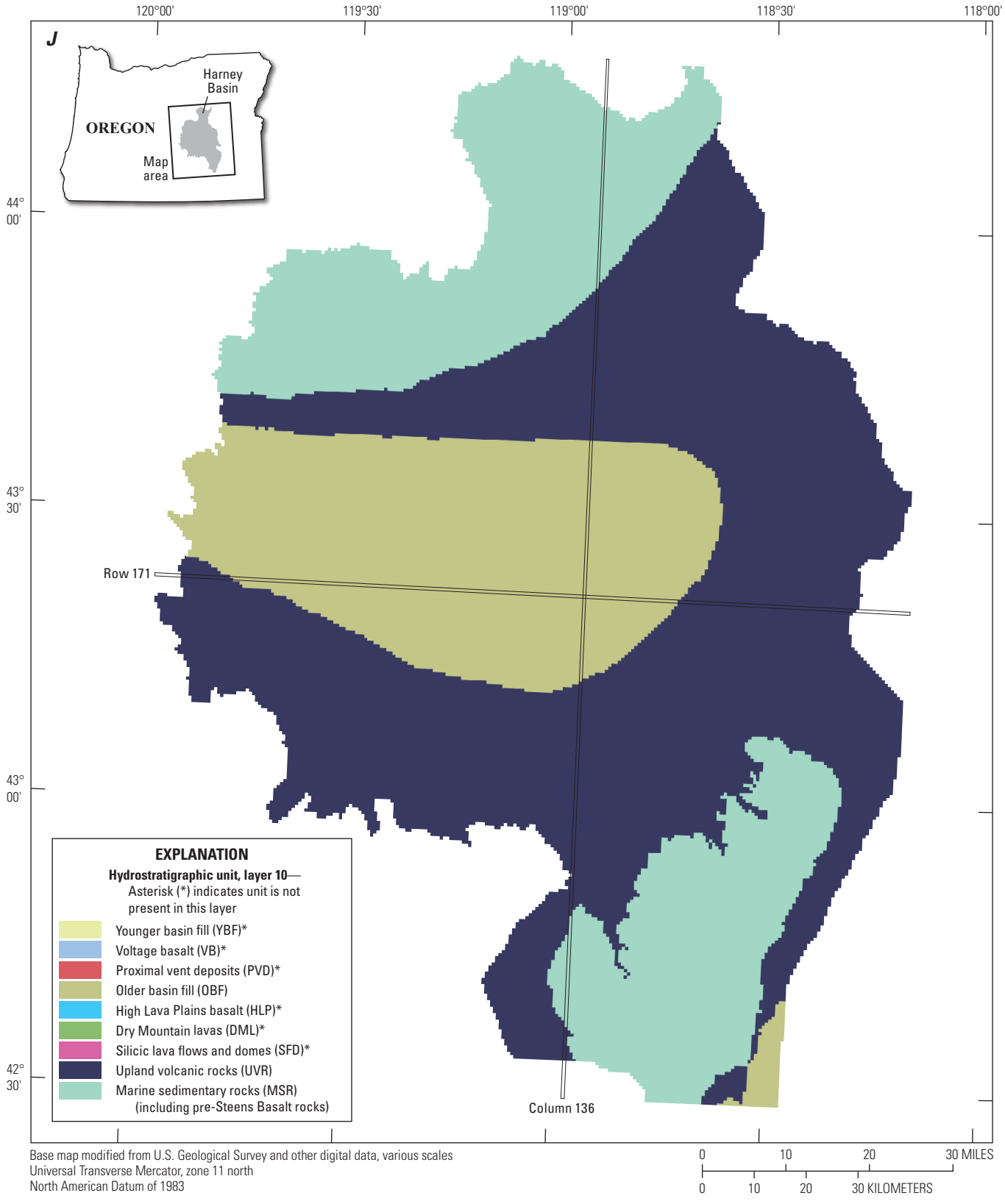

Figure 1.1.—Continued

For more information about the research in this report, contact the
Director, Oregon Water Science Center
U.S. Geological Survey
601 SW 2nd Avenue, Suite 1950
Portland, OR 97204
https://www.usgs.gov/centers/oregon-water-science-center

Manuscript approved on February 2, 2024

Publishing support provided by the U.S. Geological Survey
Science Publishing Network, Tacoma Publishing Service Center
Edited by Jeff Suwak
Layout and design by Yanis Xavier Castillo and Luis Menoyo
Illustration support by JoJo Mangano

Gingerich and others—**Groundwater Model of the Harney Basin, Southeastern Oregon**—SIR 2024–5017

ISSN 2328-0328 (online)
https://doi.org/10.3133/sir20245017